EUROPEAN COMMISSION

European Research Area

CArbon-14 Source Term

CAST

State of the art of ^{14}C in Zircaloy and Zr alloys - ^{14}C release from zirconium alloy hulls

(D 3.1)

Jean – Marie GRAS

(Andra)

Date of Issue of this report: 04/08/2014

The project has received funding from the European Union's European Atomic Energy Community's (Euratom) Seventh Framework Programme FP7/2007-2013 under grant agreement no. 604779, the CAST project.		
Dissemination Level		
PU	Public	**X**
RE	Restricted to the partners of the CAST project	
CO	Confidential, only for specific distribution list defined on this document	

EURATOM

CAST – Project Overview

The CAST project (CArbon-14 Source Term) aims to develop understanding of the potential release mechanisms of carbon-14 from radioactive waste materials under conditions relevant to waste packaging and disposal to underground geological disposal facilities. The project focuses on the release of carbon-14 as dissolved and gaseous species from irradiated metals (steels, Zircaloys), irradiated graphite and from ion-exchange materials as dissolved and gaseous species.

The CAST consortium brings together 33 partners with a range of skills and competencies in the management of radioactive wastes containing carbon-14, geological disposal research, safety case development and experimental work on gas generation. The consortium consists of national waste management organisations, research institutes, universities and commercial organisations.

The objectives of the CAST project are to gain new scientific understanding of the rate of release of carbon-14 from the corrosion of irradiated steels and Zircaloys and from the leaching of ion-exchange resins and irradiated graphites under geological disposal conditions, its speciation and how these relate to carbon-14 inventory and aqueous conditions. These results will be evaluated in the context of national safety assessments and disseminated to interested stakeholders. The new understanding should be of relevance to national safety assessment stakeholders and will also provide an opportunity for training for early career researchers.

For more information, please visit the CAST website at:
http://www.projectcast.eu

CAST		
Work package: 3 **Task: :** 3.1	**CAST document no:** CAST-2014-D.3.1	**Document type:** PU
Issued by: Andra **Internal no.:** DRFSCM140005		**Document status:** Final

Document title
State of the art of ^{14}C in Zircaloy and Zr alloys - ^{14}C release from zirconium alloy hulls

Executive Summary

This report provides a review of the current status of knowledge on various aspects related to the release of ^{14}C from zirconium alloys waste (hulls), which is of importance for long-term safety analyses of final repositories for long-lived Intermediate level waste.

Inventory and distribution of ^{14}C in Zircaloy cladding

In zirconium alloy claddings, the neutron activation of ^{14}N, impurity element of these alloys, is the main source of ^{14}C. ^{17}O coming from the UO_2 (or $(U\text{-}Pu)O_2$) oxide fuel and from water coolant is also a significant precursor of ^{14}C in the zirconia oxide layers formed in reactor on the internal and external sides of cladding respectively. The actual nitrogen content of zirconium alloys is of the order of 30 to 40 ppm, that is to say, two times lower than the maximum level of 80 ppm set as specified or contractual values.
Inventories of ^{14}C in hulls have been determined either by calculation or more rarely by direct measurement. For a fuel irradiated at ~ 45 $GWd.t_U^{-1}$, the production of ^{14}C in cladding is 30 ± 10 $kBq.g^{-1}$. The analysis of the collected data shows that the power-related ^{14}C production amounts to 1.9 ± 0.4 GBq/GWyr.ppm N. Japanese experience suggests that the calculation overestimates the inventory, even when the calculation is carried out with the actual value of the nitrogen content in alloy.
Distribution of ^{14}C between the metal cladding and the zirconia oxide layer depends on the thickness of the oxide. On PWR fuels irradiated at burn-up ≥ 45 $GWd.t_U^{-1}$, the external oxide layer contains ≤ 20 % of the ^{14}C inventory. On BWR fuels, the thinner external oxide layer contains a lower inventory.
There is a lack of reliable data on the chemical state of ^{14}C in the metal and in the zirconium oxide layer. A modelling approach at the atomic scale would be needed to identify the ^{14}C insertion sites in the metal and in the oxide.

Release rates of ^{14}C from Zircaloy hulls

The mechanisms and the rate of ^{14}C release from hulls are expected to be controlled in large part by the uniform corrosion rate of Zircaloy, the diffusion rate of ^{14}C from zirconia oxide layers and/or the dissolution rate of zirconia oxide layers, at the time of the contact between hulls and the infiltrated water under the repository conditions. However various questions arise regarding the physical condition of these hulls, i.e., their state of division and fragmentation, at this time. Indeed, the bulk Zircaloy of hulls is hydrided in reactor, linked to the burn-up, which makes the metal brittle and probably more or less fragmented if they are press compacted during waste processing.

Corrosion rates of zirconium alloys

Zirconium alloys are highly resistant to uniform corrosion at low or moderate temperatures, and their susceptibility to localized corrosion (pitting or crevice corrosion) and stress corrosion cracking appears unlikely in anaerobic groundwaters. However, as mentioned above, considerable uncertainties remain regarding the possibility of hydrogen-induced cracking of press compacted hulls under repository conditions. Nevertheless, regardless of the degree of division of hulls, it can be considered that ^{14}C in the bulk metal of hulls is released congruently with corrosion loss of zirconium alloy. During the corrosion of Zircaloy, there is a possibility of a mechanism in which ^{14}C is not released immediately by corrosion but is incorporated into the oxide film and then released by diffusion or during the zirconia dissolution. It is supported by the fact that measured ^{14}C specific concentrations in zirconia oxide layers are about twice of that of Zircaloy metal after irradiation in a reactor.

Various studies show that the uniform corrosion rates of zirconium alloys are very low in anaerobic neutral or alkaline waters at low temperature. The envelope value of 20 $nm.y^{-1}$, which has been adopted in some assessment models, seems excessively conservative. The most recent results lead to corrosion rates of 1 to 2 $nm.y^{-1}$ after a few years of a corrosion test. For a corrosion rate of 1 $nm.y^{-1}$, the lifetime of hulls, assuming they are not fractured but are corroded on both sides, would be of the order of 2.5 10^5 to 4 10^5 years, which corresponds to a corroded fraction of 2.5 10^{-6} to 4 10^{-6} y^{-1}. The thickness of metal corroded on each side of hull for 10 half-lives of ^{14}C would be only of ~ 60 µm. In other words, such low corrosion rates will lead to decay of much of the inventory of ^{14}C before release can occur.
However it should be noted that our knowledge on the corrosion resistance of zirconium alloys at low temperature regards the very beginning of the corrosion regime. Study of the corrosion behaviour of Zircaloy in high temperature water has shown that, when the zirconia oxide layer reaches a critical thickness of ~ 2.5 µm (corresponding to a weight gain of 30 to 40 $mg.dm^{-2}$), there is a change of the corrosion regime: the corrosion kinetics first follows a power law (*a priori* a cubic law) and after the break-away point corrosion follows pseudo-linear kinetics. It is not possible, at low temperature, to explore the corrosion regime which is beyond a possible phenomenon of break-away, where the corrosion kinetics could be pseudo-linear. Corrosion tests on pre-oxidized samples (oxide thickness > 10 µm) or hulls would complete the range of tests already performed.
The hydrogen pick-up ratio for Zircaloy reaches values of about 90 % in alkaline and in pure water between 30 and 50°C. So the non-corroded metal of hulls will be gradually transformed into brittle zirconium hydride, as it corrodes. This will generate on the external surface of hulls a high-density region of hydrides, acting as a brittle layer, and presumably having a corrosion behaviour different from that of zirconium metal.

Dissolution rates of zirconia oxide layer

The zirconia oxide layer formed on spent fuel rod cladding is chemically very stable in pure water (a solubility of 10^{-9} M can be considered as a conservative and realistic estimate) The solubility increases with increasing alkaline concentrations, and reaches values of the order of 10^{-6} M at pH 12.5 at ambient temperature. The zirconia solubility remains very low for carbonate concentrations lower than 10^{-2} M. At low to moderate concentrations, chloride ions do not seem to have any significant effect on the zirconia solubility, except in $CaCl_2$ solutions of concentration higher than 0.05 M at pH > 10 due to the formation of a highly soluble complex with calcium.
The dissolution rates of zirconia are less well known and have been less studied than the corrosion rates of Zircaloy. In addition, a lack of knowledge of whether the release of radionuclides can be considered as congruent with the dissolution of zirconia has led to the conservative assumption in performance assessment studies that the oxide layer provides no delay to the release of radionuclides. However, in light of some recent results, a realistic value (but possibly not conservative) of the dissolution rate of zirconia in neutral groundwaters or in cementitious environments that are weakly carbonated (< 0.01 M) and fluoride-free, could be very low (of the order of magnitude: 1 $nm.y^{-1}$).
Recent Japanese leaching experiments in alkaline solutions at pH 12.5 at room temperature suggest that ^{14}C release would be congruent with the oxide layer dissolution and metal corrosion.

Chemical forms of ^{14}C released

The aqueous C-H-O system in complete thermodynamic redox equilibrium would be dominated by carbonate and methane. However, complete stable redox equilibrium is seldom achieved in the C-H-O system at moderate temperatures. So the major uncertainties in

modelling the C-H-O system are not the uncertainties associated with the thermodynamic data but the model uncertainties, i.e. the question of metastability at moderate temperatures. The chemical stability of organic compounds under the repository conditions is poorly known.

Both organic and inorganic carbons have been identified in leaching experiments with irradiated hulls or non-activated Zr-based materials (Zr and ZrC powders), although a higher proportion is clearly released as small organic molecules. The origin of these compounds and their reaction mechanisms are not fully understood. The finding that small organic molecules such as short-chain carboxylic acids, alcohols and aldehydes are dominant species raises questions regarding the ultimate fate of such molecules. Some significant uncertainties remain with respect to speciation of ^{14}C (inorganic vs. organic), as well as the nature of the organic ^{14}C.

Contents

1 Introduction

With a half-life of 5,730 years, carbon-14 (^{14}C) is a key radionuclide in safety assessments of the geological disposal of long-lived waste. This radionuclide, of which the speciation is relatively complex, might be present in various forms among the species released into a repository including potentially mobile forms able to move in the geosphere.

The CAST (CArbon-14 Source Term) project aims to better understand the origin and the release mechanisms of ^{14}C from radioactive wastes intended to be placed in geological disposal. Among these wastes, those arising from the spent fuel rod claddings of light water reactors (LWR) after reprocessing, which constitute packages of hulls and end-pieces, form a significant part of the radiotoxic inventory of long-lived intermediate level waste (ILW) in some countries.

This report aims at providing a review of the current status of knowledge regarding the release of ^{14}C from hulls waste in the form of zirconium alloy claddings. After presenting the objects – the hulls - considered in this study and describing their state before disposal (Chapter 2), the origin and inventory of ^{14}C in claddings of fuel rods is reported (Chapter 3). We then examine in Chapters 4 and 5 the different processes that lead, during the different stages of the back-end of fuel cycle and especially in geological disposal, to a release of ^{14}C activity from the metal and the oxide layer of hulls. The state of knowledge on the speciation of carbon released from hulls is presented in Chapter 6.

The subsequent fate of ^{14}C-species released in the near field of a repository, i.e. the processes of retention and transport as well as the processes involving redox reactions *via* microbiological activity, are outside the scope of this report.

2 Zirconium alloys in the nuclear fuel cycle: from fuel rod claddings to hulls waste

2.1 Fuel rod claddings from LWRs [1]

In water reactors, the envelope of the fuel rods is constituted by a cladding tube of zirconium alloy, the dimensions of which depend on the types of reactors and fuel assembly manufacturers. The number of rods per assembly has evolved: today it is usually a 17x17

[1] The meaning of the abbreviations and acronyms cited in the text is given in the Glossary.

array for PWRs, and commonly 9x9 or 10x10 arrays for BWRs. By way of example, without implying completeness, Table 1 outlines the dimensions (outer diameter and thickness) of the fuel rod claddings of various origins used in BWRs and PWRs. Typical BWR cladding is thicker than PWR cladding: 32.0 to 34.0 mils (0.81 to 0.86 mm) thick for BWR Zircaloy-2 claddings versus 22.5 to 25.0 mils (0.57 to 0.635 mm) for PWR Zircaloy-4 claddings [DOE 1992].

Table 1: Outside diameter and thickness (in mm) of selected BWR and PWR fuel rod claddings

Reactor	**BWR**		**PWR**		
Array	8x8	9x9	14x14 to 17x17		
Outside diameter	12.5	10.05	10.75	10.72	9.50
Thickness	0.86	0.665	0.725	0.64	0.57

We will see later that, in the literature, the ^{14}C activity of the fuel rod claddings can be related to the mass of the cladding itself, to the mass of the assembly, or to the mass of fuel. To compare the data, the equivalences that apply to the 17x17 AFA-2GE assembly, manufactured by Areva NP for 900 MWe PWRs have been arbitrarily chosen and will be used as needed [AND 2012]:

- the outside diameter and thickness of cladding: 9.50 and 0.570 mm respectively;
- the mass of zirconium alloy per assembly : 125.6 kg (of which 106 kg is cladding itself) ;
- the mass of UO_2 fuel per assembly: 521.36 kg, corresponding to 0.460 t_U.

It can thus be calculated that, in the case of AFA-2GE assembly, the ratio of the zirconium alloy to the mass of initial heavy metal is 273 $kg.t_U^{-1}$. In German PWRs the mass of zirconium alloy amounts to about 290 $kg.t_U^{-1}$, in BWRs to about 320 $kg.t_U^{-1}$ (KWU – Siemens fuel assemblies) [NEE 1997].

The Japanese Radioactive Waste Management Funding and Research Center (RWMC) has developed a large inventory of the fuel assemblies intended to be reprocessed at the plant of Rokkasho. Different fuel types for BWR and PWR were characterized in terms of uranium loading and weight of cladding. For the BWR fuel type, the average mass of cladding amounts to about 365 $kg.t_U^{-1}$, for the PWR fuel type about 245 $kg.t_U^{-1}$ [SAK 2013].

2.1.1 Alloys used as cladding material

Zirconium alloys are the dominant type of fuel cladding material used in power reactors [GAR 2011]:

- in PWRs: Zircaloy-4 (in the stress relief annealed condition), advanced alloys M5™ and Zirlo™. In reactors of Soviet design (VVER), the cladding material has been principally Zr–1Nb (E110);
- in BWRs: Zircaloy-2 (in the recrystallized condition).

Zircaloy-4, reference alloy for PWR, is derived from Zircaloy-2 by elimination of nickel to reduce the hydrogen uptake during its oxidation in PWR primary water. The increase in nuclear fuel performance targeted by operators has highlighted the limits of Zircaloy-4 in relation to corrosion and led to the development of more resistant zirconium alloys containing niobium, inspired by products used for several decades by the Russians (alloy E110) and the Canadians (Zr-2.5Nb). Areva NP is oriented towards the M5™, binary alloy combining the niobium to zirconium, and Westinghouse towards quaternary alloys, the Zirlo™ and the optimized Zirlo™, combining tin, niobium and iron to zirconium.

Table 2 gives the chemical composition of these alloys for the main alloying elements.

Table 2: Main components (in weight %) of zirconium alloys used as cladding material of fuel rods in BWRs and PWRs; after [AST 2002, MAR 2008]

Alloy	Zircaloy-2	Zircaloy-4	M5™	Zirlo™
Zr	Bal.	Bal.	Bal.	Bal.
Sn	1.2 – 1.7	1.2 – 1.7 *	impurity	0.9 – 1.1
Fe	0.07 – 0.20	0.18 – 0.24	0.030	0.08 – 0.12
Cr	0.05 – 0.15	0.07 – 0.13	impurity	impurity
Ni	0.03 – 0.08	impurity	impurity	impurity
O	0.08 – 0.15	0.09 – 0.16	0.140	0.100 – 0.140
C	0.008 – 0.027	0.008 – 0.027	impurity	-
Nb	impurity	impurity	1.00 ± 0.02	0.80 – 1.20
Si	0.005 – 0.012	0.005 – 0.012	impurity	-
S	impurity	impurity	0.002	-

* The maximum tin threshold for the Zircaloy-4 standard was 1.70 %. The content of low tin Zircaloy-4 now used is 1.35 ± 0.15 %.

Table 3 specifies the contents of the elements that are precursors of ^{14}C by activation: nitrogen, carbon and oxygen (see § 3.1). Normative specifications and those of the manufacturers generally indicate a range of composition or a maximum level depending on whether the elements are introduced as an element of addition or present as an impurity. For nitrogen, which is an impurity element, the use of this maximum level, 80 ppm, gives

excessive values when it comes to assessing the actual abundance of ^{14}C formed by activation of ^{14}N with sufficient accuracy.

- In 1991, Van Konynenburg, from the Lawrence Livermore National Laboratory (LLNL), recommended for Zircaloy a value of 40 ppm [VAN 1991].
- In 2013, based on the feedback acquired at the reprocessing plant of Rokkasho, RWMC also set at 40 ppm the average nitrogen concentration in the Zircaloy-2 and -4, although lower levels can be measured [SAK 2013].
- To reduce the conservatism, CEA, Areva and EDF sought to determine more realistically the average grade of activated elements, including N, C and O present in the cladding tubes of Zircaloy-4 and M5™ alloy [MAR 2004]. For Zircaloy-4, the analysis focused on over 21 years of manufacturing, more than 100,000 fuel assemblies. The compilation and analysis of results led, in France, to adopt and recommend the actual values shown in Table 3 for the calculations of activation products inventories. It is thus noted that the nitrogen content is 34 ppm in the Zircaloy-4 and 27 ppm in the M5™.

Table 3: Specified or contractual values, and actual values of the contents (mass ppm) in precursors elements of ^{14}C in the claddings in Zircaloy-4 and M5™, after [MAR 2004]

	Specified or vendors values		Actual values derived from analysis of castings or tubes	
	Zircaloy-4	**M5™**	**Zircaloy-4**	**M5™**
N	< 80	< 80	34 ± 10	27 ± 4
C	80 - 270	< 200	140 ± 30	45 ± 8
O	900 - 1600	900 - 1600	1250 ± 170	1350 ± 70

In summary, for the activation calculations, the following values of nitrogen content may be recommended:

- for Zircaloy-2 and Zircaloy-4: 40 ppm,
- for the new advanced zirconium alloys: 30 ppm.

Nitrogen is an α-stabilizer, expanding the α region of the phase diagram by formation of an interstitial solid solution (Figure 1a). It is soluble at up to about 4 %, which is much higher than the level at which it is controlled to as an impurity. So all nitrogen should be in solid solution in zirconium alloys [ADA 2007]. Carbon has low solubility in α-Zr (~ 100 ppm) and so is generally present in the form of small precipitates of carbide fcc-ZrC (Figure 1b) [IAE 1998, ADA 2007].

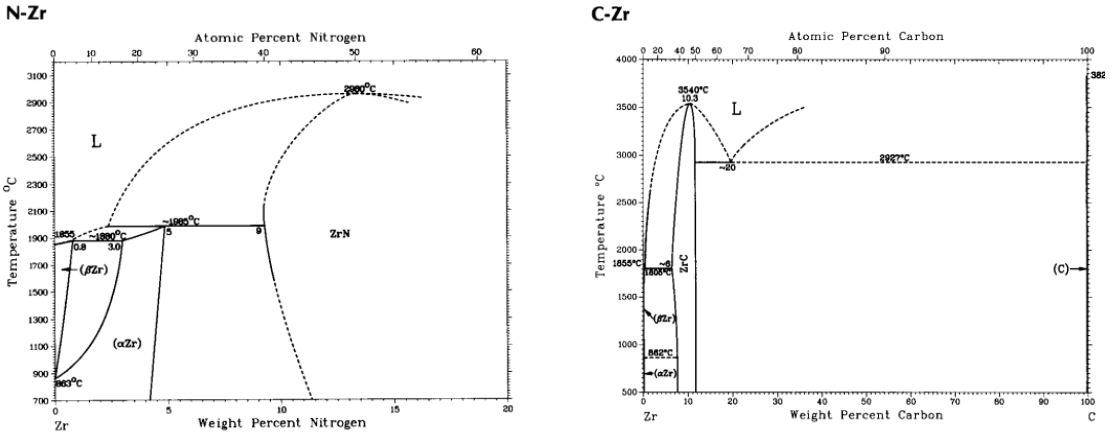

a) **b)**

Figure 1: The zirconium – nitrogen and the zirconium – carbon phase diagrams [ASM 1992]

2.1.2 Behaviour in reactor

During its passage in reactor, the fuel rods cladding is subjected to different processes:

- oxidation and corrosion, causing the growth of oxide layers on inner and outer surfaces;
- hydriding, caused by the sorption and pick-up of hydrogen formed by reduction of water;
- irradiation, leading to a change of the alloy microstructure and its mechanical properties.

The phenomena of oxidation and hydriding are the main processes to be considered in relation to the behaviour of claddings in disposal conditions and to the release of ^{14}C.

2.1.2.1 Corrosion and hydriding

2.1.2.1.1. Internal oxidation of cladding

When the gap closes between cladding and fuel pellets and the cladding comes into contact with the uranium dioxide, the high affinity of zirconium for oxygen leads to the development of an oxide layer on the cladding inner surface. The oxidation increases with burn-up: zirconia increases discontinuously, developing firstly by staining with a thickness greater than 5 µm, then covers the entire surface with a thickness that increases slowly and stabilizes around a value of 9 ± 2 µm (Figure 2a) [AND 2012]. Figure 2b shows a comparable increase in the thickness of this inner zirconia on Zirlo^{TM} claddings.

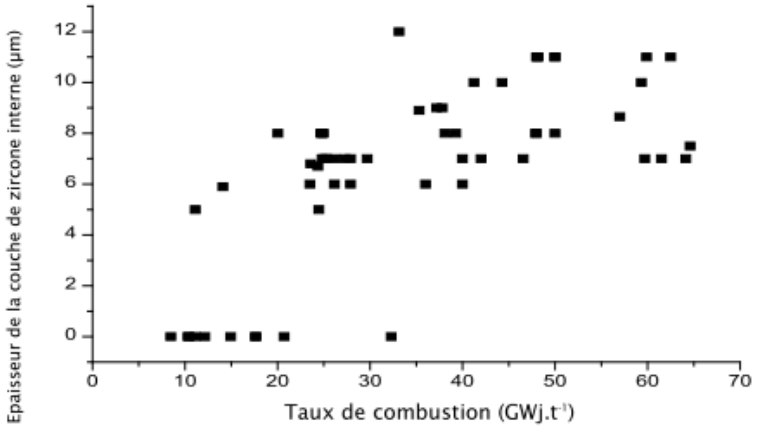

a) Zircaloy-4 (UOX or MOX fuel) [DEH 2000]

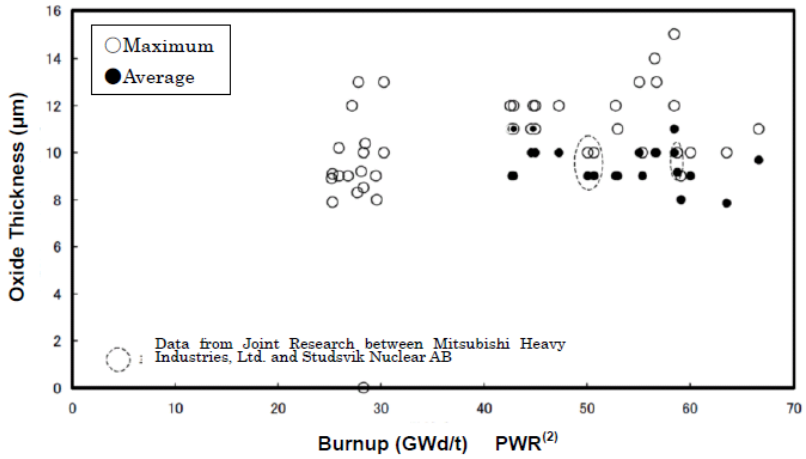

b) Zirlo™ [NIS 2009]

Figure 2: Evolution of the thickness of the internal zirconia on Zircaloy-4 and Zirlo™ cladding as a function of burn-up.

2.1.2.1.2. External corrosion of cladding

At the external surface of the cladding, the zirconium alloy reduces water to form a zirconium oxide, whose the composition is invariably considered to be ZrO_2 (zirconia), as follows [among many other references: COX 1973, COX 1976, IAE 1998, ADA 2007, ALL 2012]:

$$Zr + 2\,H_2O \rightarrow ZrO_2 + 2\,H_2 \qquad \{1\}$$

The corrosion kinetics of zirconium alloys in high temperature high pressure steam or water can be schematically described by a first "parabolic-type" regime, up to the so-called transition point, followed by a series of parabolic curves often approximated by a linear law (Figure 3a). The transition is observed for an oxide layer of thickness in the range 2 - 3 µm (corresponding to a weight gain in the range 30 - 40 mg.dm^{-2}) and is correlated with a loss of the oxide protective character. Pre-transition oxide, of tetragonal structure, is a thin, nonporous, black oxide layer that grows in thickness with the cube root of time eventually

transforming into the post-transition gray oxide layer. The post-transition gray oxide layer has some porosity; its structure is monoclinic. Thus, when a thick oxide is produced from reaction with water or steam, most of the oxide exists as the monoclinic zirconia.

Various models have been developed to account for the kinetics of uniform corrosion of Zircaloy alloys in high temperature water and in reactor [HIL 1977, GAR 1980, COX 1985, IAE 1998, COX 2005].

In practice, the corrosion of zirconium alloys in PWR and BWR results by the formation of a virtually insoluble zirconia layer at the surface of the claddings. Corrosion is similar to a simple oxidation and these are the conditions of formation of this oxide that distinguish the various forms of corrosion in reactor (Figure 3b).

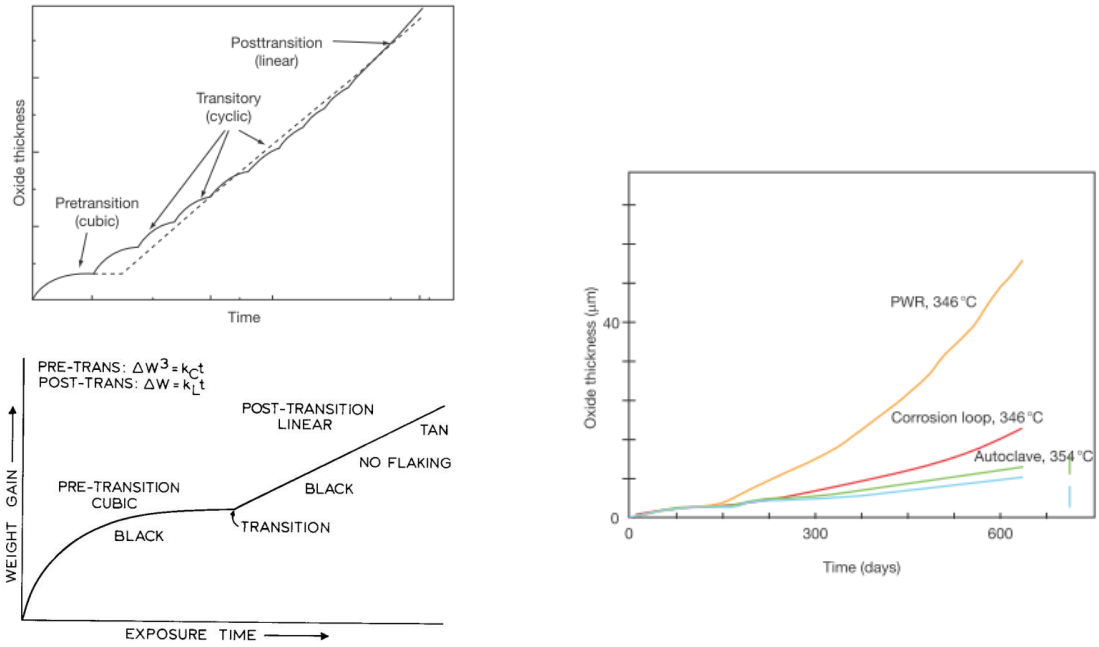

a) **b)**

Figure 3: a) Schematic representation of the corrosion of Zircaloy in the temperature range 250 – 400°C [HIL 1977, HIL 2000]
b) Influence of experimental conditions on the corrosion kinetics of Zircaloy-4: (1) isothermal conditions at 346°C and 354°C, (2) in loop at 346°C with heat flux, (3) in PWR at 346°C (cumulative effects of heat flux and irradiation) [GUE 1996, ALL 2012]

The thickness of oxide formed along the fuel rod is related to the thermal history at the metal/zirconia interface, oxidation of zirconium alloys being thermally activated. In a 900 MWe PWR, the thickness of external zirconia measured on the rods increases from the bottom of the rod until the 6th stage (8th stage in a 1300 MWe PWR) and then declines over the last two stages (Figure 4). It shows an axial profile in "roller coasters", the minima of which correspond to the location of the grids. This profile is related to the regular increase of

the external temperature from the bottom to the top of the rod and to the decrease of the temperature at the metal–oxide interface, at the level of grids and at the rod extremities.

The overall increase in oxide thickness with the burn-up is, at first, a consequence of the holding time at temperature in contact with the coolant water.

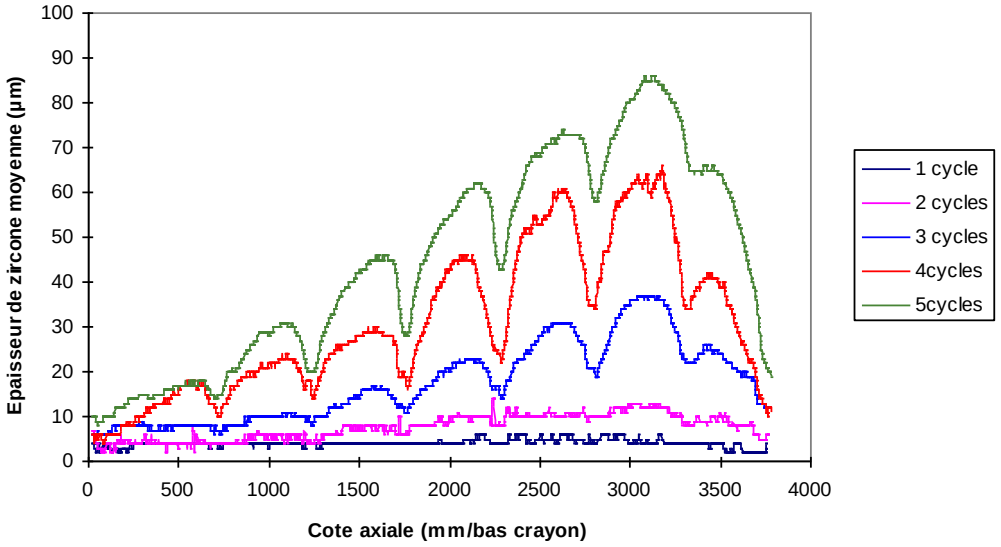

Figure 4: Zircaloy-4 claddings – Variations of the axial thickness of zirconia as a function of the number of cycles [DEH 2000]

a) Zircaloy-4 cladding

The thicknesses of the oxide layer at the most corroded stage remain below 100 µm after 4 cycles of irradiation for Zircaloy-4 cladding. Disparities may appear on the same rod from a generatrix to another.

Examinations of Zircaloy-4 claddings performed on site by EDF since 1985 have established an empirical envelope law, linking with a good statistical representativeness the thickness of the zirconia layer, *t* in µm, corresponding to the azimuthal average at the most oxidized stage, to the burn-up *BU* in GWd.t^{-1} [VRI 1994] :

$$t = 1.935\ 10^{-2}\ (BU)^{2.1} \qquad \{2\}$$

Partial peeling of the zirconia layer can be observed for greater thicknesses of the oxide and high burn-up. It is in the form of small flakes which come off the zirconia layer. This phenomenon of peeling is not normally observed for burn-up below 52 GWd.t^{-1} [AND 2012].

b) M5^{TM} cladding

The kinetics of oxidation of the M5^{TM} alloy is much lower than that measured on the claddings in Zircaloy-4 (Figure 5a). On the rods in M5^{TM}, the zirconia thickness does not exceed 30 µm after 6 cycles.

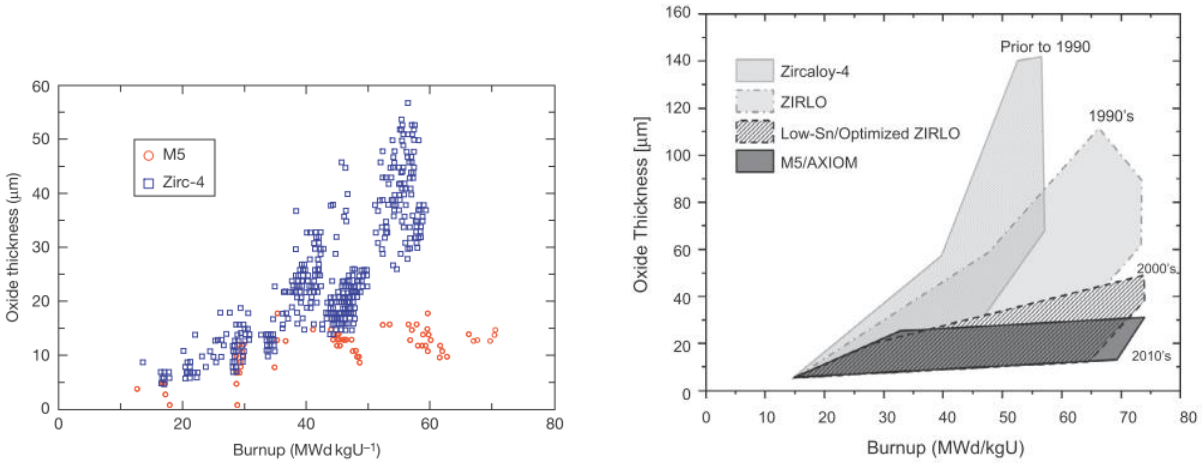

a) [BOS 2004] **b) [TER 2014]**

Figure 5: Peak oxide layer thickness as a function of burnup for Zircaloy-4, M5™ and Zirlo™.

c) Zirlo™ cladding

The Zirlo™ shows a corrosion resistance intermediate between those of Zircaloy-4 and M5™ (Figure 5b). The oxide thickness evolves axially as on Zircaloy-4. The maximum thicknesses of ZrO_2 measured on Zirlo™ claddings of French PWR are in the range 60 – 80 µm.

d) Zircaloy-2 cladding

The corrosion resistance of Zircaloy-2 in BWR is comparable to that of Zircaloy-4 could present. The BWR external oxide layer is generally thinner than on PWR cladding; it hardly ever exceeds 70 µm. Indeed the temperature of the cladding is a little lower in BWRs than in PWRs and the BWR fuel operates at a lower burn-up. Nodular corrosion occasionally occurs with zones reaching a thickness up to 100 µm (Figure 6). The water chemistry makes the alloy less liable to hydriding in BWRs than in PWRs [VID 1975, GAR 1979].

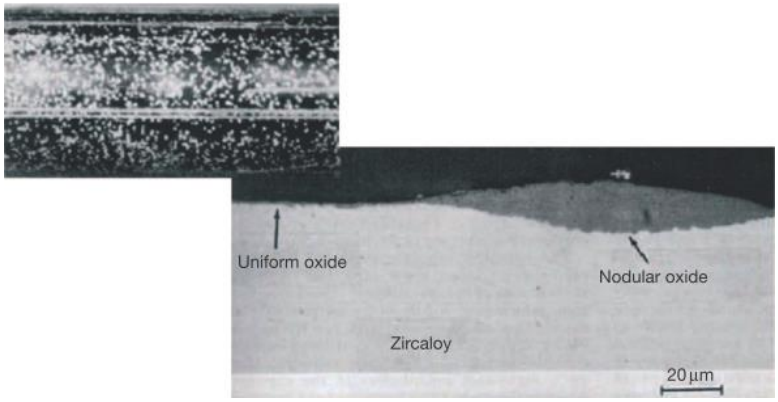

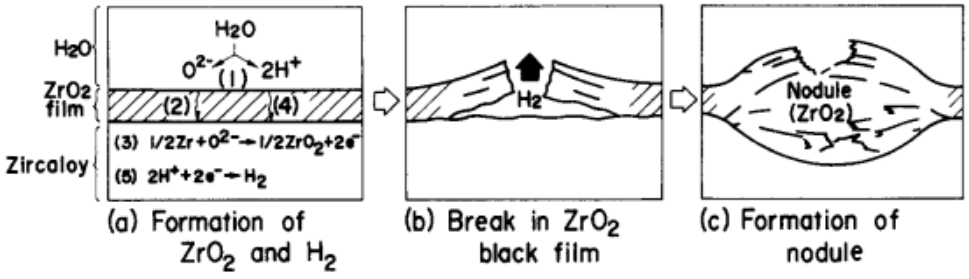

Figure 6: Typical appearance of nodular corrosion in visual inspection and metallographic examination [ALL 2012] and mechanism of formation of lenticular nodules [KUW 1983]

2.1.2.1.3. Hydriding of cladding

During the uniform corrosion of zirconium, the water reduction (cf. reaction {1}) liberates hydrogen on the reaction sites. Most of this hydrogen is released in the water, but a small portion (in the range 10-20 % for Zircaloy-4 in PWR and mostly around 15 %) is incorporated into the metal. The solubility of hydrogen in the zirconium alloy is in the range of 150 ppm at 350°C (Figure 7a). Beyond the limit of solubility, hydrogen precipitates as hydrides δ ZrH_x platelets (x between 1.5 and 1.66), which are oriented perpendicular to the tensile stress, or parallel to the planes of crystallite base in the absence of mechanical stresses (for the case of the guide tubes and grids also in zirconium alloy) [ELL 1968, COX 1976].

At temperatures reached in reactor, the hydrides are ductile and do not contribute to an embrittlement of the cladding, but, upon cooling, when the solubility of hydrogen in the zirconium is less than 1 ppm, the precipitation of hydrides involves potentially a decrease in the ductility of the cladding (Figure 7b).

The quantity of hydrogen absorbed in operation is proportional to the thickness of the zirconia layer ***t*** (Figure 8). The empirical relationship obtained for Zircaloy-4 is expressed in the following way [AND 2012]: [H] (ppm) = 8 *t* (µm). The hydrogen content in the claddings can thus be large (several hundreds of ppm).

The hydrogen uptake in PWR by the M5^{TM} alloy is very low, first because of a reduced availability of hydrogen as a consequence of lower oxidation and secondly due to lower hydrogen pick-up than for Zircaloy-4 [MAR 2008]. Figure 9 shows the evolution of the hydrogen content as function of the burn-up for M5^{TM} and Zircaloy-4. The proportional relationship between the total hydrogen content and the thickness of oxide layer is approximately 4 for the M5^{TM} [BOS 2004].

The behaviour of Zirlo^{TM} is similar to that of Zircaloy-4 in terms of hydriding.

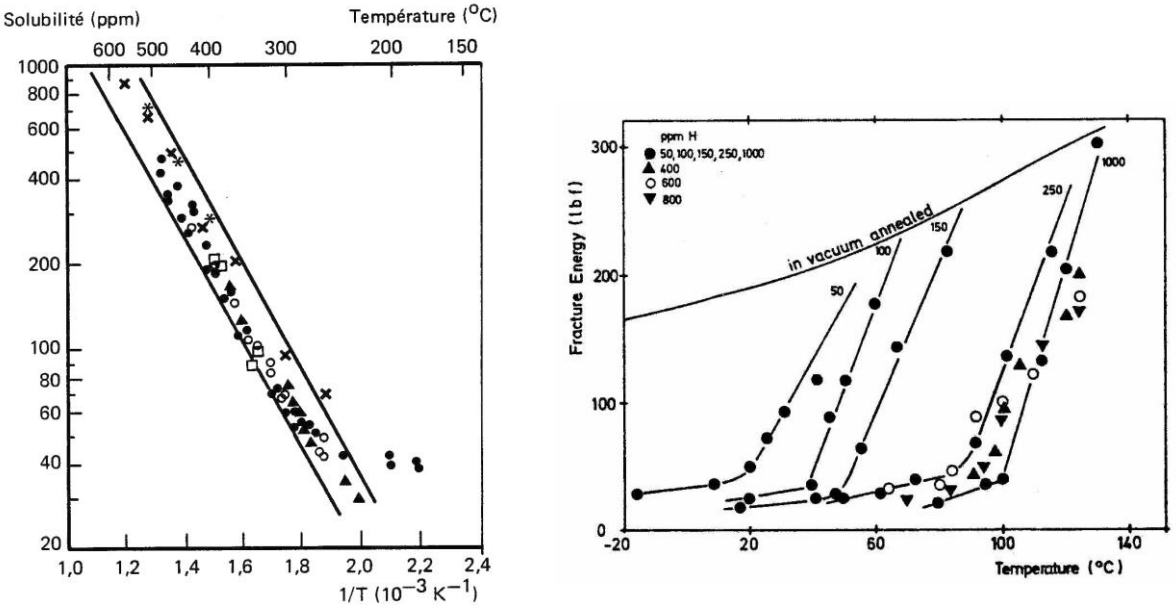

a) b)

Figure 7: Solubility of hydrogen in Zircaloy (a) and influence of hydrogen on the fracture energy transition temperature of Zircaloy (b) [DOU 1971, GAR 1979].

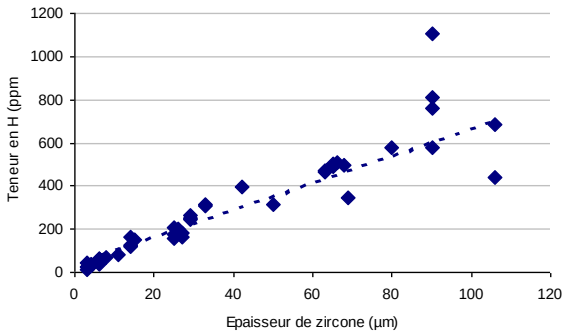

Figure 8: Relationship between the overall hydrogen content and the oxide thickness of cladding for Zircaloy-4 [BOS 2004]

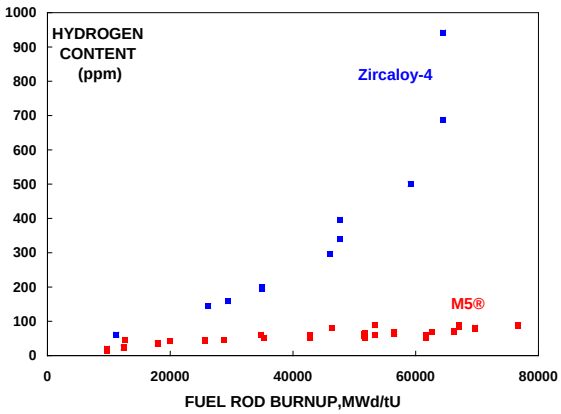

Figure 9: Comparison of the hydrogen pick-up of M5^{TM} and Zircaloy-4 as a function of the burn-up [MAR 2008]

2.1.2.2 Microstructural transformations of cladding in reactor

For Zircaloy, the two main structural transformations caused by irradiation of cladding in reactor are the following [LEM 2010]:

- a modification of the structure of dislocations (creation of <a> and <c> loops); these defects of irradiation lead to a hardening of the alloy and to a decrease of ductility, as well as to an irradiation growth;
- an evolution of the precipitation of intermetallic phases (precipitates $Zr(Fe,Cr)_2$ are the most common), resulting in amorphization, in which iron, and more slightly chromium, leave the precipitates and dissolve in the zirconium matrix. A secondary precipitation can be induced with the formation of new small precipitates ZrFeCr, Zr_5Sn_3, $Zr(Fe,Cr)_2$.

For the M5^{TM} alloy, irradiation also causes a change in the dislocation structure by creating <a> and <c>loops, these defects also leading to hardening of the alloy and to a decrease of ductility. In contrast, M5^{TM} is characterized by a microstructural stability up to high neutron fluencies (70 GWd.t_U^{-1}). Only a slight decrease is observed in the amount of niobium of β-Nb particles, correlated with a small increase in their size. The most significant microstructural change under irradiation is the appearance of precipitates of small particles in the form of needles which are rich in niobium and lead to a significant decrease of the niobium content in the matrix [AMB 2010, AND 2012].

Data on the evolution of the microstructure of Zirlo^{TM} under irradiation are fewer. Generic phenomena for the zirconium alloys such as the appearance of dislocation loops or modification of the precipitation state also occur [AMB 2010].

2.1.2.3 End-of-life condition of cladding when unloaded from reactor

When they are unloaded from reactor, the spent fuel claddings are in an oxidized and hydrided condition.

The micrographs of Figure 10 show the typical aspect of the zirconia layers present at the external surface of claddings. For Zircaloy-4 claddings (PWR), the empirical law {2} giving the oxide thickness on the most oxidized stage as a function of the burn-up leads to an outer oxide thickness of 60 µm for a spent UOX fuel irradiated for 4 cycles.

A detailed examination of these layers reveals their stratified aspect due to the presence of numerous microscopic cracks predominantly parallel to the interface metal - oxide. This cracking can sometimes lead to spalling of the zirconia layer.

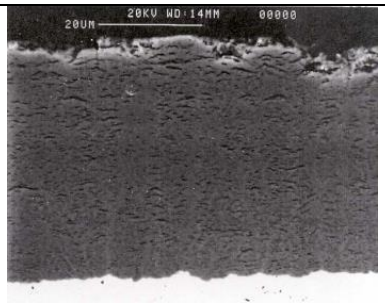

Zircaloy-4, 60 GWd.t^{-1}
[BLA 1997]

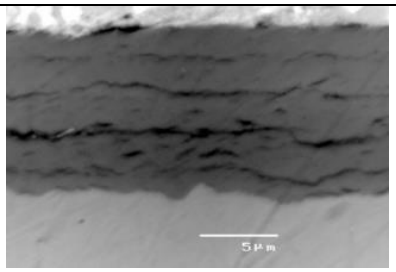

M5^{TM}, 79 GWd.t^{-1}
[BOS 2007]

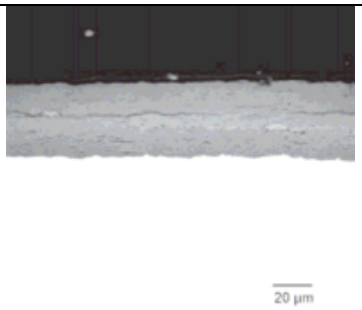

Zirlo^{TM}, 70 GWd.t^{-1}
[AMB 2010]

Figure 10: Micrographs of irradiated cladding showing the aspect of the outer zirconia layer

At the internal surface of the cladding, the zirconia layer, of average thickness 10 µm (see § 2.1.2.1.1), appears more dense than the outer oxide.

Micrographs of Figure 11 show typical morphologies of hydrides observed at room temperature on Zircaloy-4 cladding, as a function of the burn-up, and on M5^{TM} and Zirlo^{TM}. Hydrides appear circumferentially oriented and are concentrated in the cold periphery of the cladding of the fuel rods unloaded from reactors.

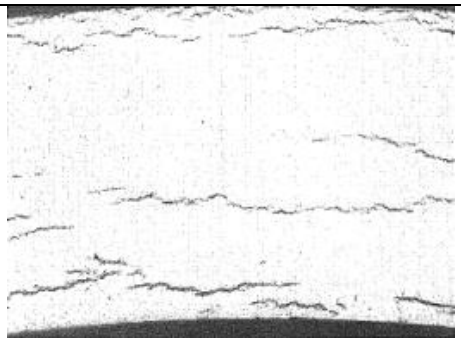

Zircaloy-4, 30 GWd.t^{-1}, stage 6
[AMB 2010]

Zircaloy-4, 65 GWd.t^{-1}, stage 6
[AMB 2010]

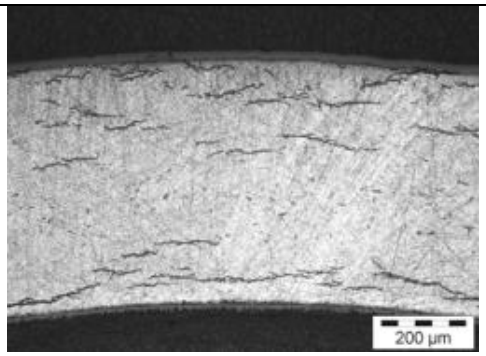

M5™, 5 cycles, stage 6
[AMB 2010]

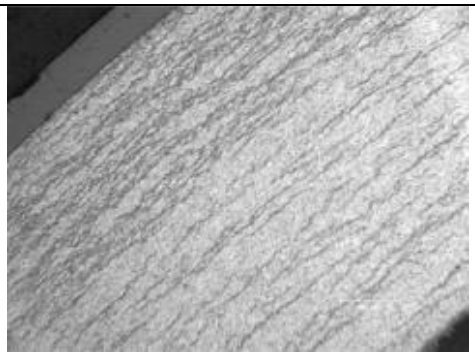

Zirlo™, 67 GWd.t^{-1}
[AND 2012]

Figure 11: Micrographs of irradiated cladding showing the hydrides distribution in the cladding thickness

2.2 Reprocessing of spent fuel

2.2.1 Consequences of transportation on the condition of cladding

After operation, the spent fuel assemblies are unloaded in the reactor pool. During the wet storage, at about 50°C, the cladding keeps its state of end-of-life in reactor.

However, during transportation in dry cask or during dry storage, the cladding is subjected to a thermo-mechanical history which may lead to:

- a thermal creep due to the tangential tensile stress induced by the internal pressure of the rod [RAS 2002];
- a partial or full recovery of irradiation defects [EPR 2006];
- a dissolution of existing hydrides and a possible redistribution of hydrogen axially and in the thickness of the cladding in the combined effect of temperature and hydrogen gradients;
- a precipitation of hydrides during cooling, their size and reorientation depending on the cooling rate and the stress state in the cladding [BIL 2013, MIN 2013, MIN 2014].

Thus, the dry transportation in cask of spent fuel to a reprocessing plant is an operation which could affect the distribution of hydrides in the cladding, and consequently in the hulls. The partial recovery of irradiation defects and a possible redistribution of hydrides are the main processes to consider for the characterization of hulls, in the framework of this study.

It was seen that after irradiation in reactor, the hydrides are distributed in the rod cladding heterogeneously in both height (depending on the stage) and in thickness, most hydrides being oriented circumferentially. During transportation, the fuel rods reach a temperature above

350°C. Hydrogen precipitated as hydride is redissolved in the cladding. During cooling, hydrogen precipitates again in the form of hydride, but in stress conditions different from those occurring in reactor. The hoop stresses induced in the cladding by the internal pressure in the fuel rod may then result in the formation of radial hydrides [PIC 1972, KAW 1974, COL 1985, EIN 2005, BIL 2013, MIN 2014]. In the case where radial hydrides appear, the ductility of the material decreases; the embrittlement becomes itself an indicator of the hydrides reorientation [HSU 2011].

The radialization of hydrides depends mainly on three parameters:

- the temperature: the radialization threshold is all the lower than the temperature before cooling is high;
- the hydrogen content of the cladding;
- the internal pressure inside the rod: the fraction of radial hydrides increases with the stress, that is to say with the internal pressure in the rod. So the phenomenon has a tendency to affect the claddings of highly irradiated fuel rods.

Note that the parameters temperature and internal pressure in the rod are coupled in the creep phenomenon of cladding. Indeed, during transportation, the creep deformation of cladding (T > 350°C) involves a decrease of the pressure in the rod and thus the stress in the cladding as well. Reorientation of hydrides should thus be limited.

For illustration, Figure 12a shows the hydrides morphology observed in Zircaloy-4 after a thermo-mechanical history causing a radialization of hydrides. Similar observations were made for other cladding alloys, they are in a stress relief annealed or recrystallized condition: Zircaloy-2 [AOM 2007], Zirlo™ [BUR 2010, BIL 2013] (Figure 12b), Zr-Nb [SIN 2004, MIN 2014].

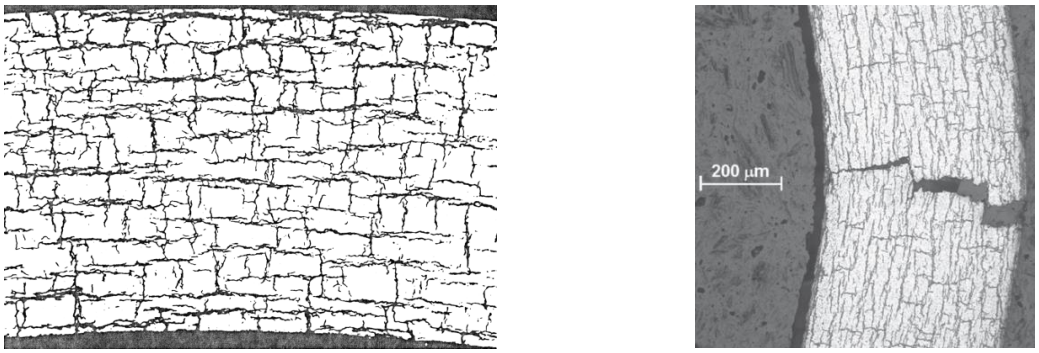

a) **b)**

Figure 12: Examples of redistribution of hydrides observed: a) in Zircaloy-4 after cooling from 300°C under a stress of 140 MPa [PIC 1972]; b) in Zirlo™ with 630 ± 110 ppm H [BIL 2013].

2.2.2 From spent fuel claddings to hulls waste

At the reprocessing facility, after being discharged from the transportation cask (Figure 13), the spent fuel assemblies are first stored in the deactivation pool. After a few years (one to four), they are sheared in order to dissolve the fuel pellets, the essential operation of the reprocessing process (Figure 14).

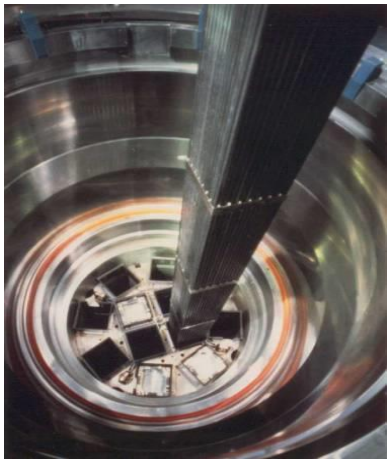

Figure 13: Dry unloading of spent fuel at the reprocessing plant (Areva NC photograph)

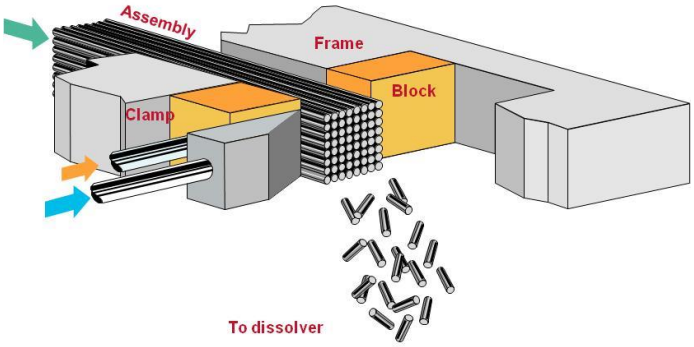

Figure 14: Principle of mechanical shearing treatment of fuel assemblies at the La Hague (Areva NC picture)

The shearing of the entire assembly is provided by a hydraulically actuated blade; the operation is made dry. The shears cut PWR and BWR fuel assemblies of all sizes. The assembly is thus cut up into pieces of average length of 35 mm that feed the dissolver (Figure 15) [BOU 2000]. Boiling concentrated nitric acid solution is used to dissolve as fully as possible the nuclear matter contained in the pieces. The cladding pieces – the hulls - are not attacked. They are rinsed with acid, then with water at ~ 80°C and then transferred to the packaging plant of hulls waste. In principle, these steps do not affect the retention of the zirconia layers, or the corrosion resistance of the hulls[2].

[2] Corrosion tests of zirconium in nitric acid fluorine-free solutions, at temperatures near the boiling point indicate that general corrosion rates are less than 1 µm.y^{-1}.

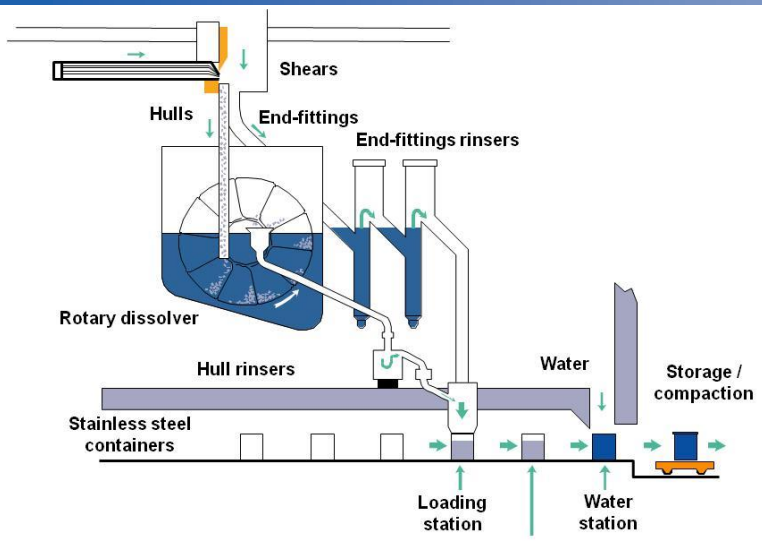

Figure 15: Schematic diagram of the dissolver of the reprocessing facilities at La Hague (Areva NC picture)

Figure 16 schematically shows the aspect of hulls at this stage and the distribution and location of radionuclides in the cladding. Three main types of radionuclides may be distinguished:

- activation products formed under neutron flux and distributed in the mass;
- fission products implanted by recoil fission on the internal surface of cladding and those contained in the deposits and residues after the reprocessing operations;
- actinides that could not be recovered by dissolving and rinsing operations.

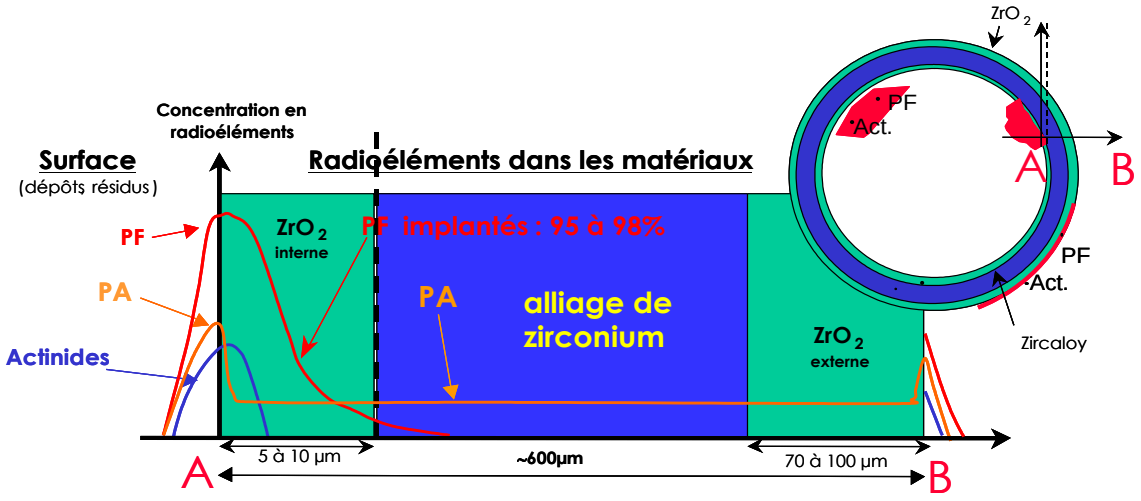

Figure 16: Schematic representation of the location of radionuclides in hulls [AND 2005].

In the La Hague reprocessing plant, the structural waste from spent fuel (hulls, end-pieces, spacers, springs) were cemented until August 1995. Hulls and end-pieces produced after this date are press compacted in *galettes* (Figure 17). Press compacting induces mechanical deformations that may cause fragmentation of hulls. Moreover the radialization of hydrides in highly irradiated Zircaloy and Zirlo^{TM} claddings could likely promote the production of small metallic fragments.

Figure 17: On the left, hulls and *galette* of press compacted hulls and end-pieces; on the right, stack of *galettes* of press compacted waste in CSD-C waste package (Areva NC photographs)

3 Origin and inventory of ^{14}C in fuel rod cladding

3.1 Radioactive origin of ^{14}C

^{14}C is a pure beta emitter (decay in ^{14}N) of low energy (average energy: 49.44 keV, maximum energy: 156.47 keV). Its half-life is 5,730 years. Its specific activity is 1.65 10^{11} $Bq.g^{-1}$ [IRS 2001].

^{14}C is mainly formed by thermal neutron activation of ^{14}N and ^{17}O in LWRs according to the transmutation reactions $^{14}N(n,p)^{14}C$ and $^{17}O(n,\alpha)^{14}C$ (Table 4). Other reactions (neutron activation of ^{13}C, ternary fissions) have a negligible or inconsequential impact in water reactors, i.e. the ^{14}C production rate per ppm of ^{13}C is lower than the ^{14}C production rate per ppm of nitrogen by a factor of approximately 10^{-5} [EPR 2010]. The neutron cross-sections for these three reactions are shown in Figure 18. Table 5 indicates the respective importance of

the two major reactions in various calculations of the ^{14}C production in the materials of the fuel assembly (UO_2 fuel and metal structures).

Table 4: Reactions forming ^{14}C in the LWR [MAG 2007, EPR 2010]

Neutron induced reaction	Isotopic abundance of precursor element (%)	Cross-sections (barn)	
		thermal	resonance
^{14}N (n, p) ^{14}C	99.632	1.82	0.818
^{17}O (n, α) ^{14}C	0.038	0.235	0.106
^{13}C (n,γ) ^{14}C	1.07	$1.37\ 10^{-3}$	$5.93\ 10^{-4}$

Table 5: Production of ^{14}C (in $GBq.GWe^{-1}.y^{-1}$) in LWR fuel assemblies [EPR 2010]

	Precursor	Bonka *et al.* [BON 1974]	Kelly *et al.* [KEL 1975]	Fowler *et al.* [FOW 1976]	Davis [DAV 1977]	Hayes *et al.* [HAY 1977]
BWR	^{14}N	477	403	666	426	784
	^{17}O	311	100	148	122	403
PWR	^{14}N	451	403	666	-	281
	^{17}O	263	100	148	130	148

In the claddings themselves, the ^{14}C production results very predominantly from the activation of nitrogen as an impurity element in zirconium alloys; the reaction $^{17}O(n,\alpha)^{14}C$ is very minor, the majority of this reaction for the fuel assembly (see Table 5) coming from the important contribution of the oxide UO_2.

Data provided by EDF [BOR 2008], established by using the code Apollo-Pépin-Darwin developed by the CEA, show, for an UO_2 fuel irradiated to 45 $GWd.t_U^{-1}$, that the cladding and the fuel pellet contribute 50 % each to the ^{14}C production. The origin of ^{14}C for both materials is detailed in Table 6.

Table 6: Origins of ^{14}C in an UO_2 (3.70 % ^{235}U) PWR fuel assembly irradiated to 45 $GWd.t_U^{-1}$ [BOR 2008]

	^{14}N	^{17}O	^{13}C
In UO_2 (11.9 % O ; 7.5 ppm N ; 15 ppm C)	36.9 %	63.1 %	< 0.01 %
In the cladding ($M5^{TM}$ alloy) (1,700 ppm O ; **80 ppm N** ; 120 ppm C)	99.8 %	0.2 %	< 0.01 %
For the fuel assembly	69 %	31 %	-

However, it may be observed that these results tend to overestimate the contribution of nitrogen in so far as the calculations were carried out for the maximum limit of 80 ppm nitrogen imposed by specifications. Indeed, it was reported above (Table 3) that the nitrogen

content in the M5^{TM} alloy is actually 27 ± 4 ppm (34 ± 10 ppm for Zircaloy-4). However, these calculations do not take into account the contribution of the oxygen supplied by the coolant water (transmutation of ^{17}O in H_2O) to form the outer layer of zirconia.

Balances of inventories carried at the spent fuel reprocessing plant confirm that the ^{14}C is distributed in an approximately equivalent way between the fuel itself and the cladding. Indeed, 40 to 45 % of the ^{14}C inventory are released during the dissolution step of the fuel, and 55 to 60 % remain in the hulls and other metal waste [IAE 2004].

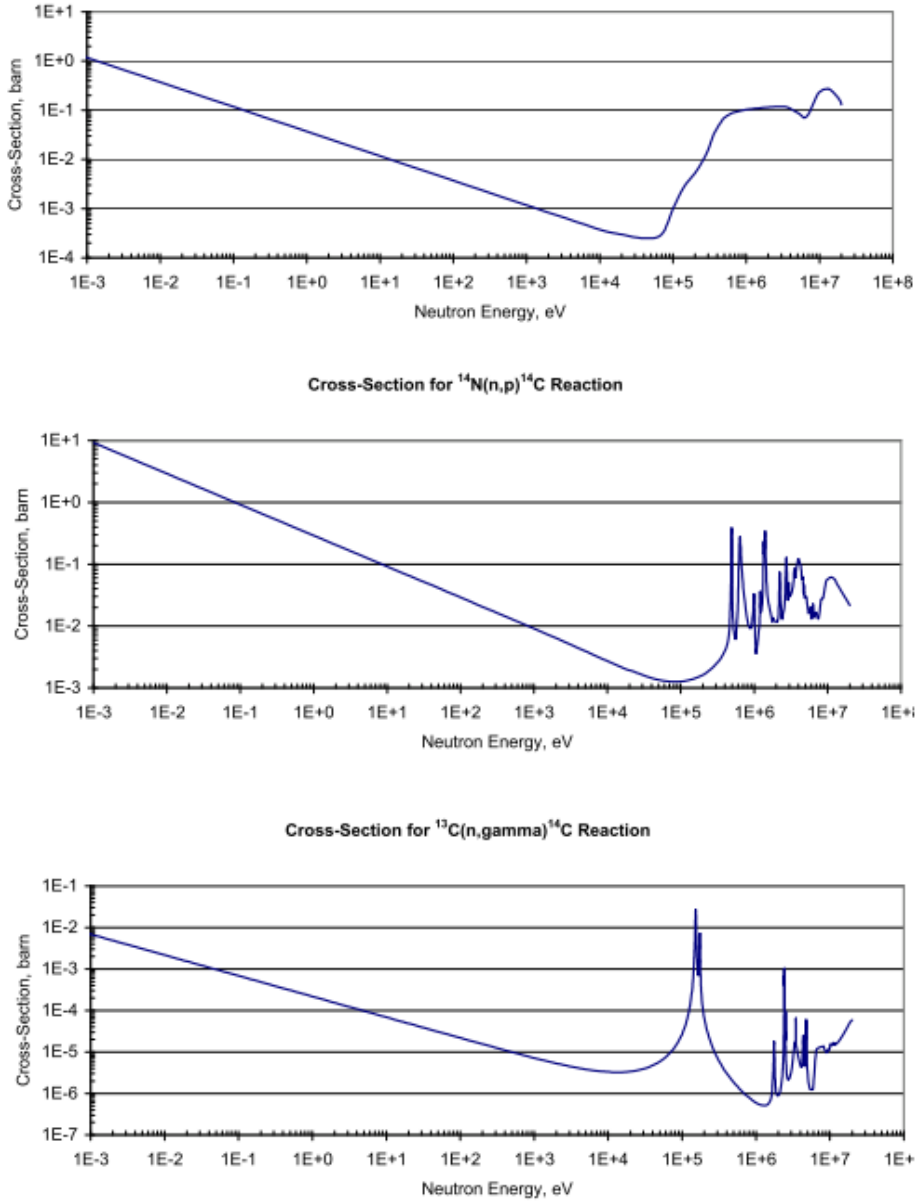

Figure 18: Cross sections for $^{17}O(n, \alpha)^{14}C$, $^{14}N(n, p)^{14}C$ and $^{13}C(n,\gamma)^{14}C$ reactions; ENDF, National Nuclear Data Center, Brookhaven National Laboratory [EPR 2010]

3.2 ^{14}C inventory in hulls

3.2.1 Distribution of ^{14}C between the metal and the oxide layer

Using the code CESAR, the CEA determined the inventory of activation products present in the Zircaloy-4 cladding of a PWR 900 MWe assembly irradiated to 45 $GWd.t_U^{-1}$: for ^{14}C, approximately 80 % are found in the Zircaloy metal, the remaining 20 % being in the outer oxide layer (100 µm thick) [HÉL 2004, AND 2005].

Tanabe *et al.* (RWMC) measured separately the ^{14}C inventory in the non-oxidized metal cladding and in the zirconia layer [YAM 1999, TAN 2007]. For a PWR fuel irradiated to 47.9 $GWd.t_U^{-1}$, they found that the oxide layer (the thickness of which would be ~ 55 µm according to the empiric law given by RWMC in [SAK 2013]) contains 17 % of the ^{14}C inventory. For a BWR fuel irradiated to 39.4 $GWd.t_U^{-1}$, the thickness of the external oxide layer is 20 µm and 96 % of the ^{14}C inventory is found in the unoxidized metal. The results thus show that, logically, the amount of ^{14}C in the oxide increases with its thickness, that is to say with the burn-up and that, in a strongly irradiated PWR fuel, zirconia may contain up to 20% of the ^{14}C inventory of the cladding. We will return to this result in the following paragraph.

3.2.2 Inventory of ^{14}C

The determination of the amount of ^{14}C produced in the spent fuel claddings has been carried out either by calculation, using codes like ORIGEN or CESAR, or by experimental measurement. Two main methods for measuring the ^{14}C content in the claddings or hulls have been carried out:

- combustion of a sample in an oxygen or air atmosphere; CO_2 is collected and the ^{14}C measured by beta liquid scintillation counting. Guenther *et al.* estimate the uncertainty of this method to ± 5.6 % [GUE 1994];
- dissolution of a sample by acid, and analysis of ^{14}C in the solution and the off-gas, after an eventual sodium hydroxide trapping. ^{14}C activity is determined by liquid scintillation counting. The method was improved by Takahashi *et al.* for the analysis of ^{14}C inventories and ^{14}C release in aqueous solutions (see § 6.3) [TAK 2013].

Bleier *et al.* [BLE 1987, NEE 1997] have measured the ^{14}C activity of claddings irradiated in German reactors (KWU): the Zircaloy-2 cladding (nitrogen content: 35 ppm) of a BWR fuel irradiated to 22.4 $GWd.t_U^{-1}$ contained 23 $kBq.g^{-1}$ of ^{14}C; the Zircaloy-4 cladding (nitrogen content: 40 ppm) of a PWR fuel irradiated to 35.7 $GWd.t_U^{-1}$ contained 17 $kBq.g^{-1}$.

Van Konynenburg (LLNL) reported the following values calculated for Zircaloy cladding of PWR fuel irradiated to 33 $GWd.t_U^{-1}$ and BWR fuel irradiated to 27.5 $GWd.t_U^{-1}$: 0.18 and 0.38 $Ci.t_U^{-1}$ respectively [VAN 1991]. If we assume that the ratio of the mass of heavy metal to this one of Zircaloy is similar on the concerned assemblies and on the AFA-2G assembly (cf. § 2.1), i.e. 273 kg of Zircaloy by t_U, these activities are equivalent to ~ 24 $kBq.g^{-1}$and ~ 52 $kBq.g^{-1}$ of cladding respectively.

Einziger, from Pacific Northwest Laboratory (PNL), sought to evaluate the amount of ^{14}C released from the claddings of the fuel rods where they oxidize in dry storage in the presence of air. He retained the following values measured by Guenther *et al.* [GUE 1994] on cladding of fuel irradiated to 33 $GWd.t_U^{-1}$ (PWR) and 27.5 $GWd.t_U^{-1}$ (BWR): 0.4 to 0.9 $\mu Ci.g^{-1}$ for the first, 0.4 to 1.4 $\mu Ci.g^{-1}$ for the latter [EIN 1991].

Using the code CESAR, the CEA calculated the amount of ^{14}C produced in the 125.6 kg of Zircaloy-4 cladding of an assembly AFA-2G 900 MWe irradiated to 50 $GWd.t_U^{-1}$; for a content of 34 ppm nitrogen it is 2.51 10^{-2} g at 10 years [MAR 2003], which corresponds to a mass of 2 10^{-7} g ^{14}C per gram of cladding, or to a ^{14}C specific activity of 33 $kBq.g^{-1}$.

Using the code Apollo2-Darwin developed by the CEA, EDF calculated the amount of ^{14}C produced in Zircaloy-4 or M5^{TM} cladding of an UO_2 fuel (4.95 % ^{235}U) irradiated to 70 $GWd.t_U^{-1}$ and cooled 3 years: calculated for a maximum content of 80 ppm nitrogen (0.125 % O and 200 ppm C), it is 96.7 $kBq.g^{-1}$ [LAU 2003]. In a first approximation, the ^{14}C activity corresponding to a content of 40 ppm nitrogen would be half of this value, that is to say 48.3 $kBq.g^{-1}$.

Tanabe *et al.* (RWMC) measured separately the ^{14}C inventory in the non-oxidized metal of cladding and in the zirconia layer [YAM 1999, TAN 2007, TAK 2013]. Hulls taken from Zircaloy cladding of two fuel rods were thus characterized: a PWR fuel irradiated to 47.9 $GWd.t_U^{-1}$ (nitrogen content of cladding: 47 ppm) and a BWR fuel irradiated to 39.4 $GWd.t_U^{-1}$ (nitrogen content of cladding: 34 ppm). The reported inventory and ^{14}C distribution are shown in Table 7. Comparison of ^{14}C inventories in metal and oxide layer shows that the inventory in oxide layer is roughly twice its concentration in the base metal, in both PWR and BWR cases. The activation calculation results suggest that the $^{17}O(n,\alpha)^{14}C$ reaction would justify this inventory increase into the oxide layer, in addition to the $^{14}N(n,p)^{14}C$ reaction in which the nitrogen concentration was assumed to be the same as in the base Zircaloy [SAK 2013]. In the case of PWR hull, the measurement result and the ORIGEN calculation result are similar [TAN 2007].

Table 7: Measurement results of RWMC [TAN 2007]: distribution of ^{14}C in metal and oxide layer of irradiated Zircaloy claddings

Origin of cladding	Thickness (µm)		^{14}C activity (kBq.g^{-1})		
	Metal cladding	Oxide layer	Metal cladding	Oxide layer	Ratio oxide/metal
PWR, 47.9 GWd.t_U^{-1}	-	-	30	44 (59)*	1.5 (2.0)*
BWR, 39.4 GWd.t_U^{-1}	752	20 outer	19	33 (44)*	1.7 (2.3)*

* in terms of metal weight (M_{ZrO2}/M_{Zr} = 1.35)

More recent results were published by RWMC [SAK 2013], which cover a large amount of hull and end-piece wastes generated from the Rokkasho reprocessing plant in Japan and corresponding to 32,000 t_U (16,000 t_U for each reactor type, BWR and PWR). Table 8 shows the results of ^{14}C inventory calculations using the code ORIGEN 2.2. Values of zirconia layer thicknesses selected for the study were taken from a linear relationship between maximum

Table 8: Calculation results of RWMC [SAK 2013]: inventory of ^{14}C in hulls (metal and oxide) for BWR and PWR fuel assemblies

Fuel type	Burn-up (GWd.t^{-1})	Zircaloy (tons)	Oxide thickness (µm)	^{14}C inventory (Bq)		^{14}C activity	
				Hull metal	Hull oxide	Hull (kBq.g^{-1})	% oxide
BWR							
New 8x8	29.5	84.4	66	$1.85\ 10^{12}$	$1.18\ 10^{11}$	23.3	6
STEP I	33.0	188.9	39	$4.91\ 10^{12}$	$1.78\ 10^{11}$	26.9	3
STEP II	39.5	1576.1	10	$4.37\ 10^{13}$	$3.95\ 10^{11}$	28.0	1
STEP III	45.0	4264.5	6	$1.27\ 10^{14}$	$7.90\ 10^{11}$	30.0	1
PWR							
14x14, 2 loops	31.5	116.9	34	$2.93\ 10^{12}$	$1.82\ 10^{11}$	27.9	10
15x15, 3 loops	32	50.5	35	$1.29\ 10^{12}$	$8.15\ 10^{10}$	28.5	10
17x17, 3 loops	31	49.5	34	$1.21\ 10^{12}$	$8.11\ 10^{10}$	27.7	12
17x17, 4 loops	31	91.9	34	$2.25\ 10^{12}$	$1.51\ 10^{11}$	27.7	12
14x14, 2 loops	41	405.5	45	$1.14\ 10^{13}$	$9.55\ 10^{11}$	31.4	10
15x15, 3 loops	43	240.4	47	$7.12\ 10^{12}$	$6.31\ 10^{11}$	33.1	10
17x17, 3 loops	40	511.3	44	$1.39\ 10^{13}$	$1.24\ 10^{12}$	30.8	12
17x17, 4 loops	43	770.6	47	$2.27\ 10^{13}$	$2.20\ 10^{12}$	33.4	12
14x14, 2 loops	51	379.0	58	$1.17\ 10^{13}$	$1.31\ 10^{12}$	34.5	11
15x15, 3 loops	49	247.3	55	$7.51\ 10^{12}$	$8.10\ 10^{11}$	33.9	10
17x17, 3 loops	49	427.7	55	$1.26\ 10^{13}$	$1.48\ 10^{12}$	33.4	12
17x17, 4 loops	50	662.9	56	$1.99\ 10^{13}$	$2.40\ 10^{12}$	34.1	12

oxide thickness and burn-up for each fuel type. The ^{14}C activities deduced from the inventories of hulls (metal and oxide) for each fuel type are between 23.3 and 34.5 kBq.g^{-1}. As expected, we note that they depend on the burn-up. The oxide layer contains a fraction of inventory that does not exceed 12 %, but we also note that the calculations were made with relatively moderate oxide thicknesses, not exceeding 60 µm. As a result of the difference of the estimated oxide thickness between BWRs and PWRs, the ^{14}C inventory is lower in BWR oxide than in PWR oxide.

All the results presented above are summarized in Table 9 and the ^{14}C activities in hulls resulting of calculations or measurements are plotted as a function of the burn-up in Figure 19.

Table 9: Results of calculations and measurements of ^{14}C activity into the Zircaloy claddings of PWR and BWR spent fuel.

Reactor	Burn-up (GWd.t^{-1})	N content in cladding (ppm)	Result *	^{14}C activity (kBq.g^{-1} of hull **)	Ref.
BWR	22.4	35	m	23	[BLE 1987]
	~ 27.5	40 ?	c	52 ***	[VAN 1991]
	~ 27.5	-	m	15 to 52	[EIN 1991]
	39.4	34	m	19 (metal)	[TAN 2007]
	29.5	40	c	23.3	[SAK 2013]
	33.0	40	c	26.9	[SAK 2013]
	39.5	40	c	28.0	[SAK 2013]
	39.7	-	m	17.4 (metal)	[YAM 2013]
	45.0	40	c	30.0	[SAK 2013]
PWR	~ 28	-	m	17	[SMI 1993]
	35.7	40	m	17	[BLE 1987]
	~ 33	40 ?	c	24 ***	[VAN 1991]
	~ 33	-	m	15 to 33	[EIN 1991]
	50	34	c	33	[MAR 2003]
	70	40	c	48.3 ***	[LAU 2003]
	47.9	47	m	30 (metal)	[TAN 2007]
	47.9	47	c	40 (metal)	[TAN 2007]
	31.5	40	c	27.9	[SAK 2013]
	32	40	c	28.5	[SAK 2013]
	31	40	c	27.7	[SAK 2013]
	31	40	c	27.7	[SAK 2013]
	41	40	c	31.4	[SAK 2013]
	43	40	c	33.1	[SAK 2013]
	40	40	c	30.8	[SAK 2013]
	43	40	c	33.4	[SAK 2013]
	51	40	c	34.5	[SAK 2013]
	49	40	c	33.9	[SAK 2013]
	49	40	c	33.4	[SAK 2013]
	50	40	c	34.1	[SAK 2013]

* m = measured; c = calculated
** unless otherwise specified
*** value deduced

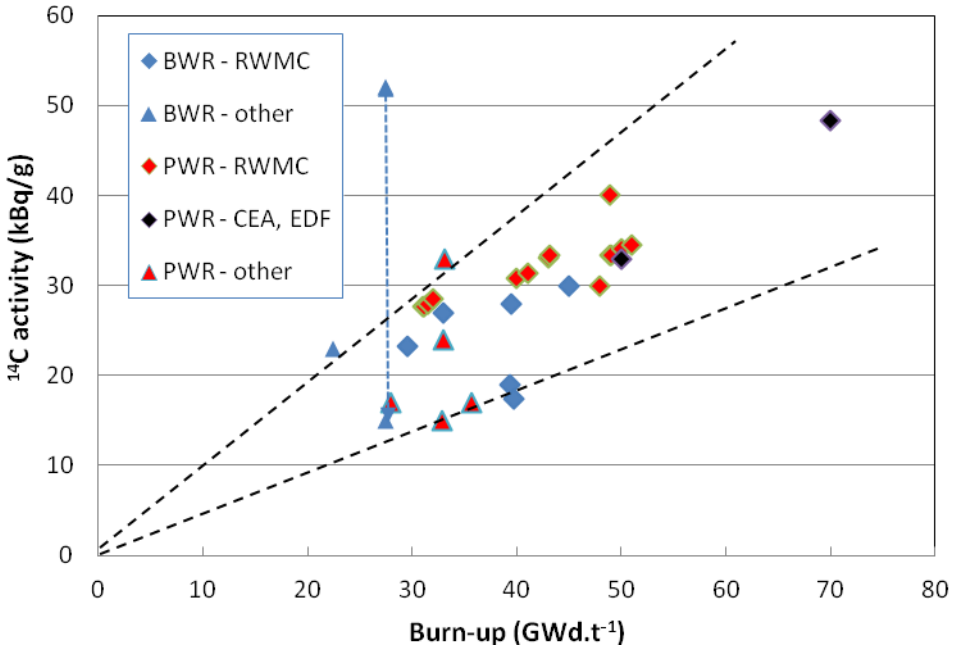

Figure 19: ^{14}C activity concentrations in BWR and PWR fuel Zircaloy claddings (nitrogen content ~ 40 ppm) as a function of the burn-up.

The set of data is between the lines of slope 0.5 and 1.0 kBq/g.GWd.t^{-1}. As expected, it does not show significant difference between the cladding of BWR and PWR fuel. These values are lower than those reported in a previous study, which were based on the older inventory data [BOU 2003].

One can try to normalize the production of ^{14}C in the cladding taking into account the concentration of nitrogen in the alloy. With the concentrations of nitrogen actually measured in the Zircaloy, the results reported in Table 9 lead to a value of the power-related ^{14}C production of 1.9 ± 0.4 GBq/GWy.ppm N (the calculation was made based on a simplifying assumption of 273 kg of Zircaloy for 1 t_{HMi}, whatever the type of reactor; cf. § 2.1).

3.3 Chemical forms of ^{14}C in the hulls

It has been shown that the ^{14}C radiologic activity in spent fuel claddings and in hulls is distributed mostly in the mass of the alloy (> 80 %) and in lesser quantities in the oxide layers (< 20 %). Because the impurities (nitrogen) or alloying elements (oxygen) in the zirconium alloys are uniformly distributed, and the temperature gradient in the cladding during in-reactor irradiation is relatively low, as well as the associated solid-state diffusion rates, the activation products would be expected to be likewise uniformly distributed on a microscopic scale [JOH 2002]. Thus, as a first approach, it is believed that ^{14}C is homogeneously

distributed in the bulk of material, in the metal and in the oxide, although there is evidence that ^{14}C has a higher concentration in the oxide layer than in the underlying alloy [YAM 1999].

However we have also seen that ^{14}C is mainly formed from ^{14}N and ^{17}O. These two elements occupy specific positions into the structure of the alloy and the zirconia lattice.

In the bulk of the cladding, ^{14}C is probably present in solution in the matrix of zirconium or/and in carbide precipitates [SMI 1993, IAE 1998, AOM 2007]. Kaneko *et al.* [KAN 2002] compared the chemical forms of carbon released in alkaline solutions by a zirconium (non-activated) powder, containing 0.02 wt % C, and zirconium carbide powder (see § 6.3); they deduced that one of the chemical forms of carbon in metals could indeed be a carbide. It should be noted, however, that stable carbon and ^{14}C could have different chemical environments: either bound as interstitial solid solution by neutron activation of ^{14}N or as substitutional solid solution by isotopic exchange with carbide from non-activated material.

The oxide itself, consisting of sub-stoichiometric zirconia, is filled with point defects. It is likely that ^{14}C is trapped in these defects which undoubtedly play an important role. But one might think that the ^{14}C formed from ^{17}O of the oxide lattice is not bound into the oxide matrix in the same way as this one formed from nitrogen impurity, in solid solution in ZrO_2 when the zirconium matrix is oxidized [AOM 2007]. The experiments on thermally-activated release (see § 4.2.2) suggest that there at least two types of sites occupied by the ^{14}C atoms in the oxide layer: ^{14}C adsorbed on the surface of oxide, which is observed to desorb first, and ^{14}C occluded within the zirconium oxide layer that requires more time for release [SMI 1993].

Inspite of these indications, we conclude that there is a current lack of reliable data on the chemical state of ^{14}C in the metal and in the zirconium oxide layer. A modelling approach at the atomic scale would undoubtedly be a valuable aid to identify the ^{14}C insertion sites in the metal and in the oxide.

4 Release mechanisms of ^{14}C. Thermal release of ^{14}C

4.1 General outline on the release mechanisms of ^{14}C

The mechanisms and the rate of ^{14}C release from hulls depend on different processes. It is expected to be controlled in large part by the uniform corrosion rate of Zircaloy, the diffusion rate of ^{14}C from zirconia oxide layers and/or the dissolution rate of zirconia oxide layers, at the time of the contact between the hulls and the infiltrating water under the repository

conditions. Dissolution of zirconia layers and corrosion of Zircaloy are discussed further below.

Regarding the radionuclides contained in the mass of the zirconium alloys, it can be considered as a first approach that their release is congruent with the corrosion of the alloy. Thus it is assumed that diffusion of radionuclides in solid phase in the metal at the temperature of disposal (between 20 and 50°C for the most exothermic ILW packages) is not significant and that the radionuclides release is only due to the alloy corrosion. This hypothesis of a congruent release of radionuclides with the metal corrosion may lead to an overestimate of their release. Indeed, a significant fraction of the radiological inventory is likely to end up "trapped" in the zirconia formed during metal corrosion.

Other mechanisms may be possibly involved and explain that some ^{14}C might be lost from cladding or hull waste before disposal and leaching of waste in repository:

- mechanisms related to a thermal release and diffusion of ^{14}C;
- mechanisms related to the mobile character of some form of ^{14}C within the zirconia layers, as far as the layered structure of oxide results in multiple reservoirs or inventories of ^{14}C (^{14}C adsorbed, ^{14}C physically or chemically occluded, ^{14}C organic volatile or dissolved species).

The release mechanisms in aqueous media will be investigated in the next chapter (Chapter 5). The purpose of this one relates exclusively to the influence of the temperature and to identify the steps during waste management that could lead to a thermal release of activity.

4.2 Diffusion of carbon in Zr alloys and ZrO_2. Thermal release of ^{14}C

4.2.1 Diffusion of carbon in Zr alloys and in zirconia oxide layer

Agarwala *et al.* [AGA 1975] determined the diffusion of ^{14}C in Zr alloys above 873 K, using the residual activity technique. For their part, Smith *et al.* investigated the diffusion of ^{14}C on both pre- and post-transition oxide cladding samples in both argon and air, in the range 373 – 623 K [SMI 1993]. These authors find differences in the ^{14}C release mechanisms in air versus argon: in the argon environment, the ^{14}C release shows a small and lower temperature sensitivity than in air. The initial release observed under both air and argon atmospheres suggests an initial desorption of $^{14}CO_2$ from the surface. Both surface desorption and bulk diffusion may be rate-controlling at different times. At later times, desorption becomes less

important while diffusion becomes the dominant rate-controlling step. The samples with post-transition oxide (8-20 µm thick) generally released more ^{14}C than the samples with pre-transition oxide (3-8 µm thick).

The values of the diffusion coefficients reported in these two studies are given in Table 10 and represented on an Arrhenius plot in Figure 20. This figure shows that the ^{14}C diffusivities in the three Zr alloys are of the same order of magnitude, suggesting that carbon atoms while diffusing come across almost similar surroundings in the three materials [AGA 1975]. It shows that the diffusivities of carbon in ZrO_2 layers are considerably higher than those in the Zr alloys. For example, at 300°C (573 K), the calculated diffusion coefficient is about 5 10^{-22} $m^2.s^{-1}$ for Zircaloy, compared to 2.5 10^{-14} $m^2.s^{-1}$ for post-transition zirconia layer.

Table 10: Diffusion coefficients D = Do exp (- Ea/RT) of ^{14}C in Zr alloys and ZrO_2 (tests in air)

	Temperature range (K)	Do ($m^2.s^{-1}$)	Ea ($kJ.mol^{-1}$)	Ref.
Zr alloys				
Zr	873 - 1123	(2.00 ± 0.37) 10^{-7}	151.59 ± 2.51	[AGA 1975]
Zircaloy-2	873 – 1043	(1.41 ± 0.32) 10^{-7}	158.99 ± 3.14	[AGA 1975]
Zr-2.5Nb	753 - 873	(4.68 ± 0.88) 10^{-7}	159.98 ± 2.97	[AGA 1975]
Zirconia oxide layer				
Pre-transition ZrO_2	373 – 623	6.73 10^{-6}	103 ± 23	[SMI 1993]
Post-transition ZrO_2	373 - 623	3.30 10^{-7}	78 ± 12	[SMI 1993]

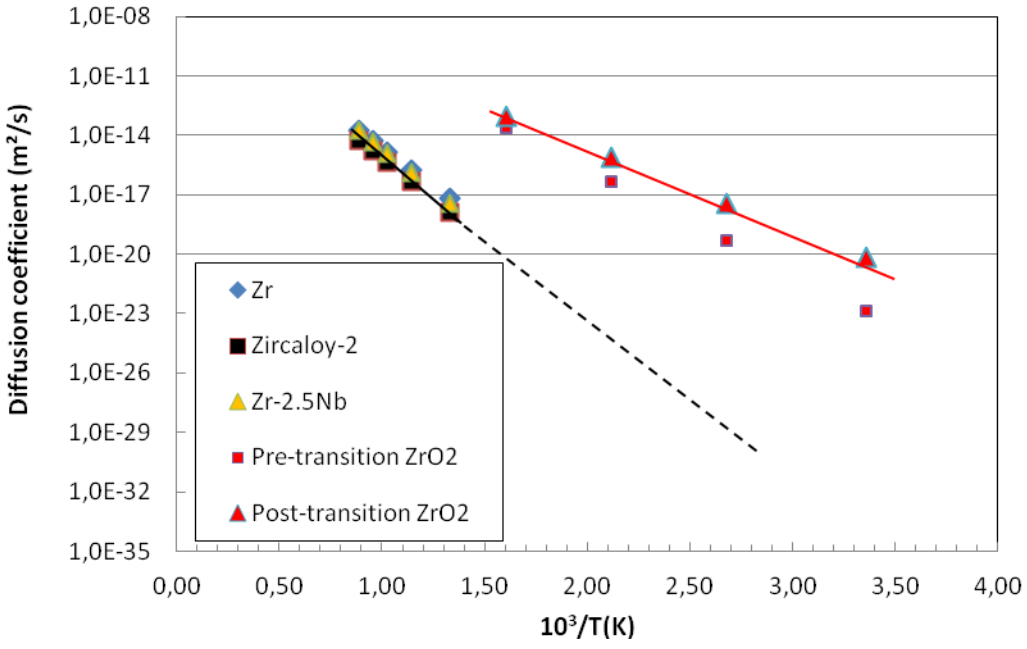

Figure 20: Arrhenius plot of diffusion coefficients of ^{14}C in Zr alloys [AGA 1975] and ZrO_2 oxide layers (pre- and post-transition oxide cladding) [SMI 1993]

4.2.2 Thermally-activated release of ^{14}C

The management of spent fuel comprises steps during which it remains at a high enough temperature that the question arises of a possible thermally-activated release into the surrounding atmosphere of ^{14}C contained in the cladding, at least from the zirconia layer. In addition, the very long periods involved in geological disposal also raise the question of a possible release of ^{14}C into the near-field of a repository by thermal diffusion.

4.2.2.1 During transportation and dry storage of fuel assemblies

The steps in the back-end of fuel cycle at a relatively high temperature are the following:

- transportation from the nuclear power plant (NPP) to the reprocessing plant. This operation is classically carried out in dry canister under inert atmosphere and lasts typically a week for spent fuel discharged from the French PWRs and transported to La Hague;
- dry storage on the sites of NPPs, under inert atmosphere, for some time waiting for their further management.

During transportation and dry storage, at least during the early years, the surface temperature of the rods may be as high as 300 to 350°C. But, as shown by Smith *et al.*, the release under an inert atmosphere may be less sensitive to temperature than in air, if the oxidation in air is important for release, or if natural CO_2 in the air facilitates release by exchanging with adsorbed $^{14}CO_2$ on the cladding [SMI 1993].

To give some orders of magnitude, let us calculate the characteristic term $(D.t)^{½}$ at 300°C as function of time for the diffusivity of ^{14}C in Zircaloy and in post-transition oxide layer (Table 11). It is thus observed that a transportation operation of spent fuel is likely to affect entire inventory present in the oxide layer (recall that the maximum thickness of the zirconia layer on the cladding of spent fuel does not exceed 100 µm in principle). In contrast, the ^{14}C dissolved or precipitated in the metal can be considered as immobile during transportation of spent fuel as well as for dry storage.

For safety case considerations, some authors have made estimates of the rate of ^{14}C release in dry storage facilities for spent fuel or within the disposal concept that was envisaged in Yucca Mountain. Some of their results are given in Table 12. The estimated releases can be an

important fraction of the ^{14}C present in the cladding, depending on the temperature and its duration.

Table 11: Values of the characteristic term $(D.t)^{½}$ (in µm) at 300°C as function of time for Zircaloy and oxide layer

Time	Zircaloy	Oxide layer
1 week	0.02	120
1 year	0.12	880
10 years	0.38	2,800

Table 12: Some data of ^{14}C release from irradiated cladding after keeping in air

Temperature (°C)	Duration	^{14}C release (%)	Ref.
200	4 months	1.5	[KOP 1990]
275	1 month	1.0	[VAN 1985]
275	8 h	3	[SMI 1993]
400	4 months	25	[KOP 1990]

Releases of ^{14}C also have been detected in dry storage cask tests by analysis of the cask cover gas and the highlighting of very low concentrations of $^{14}CO_2$ and ^{14}CO [EPR 1989, STE 1996, EPR 2000]. Releases appeared to be lower than would be predicted from the results of Smith *et al*. Various reasons may explain this discrepancy, in particular the fact that dry storage of LWR spent fuel is carried out under inert atmosphere (usually helium).

Release of ^{14}C was also highlighted in wells of a dry storage facility where naval nuclear fuel was loaded; the spent fuel was weakly irradiated compared to fuel power generating reactors [BON 1992].

4.2.2.2 Under repository conditions

The results given by Smith and Baldwin [SMI 1993] lead to values of the apparent diffusion coefficient of ^{14}C in the post-transition zirconia equal to $3.85\ 10^{-21}\ m^2.s^{-1}$ and $7.58\ 10^{-20}\ m^2.s^{-1}$ to 20°C and 50°C respectively. The variations of the term $(D.t)^{½}$, calculated for these two temperatures, are shown as a function of time in Figure 21. It can be concluded that the thermal diffusion is a phenomenon that is *a priori* to be taken into account in the process of release of ^{14}C in disposal. In the first times, when the hulls packages are still warm, the term $(D.t)^{½}$ is not negligible (e.g. ~ 5 µm for a duration of 10 years at 50°C).

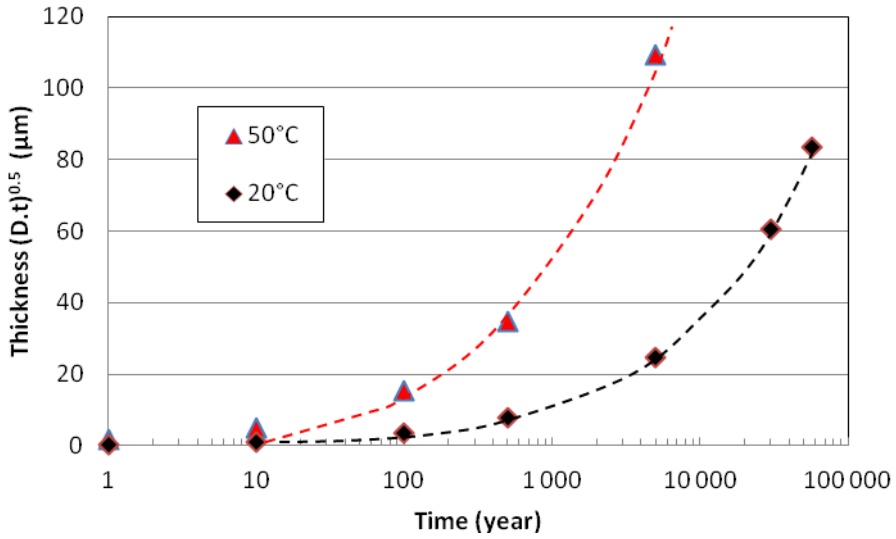

Figure 21: Characteristic term $(D.t)^{½}$ for the diffusion of ^{14}C in post-transition ZrO_2 at 20 and 50°C, according to the data of Smith and Baldwin [SMI 1993]

5 Environment assisted release of ^{14}C

The ^{14}C inventory being located in both the oxide layers (≤ 20 %) and the metal of hulls (≥ 80 %), it is necessary to examine in turn the behaviour of zirconia, formed in reactor, and zirconium alloys under the expected repository conditions. *A priori* most of the release of radionuclides will come from the dissolution of oxides on the one hand, and from the uniform corrosion of Zircaloy on the other hand, the overall rate of release being controlled by the rate of these two processes.

The dissolution of oxide layers and the corrosion of the zirconium alloys, and thus radionuclide release, will depend on the properties of the groundwater, eventually modified by the materials placed in the environment of waste. Of particular importance will be the groundwater composition, its redox potential and pH.

In most concepts envisaged for disposal of long-lived intermediate level waste, the packages of hulls and end-pieces waste will be placed in the vicinity of concrete structures and thus exposed to water in equilibrium with these cement-based materials. In the early years after closure, residual oxygen will be consumed and therefore anaerobic conditions will be imposed within the repository. So, anaerobic alkaline conditions constitute an environment that will prevail during the long post-closure phase of the disposal of hulls waste.

If concrete or a cement backfill or an internal waste package grout are not used, neutral reducing waters and groundwaters representative of deep argillaceous or crystalline rock site must also be considered.

We will begin by making a state of knowledge, seeking in particular to establish dissolution rates of zirconia layers (section 5.1) and corrosion rates of zirconium alloys (section 5.2) realistic and representative of those expected under the repository conditions. In the section 5.3, we will report the results available on leaching of irradiated hulls in aqueous solutions and release of ^{14}C. We will consider, in particular, whether the measured release rates are consistent with the corrosion (or dissolution) rates.

5.1 Dissolution of the zirconia layer

It is known that the zirconia oxide layer formed on spent fuel rod cladding is chemically very stable in pure water at reactor operation temperatures. This observation has led several authors to consider zirconia of potential interest for the safe disposal of high-level waste and plutonium derived from the decommissioning of strategic nuclear weapons [LUM 1999, DEG 2007].

The issue is to evaluate whether the conditions prevailing in a repository are capable of enhancing the solubility of zirconia, which is very low in pure water [BAE 1976].

5.1.1 Influence of pH and redox conditions

Data of zirconia solubility in water at 25°C reported in the literature were compiled by Andra and the Paul Scherrer Institute (PSI), and plotted as a function of pH (Figure 22). In neutral pH, the zirconia solubility reaches 10^{-12} M according to PSI [CUR 2002]. For other authors, the minimum solubility of zirconia would be one or some orders of magnitude higher [KOB 2007]. According Bruno *et al.*, a solubility of 10^{-9} M can be considered as a conservative and realistic estimate of the behaviour of zirconium as it is released from the Zircaloy elements [BRU 1997]. For a reference argillaceous groundwater, Andra calculated an average solubility of 2 10^{-8} M, ranging between 10^{-11} M and 3 10^{-6} M taking into account the uncertainties [AND 2005b].

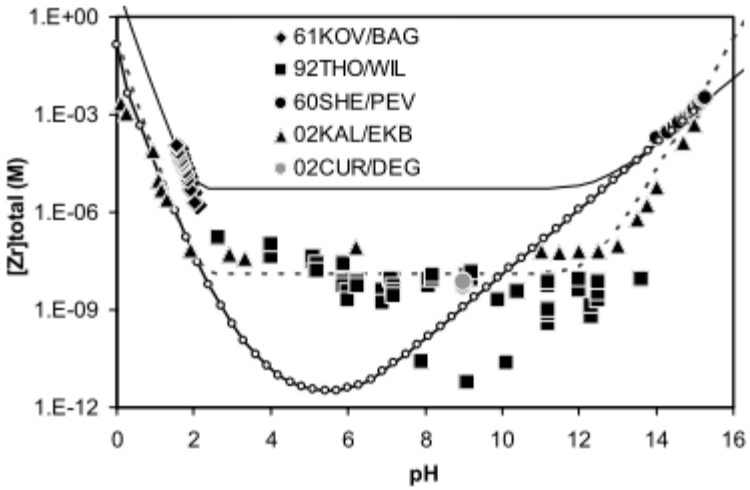

a) Compilation performed by Andra [AND 2005b]

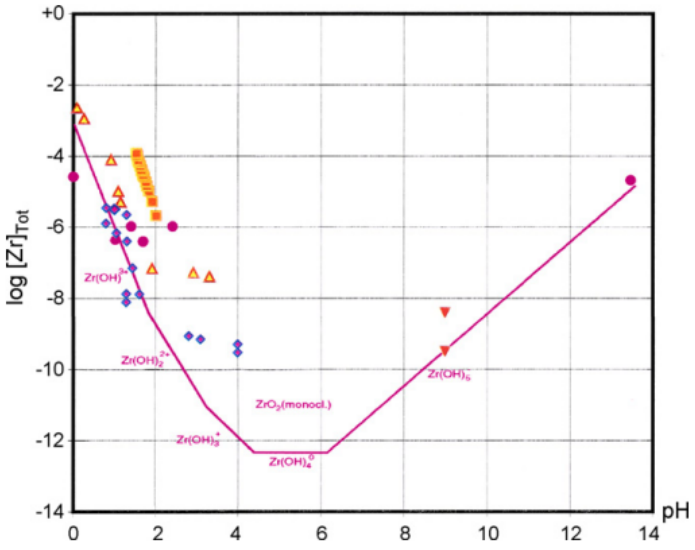

(■) Kovalenko and Bagdasarov [29]; (●) Adair et al. [30]; (▼) Pouchon et al. [31]; (▲) Ekberg et al. [32]; (♦) Michel [28].

b) Compilation performed by PSI [DEG 2007]

Figure 22: Solubility of monoclinic zirconia and oxy-hydroxide precipitate as a function of pH.

It may also be recalled that no zirconia dissolution is measurable in PWR primary water, which is not the case for austenitic stainless steels and nickel-based alloys [COH 1980, ROB 1989, NEE 1997]. This almost negligible release of zirconia in water precisely justifies that the corrosion of zirconium alloys can be deduced from measurements of weight gain, at least in neutral or slightly alkaline water, which would not be possible if the zirconia dissolved in significant proportions (see Appendix 1).

Anyway, the solubility of ZrO_2 may be considered as very low in the pH range for ground-waters (~ 6 to 9) [SHO 2010]. The solubility increases with increasing acidic and alkaline

concentrations, and can reach values of the order of 10^{-6} M. Similar dissolution behaviour is also observed in the solubility tests of hydrous zirconium oxide.

In strongly alkaline solutions the solubility increases with increasing pH due to the formation of the zirconate ion $HZrO_3^-$ (see below Figure 29) or $Zr(OH)_5^-$.

Zirconium being a non redox-sensitive element (it occurs in the IV valence state), no effects are observed due to the change in the redox conditions of the system. Duro *et al.* have calculated that the solubility of Zr in the form $Zr(OH)_4$ in water at 15°C is the same, i.e. 9.7 10^{-9} M, under a partial pressure of oxygen of 0.2 atm and under a partial pressure of hydrogen of 10^{-7} or 10^{2} atm [DUR 2006].

5.1.2 Influence of complexing species

Among the species present in the pore water permeating a typical repository environment, the effect of dissolved ligands has to be evaluated. The influence of chloride and carbonate ions, the presence of which is expected in the groundwaters, should especially be regarded. For the disposal of ILW, the leaching of cementitious waste forms could lead to alkaline $CaCl_2$ solutions.

5.1.2.1 Chloride ions

At low to moderate concentrations, chloride ions do not seem to have any significant effect in neutral waters on the zirconia solubility.

Figure 23 shows solubility data measured with zirconium oxide in 1.0 M $NaClO_4$ and in 0.5 and 1.0 M NaCl over a large pH range. In the range pH 3 - 13, the zirconium concentration is at a constant level [BRE 2007]. At pH > 13, the solubility curves (log [Zr] vs pH) show a distinct increase with a slope of 2 due to the formation of a complex.

In $CaCl_2$ solutions of concentration higher than 0.05 M, this solubility increase is more pronounced and already observed at significantly lower pH values (pH > 10). The solubility in 0.5 and 1.0 M NaCl/NaOH solutions is orders of magnitude lower than those in $CaCl_2$ solutions with similar chloride concentrations. This solubility increase is caused by the formation of a ternary complex $Ca_3[Zr(OH)_6]^{4+}$, which causes unexpectedly high solubilities of zirconium hydrous oxides, above 10^{-3} M at pH 12 [BRE 2007].

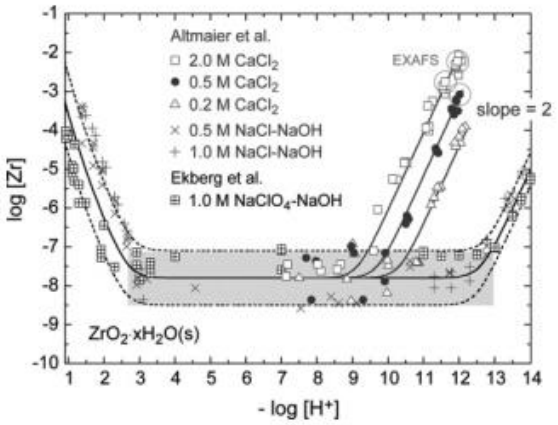

Figure 23: Solubility of $ZrO_2.xH_2O$ in $NaClO_4$, NaCl and $CaCl_2$ solutions at 20 – 25°C [BRE 2007]

5.1.2.2 Carbonate ions

The zirconia solubility remains very low for carbonate concentrations lower than 10^{-2} M (Figure 24). For concentrations higher than 10^{-2} M, experiments conducted by PSI at pH 9 and 25°C clearly indicate that the addition of bicarbonate ions in aqueous solutions increases the solubility of both cubic and monoclinic zirconia by some orders of magnitude. Whereas in pure water, the solubility of zirconia proves to be very low (~ $l0^{-12}$ to 10^{-8} M), it increases to 10^{-6} M in the presence of 0.05 M $NaHCO_3$, indicating the formation of carbonate complexes such as $Zr(OH)_5^-$, $Zr(CO_3)_5^{6-}$ and $Zr(OH)_3CO_3^-$ [CUR 1999]. The PSI results indicate a zirconia solubility in the order of 10^{-6} M for typical repository conditions. Figure 25 shows a typical speciation for conditions relevant to a repository environment at pH 9.

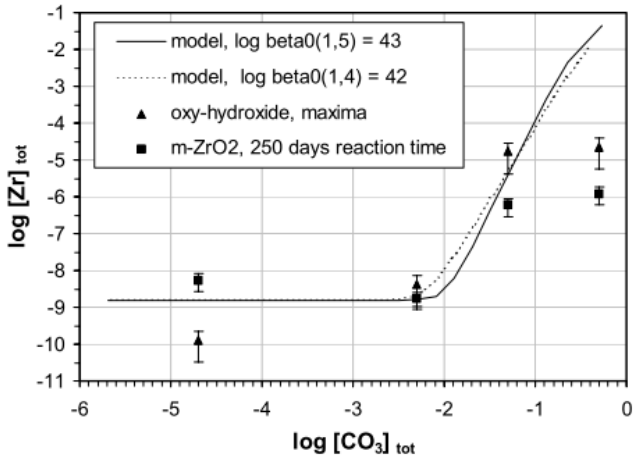

Figure 24: Solubility of monoclinic zirconia and of freshly precipitated Zr oxy-hydroxide as a function of total carbonate concentration [HUM 2002]

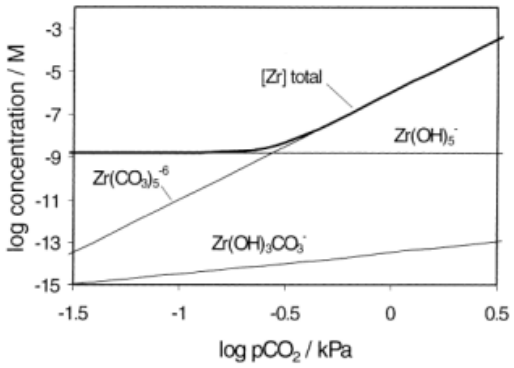

Figure 25: Zr speciation in equilibrium with monoclinic zirconia as a function of the carbon dioxide partial pressure, for pH 9 (in normal atmospheric conditions, $pCO_2 = 10^{-1.5}$ kPa) [CUR 1999]

5.1.3 Influence of γ-irradiation

The effect of irradiation on corrosion results from a series of phenomena which are attached either to a chemical modification of the medium (radiolysis effect) or a modification of the material microstructure (creation of structural defects). For waste containing activation products, such as the packages of hulls and end-pieces, the main source of irradiation is the β and γ emissions. Above a certain value of the dose rate, the γ-irradiation involves water radiolysis and thereby the creation of new molecular and radical species capable of causing a change in the chemistry of the water present in contact with waste. Water radiolysis can result, in particular, in alteration of the redox properties of the medium. However, as discussed above (see § 5.1.1), zirconium is a non redox sensitive element. It is therefore expected that there would be little, if any, effect of γ-irradiation on zirconia dissolution under disposal conditions.

For CSD-C waste packages manufactured at La Hague by Areva NC, the average γ-ray dose rate on contact is 25 $Gy.h^{-1}$ for a standard package when it is removed from storage. The dose rate decreases relatively rapidly with time. In contact with these packages, dose rates are about 0.25 $Gy.h^{-1}$ after 100 years and 0.03 $Gy.h^{-1}$ after 1,000 years [AND 2013]. So, for this second reason, any hypothetical effect of water radiolysis on zirconia layer dissolution will be *a priori* unsignificant under repository conditions.

Nishino *et al.* [NIS 1997] studied the effect of a high γ-dose rate (~ 30 $kGy.h^{-1}$) on the dissolution rate of a zirconia layer formed beforehand on Zircaloy-2 in high temperature water. Tests, lasting 200 hours, were conducted at 288°C in neutral water and in a slightly alkaline water. The dissolution of zirconia was determined from weight loss measurements. It was observed that the dissolution of ZrO_2 is more important at alkaline pH and that it is about

30 - 40 % larger under γ-ray irradiation (Figure 26). So γ-ray irradiation enhances the dissolution of zirconium oxide layer, at least at high dose rates.

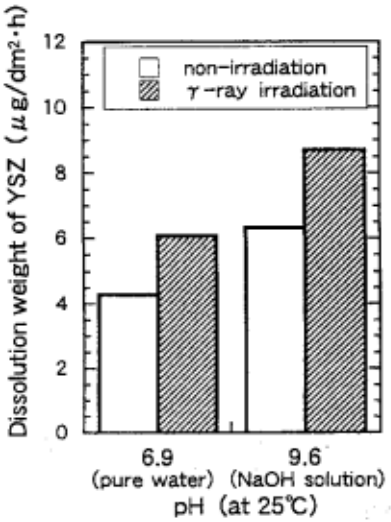

Figure 26: Dissolution of yttria-doped ZrO_2 at 288°C in pure water (pH 6.9 at 25°C) and in 4.4 10^{-5} M NaOH (pH 9.6 at 25°C), both with and without γ-ray irradiation (experiments of 200 h, dose rate of γ-irradiation ~ 30 kGy.h^{-1}) [NIS 1997].

In another study, the kinetics of dissolution of the oxide layer formed on Zircaloy 4 was compared under non-irradiated or irradiated (3.5 kGy.h^{-1}) conditions, at room temperature, in water at pH between 5 and 12 [GUI 2009]:

- without irradiation, the dissolution rate of zirconia in alkaline water is lower than the detection limit of the techniques used, i.e. less than 0.4 nm.y^{-1} ;
- under irradiation, after a test duration of 360 h, corresponding to a total dose received by a CSD-C waste package after 100,000 years, the thickness of oxide dissolved is 0.19 nm.

Thus the influence of γ-radiolysis of water on the dissolution of zirconia appears very moderate, even for very high dose rates. This result may be related to the fact that the solubility of zirconia in water is insensitive to redox.

5.1.4 Dissolution rates of zirconia

Shoesmith *et al.* present the results of some authors who have measured oxide dissolution rates on zirconium specimens prepared electrochemically by anodic oxidation [SHO 2010]. Dissolution rates were determined using capacitance measurements which allow determination of the change in oxide film thickness with time. The films grown in this manner consist of two layers: an outer hydroxide or hydrated ZrO_2 layer which dissolves rapidly and

an inner barrier layer with properties which more closely resemble those of a stable passive film. Figure 27 shows measurements of the dissolution rates for the inner barrier layer oxide. They depend very much on the preparation conditions of specimens, especially in acidic solutions. The dissolution rates measured in neutral solutions are in the range 5 to 20 $nm.y^{-1}$. The authors remark that all the rates plotted in Figure 27 may be conservatively high.

Some leaching experiments have been conducted with zirconia in alkaline solutions over periods of time not exceeding a few weeks (Table 13). Therefore, these data yield short-term leaching rates that are likely to be higher than rates which would be measured over a long time (several years) and conservative with respect to the corrosion rate of the zirconia of hulls under the repository conditions. The experimental techniques used to measure the zirconia dissolution differ between the authors and the ratio of specimen surface to volume of solution (S/V) is rarely indicated in these studies. The results of the Guipponi's thesis show that the dissolution rate of ZrO_2 in alkaline solutions at ambient temperature is extremely low ($< 0.4\ nm.y^{-1}$) [GUI 2009]. The results of Poulard, which were established using europium as a surface marker of zirconia, would lead to an apparent activation energy of dissolution of the post-transition zirconia equal to $57.9 \pm 19\ kJ.mol^{-1}$ [POU 2001a]. Assuming that the mechanism of zirconia dissolution remains unchanged at a lower temperature, a dissolution rate of zirconia in cementitious environment in the range 25 – 50°C significantly lower than $1\ nm.y^{-1}$ ($4\ 10^{-2}\ nm.y^{-1}$ at 50°C) could be inferred from these data. However, we will see below (§ 5.2.1) that zirconia can be considered as thermodynamically stable in alkaline solutions (pH ≤ 12.5) at low temperature, but not at high temperature.

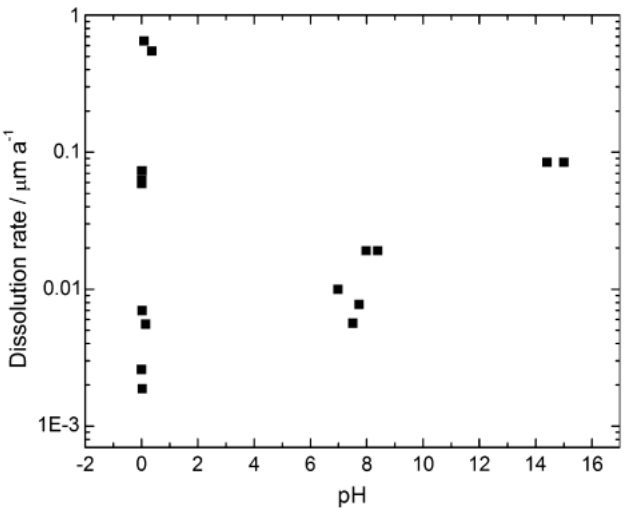

Figure 27: Dissolution rates of anodically grown oxides on Zr as a function of pH at ambient temperature [SHO 2010]

Table 13: Dissolution rates of ZrO_2 in alkaline solutions

Solution	$pH_{25°C}$	Temperature (°C)	Test duration (week)	r_{corr} * ($\mu m.y^{-1}$)	Ref.
NaOH	11.8	25	2	$< 4\ 10^{-4}$	[GUI 2009]
NaOH	9.6	288	1.2	1.0	[NIS 1997]
KOH + NaOH	13.5	250	12	a) 0.12 – 0.17 b) 0.13 – 0.14	[POU 2001a]
KOH + NaOH	13.5	275	12	a) 0.23 – 0.24 b) 0.21 – 0.24	[POU 2001a]
KOH + NaOH	13.5	300	12	a) 0.37 – 0.41 b) 0.34 – 0.37	[POU 2001a] [POU 2001b]

* When indicated: a) pre-transition zirconium oxide, b) post-transition oxide

The rate of zirconia dissolution has been found constant in alkaline solutions at high temperature up to 12 weeks [POU 2001a], but lower temperature tests suggest that the concentration of dissolved zirconia first increases and then decreases before reaching equilibrium (Figure 28). Dissolution equilibrium appears to be reached faster at 25°C than at 100°C [QIU 2009]. Curti *et al.* relate this behaviour, also observed for both monoclinic and cubic ZrO_2 dissolution in water, to the reordering of the surface structure from a soluble, amorphous structure to a less soluble crystalline form [CUR 2002]. Other authors suggest a mechanism of incongruent dissolution of zirconia.

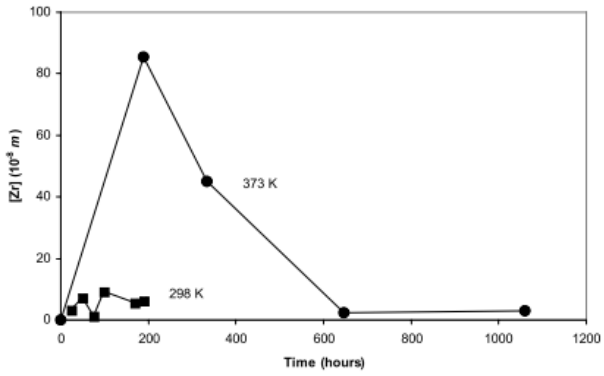

Figure 28: Dissolution kinetics of ZrO_2 in LiOH solutions with initial pH values of 10.0 and 10.48 at 298 and 373 K respectively [QIU 2009]

In conclusion, a realistic value, but possibly not conservative, of the dissolution rate of zirconia in neutral groundwaters or in cementitious environments, weakly carbonated (< 0.01 M) and fluoride-free, could be ~ 1 $nm.y^{-1}$. For an oxide layer thickness supposed of 50 µm and assuming that the oxide dissolution occurs only on its external face, a corrosion rate of 1 $nm.y^{-1}$ would correspond to a fractional release of $2\ 10^{-5}\ y^{-1}$.

The possible role of certain complexing molecules must however be subject to specific consideration depending on the chemistry of groundwaters of disposal sites considered.

5.2 Corrosion of zirconium alloys

The corrosion resistance of hull waste in disposal conditions is a key issue in the assessment of disposal performance for activated waste, because corrosion is expected to initiate and control the release of radionuclides from the waste by leaching. Zircaloy-2 and Zircaloy-4 have both been extensively studied for their corrosion and oxidation properties in nuclear power plants, in high temperature water and in steam, but few studies have been performed until recent years on the corrosion resistance of either alloy under the expected repository conditions, especially in cementitious environments.

5.2.1 Overview. Modes of corrosion expected under repository conditions

The potential - pH equilibrium diagram of zirconium in water at 25°C shows that the range of stability of the zirconia is between pH 3.5 and pH 12.5 (Figure 29). In this area, the zirconium is likely to be passivated by ZrO_2 and corrode extremely slowly. The stability domain of zirconia also depends on the concentration of zirconium ions in solution. Thus, this area is significantly larger when the concentration of zirconium in solution increases. For pH values above 12.5, the thermodynamically stable form of zirconium is the $HZrO_3^-$ anionic species. However, the conditions in repository (low amount of water in contact with the waste, limited renewal of the solution, large surface of Zircaloy accessible) will likely lead, in cementitious environments, to a content of dissolved zirconium sufficient to stabilize ZrO_2 at the highly alkaline pH, at least at low temperature.

Indeed, when temperature increases, the thermodynamic stability area of ZrO_2 is gradually reduced, while that of the $HZrO_3^-$ anionic species broadens as much (Figure 30). This effect of temperature on the stability range of zirconia has two consequences: (i) it explains the high solubility and high dissolution rates of zirconia in basic solutions at high temperature (see Table 13); (ii) the corrosion rates measured in basic solutions at high temperature cannot be extrapolated without precaution at low temperatures.

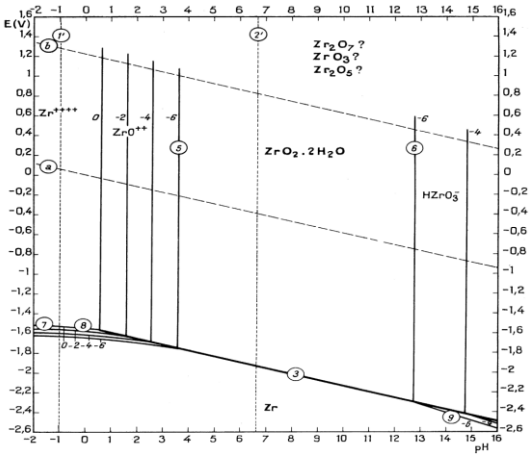

Figure 29: Potential – pH diagram of zirconium in water at 25°C [POU 1963]

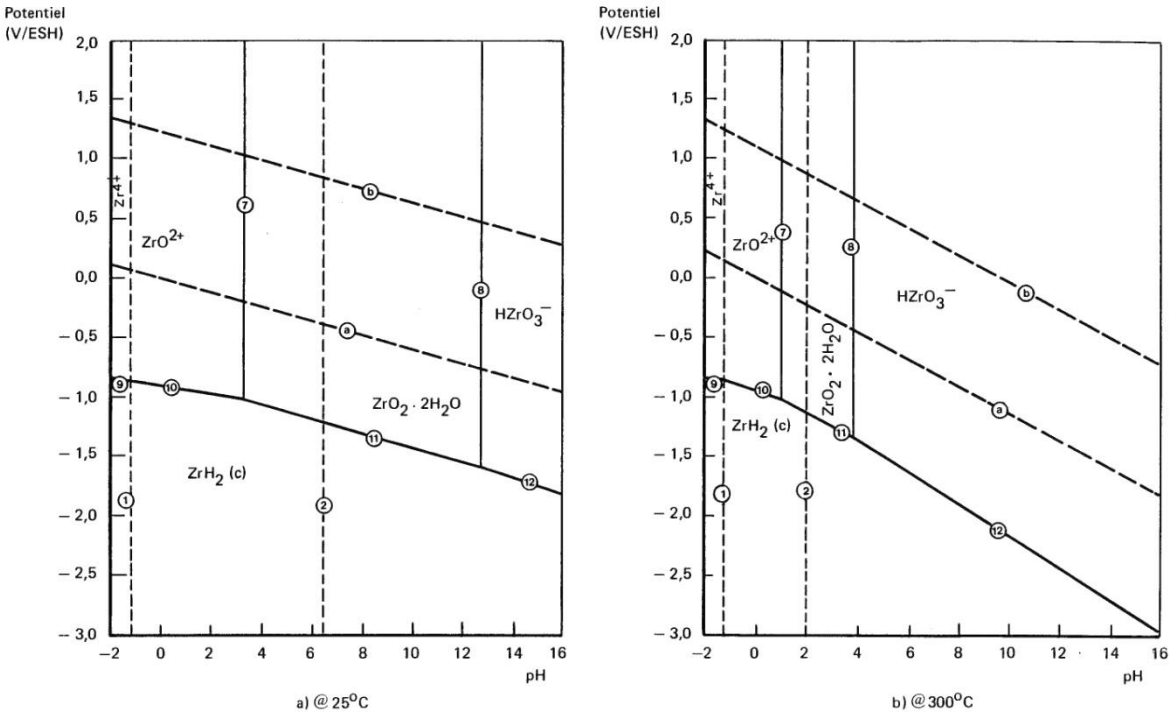

Figure 30: Potential – pH diagrams of the system zirconium – water at 25 and 300°C (activity of ionic and solid species taken equal to 10^{-6} and 1 respectively) [CHE 1983]

The processes which could lead to corrosion of zirconium alloys under repository conditions are related to the behaviour of the passive layer (or film) of ZrO_2:

- the presence of this layer is governed by a mechanism of passivation;
- the breakdown of this layer may involve pitting or crevice corrosion under oxidizing conditions;
- the formation of this layer could be prevented in certain circumstances, for example in case of adversely galvanic coupling.

These modes of corrosion involve a loss (dissolution) of metal; so they are important to investigate in the context of this study on the release of radionuclides. The following paragraphs are devoted to them.

Other damage modes, which may induce a loss of mechanical integrity of structures, but do not cause, strictly speaking, a dissolution of metal are also to be considered: stress corrosion cracking (SCC) and hydrogen embrittlement. Nevertheless, they may intervene in the kinetics of release: cracking of hulls could increase the areas affected by the general corrosion and therefore the fraction released of ^{14}C.

- SCC of zirconium alloys is not expected in repository conditions. Zirconium and its alloys are resistant to SCC in seawater and most aqueous environments. SCC of Zircaloy can occur in concentrated methanol, solutions containing heavy metal chlorides, ferric chloride solutions, copper chloride solutions, organic solutions with chloride, gaseous iodine or fused salts [COX 1990, NAK 1993].
- On the contrary, hydrogen embrittlement cannot be excluded, although its probability is low. While evidence is presented that hydrogen embrittlement failure is not likely to occur, it is difficult to demonstrate this conclusively because the process is not clearly understood and data relevant to the disposal of compacted hydrided hulls are limited. It was shown above (see §§ 2.1.2.1.3 and 2.2.1) that cladding contains hydrides after reactor operation and that transportation of spent fuel may induce a reorientation of these hydrides. In a repository, the hulls might also pick up more hydrogen from general corrosion of Zircaloy but *a priori* stresses are too low to cause a propagation of cracks or hydride embrittlement. Further work would be required to attempt to rule out with greater certainty a potential risk of compacted hulls fragmentation by a phenomenon of hydrogen embrittlement.

5.2.2 Localized corrosion of Zr-based alloys

5.2.2.1 Pitting and crevice corrosion

Zirconium and Zr alloys are known to be susceptible to pitting and crevice corrosion in halide solutions with chloride ions being the most aggressive, followed by bromide and finally iodide [KNI 1984]. The effect of the Cl^- ion content on the pitting potential measured by several electrochemical methods is illustrated in Figure 31.

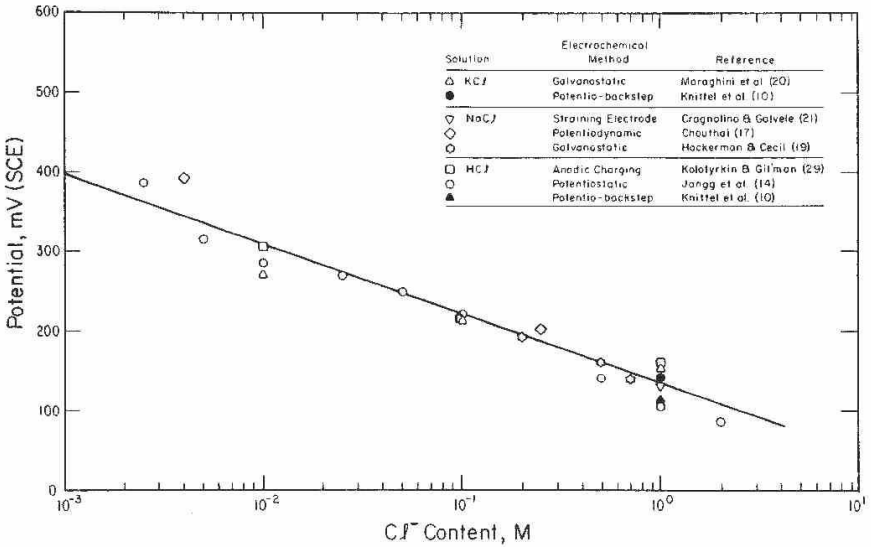

Figure 31: Effect of Cl^- ion content on the pit nucleation potential E_p at room temperature. E_p follows the relationship: E_p (V_{SCE}) = 0.134 – 0.088 log [Cl^- (M)], after [KNI 1984]

A susceptibility to pitting or crevice corrosion is possible when the environment is sufficiently oxidizing to polarize the free corrosion potential (E_{corr}) of the material into the potential range of susceptibility. Initiation and propagation of pitting (or crevice corrosion) are characterized by the existence of critical potentials obtained from an anodic potentiokinetic scan [POU 1970] (Figure 32):

- for potentials higher than the initiation pitting potential (E_p for pitting, E_{cr} for crevice corrosion), there is initiation and propagation of localized corrosion. The pitting potential is all the higher that the material is resistant to the environment;
- for potentials lower than the repassivation potential (E_{rp}), there is neither initiation nor propagation of localized corrosion. This potential is in fact the minimum potential required to maintain in the occluded cell a sufficiently aggressive medium for the active dissolution to continue;
- for potentials between E_p (respectively E_{cr}) and E_{rp}, pitting (respectively crevice corrosion) does not initiate, but existing pits continue to propagate.

Very generally, crevice corrosion initiates more easily than the pitting which results in lower initiation potential on polarization curves. The demonstration of the absence of risk of localized corrosion in the repository conditions is based on the existence of a repassivation potential higher than the corrosion potential of the material.

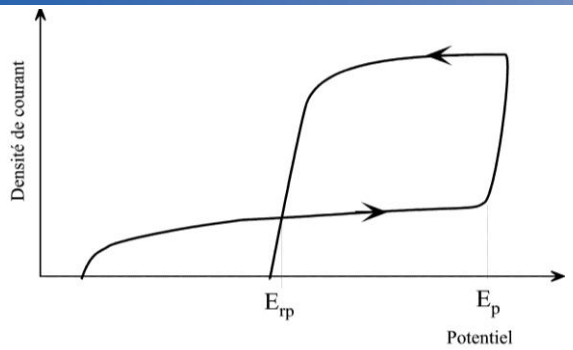

Figure 32: Current-potential curve of a passivating material in chloride solution: initiation pitting potential (E_p) and repassivation potential (E_{rp}). E_{corr} would be at the lower potential limit.

Under repository conditions, the source of oxidants within a failed package of hull waste may have two origins: (i) residual oxygen present in the early years after closure, but this oxygen will be consumed and therefore anaerobic conditions will impose, (ii) the hull γ-radiation which could lead to water radiolysis products such as hydrogen peroxide H_2O_2. A potential influence of γ-ray on corrosion of zirconium alloys might thus occur through an increase in the free corrosion potential and hence an increased risk of pitting or crevice corrosion.

Shoesmith *et al.* cite data showing that the range of corrosion potentials E_{corr} of Zr alloys measured in a series of neutral pH sulfate, chloride or perchlorate (0.1 $mol.L^{-1}$) solutions is close to, if not in, the susceptibility region for pitting [SHO 2010]. These authors also suggest that Zr alloys are susceptible to pitting at very low potentials providing the concentration of chloride is high enough (Figure 33) and that Zircaloy cladding could be susceptible to pitting in crystalline rock groundwaters ($0.2\ mol.L^{-1} \leq [Cl^-] \leq 1\ mol.L^{-1}$) and especially in sedimentary rock groundwaters ($0.3 \leq [Cl^-] \leq 5.7\ mol.L^{-1}$).

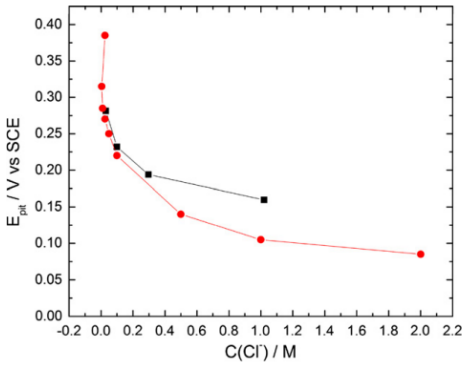

Figure 33: Pitting breakdown potentials recorded on Zr as a function of chloride concentration (C) at ambient temperature [SHO 2010].

To acquire data for the judgement and assessment of the risk of premature failure of fuel cladding in the proposed geological repository of Yucca Mountain, the Center for Nuclear Waste Regulatory Analyses (CNWRA) studied the pitting corrosion of Zircaloy-4 as a function of temperature (25 to 95°C), chloride concentration (1 mM to 4.0 M) and pH (2.1 to 10.7) in solutions containing the predominant anions of the groundwater [BRO 2000, PAN 2001]. A typical polarization curve in deaerated simulated groundwater (pH 8.4) containing 0.1 M Cl^- at 95°C shows a wide passive range that extends over almost 1 V above the corrosion potential, which is approximately -0.7 V_{SCE} (-0.46 V_{SHE}) in the deaerated solution, a pitting potential of about 0.20 V_{SCE} and a repassivation potential of about 0.10 V_{SCE} (Figure 34). Figure 35 illustrates the effect of chloride content and pH on the pitting potential (here called breakdown potential) and the repassivation potential at 95°C. The authors have also examined the effects of a pre-oxidation in water at 300°C (oxide thickness: 1.7 and 3.4 µm) on the corrosion of Zircaloy-4: it involves an increase of the breakdown potential (Figure 35b). They conclude that a thicker oxide affects significantly the pit initiation process [PAN 2001].

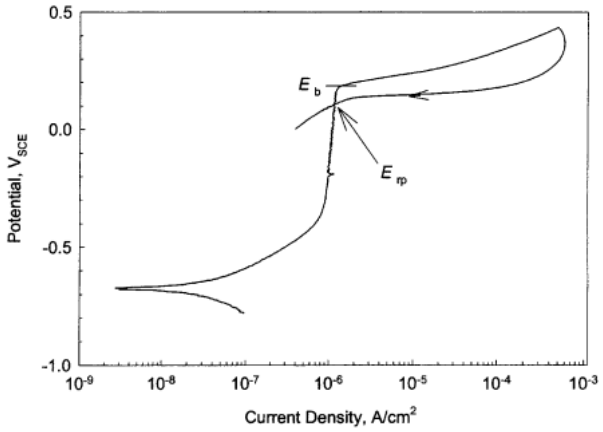

Figure 34: Potentiodynamic polarization curve for Zircaloy-4 in deaerated simulated J-13 well water (pH 8.4) containing 0.1 M NaCI at 95°C (scan rate of 0.167 mV.s^{-1}) [PAN 2001]

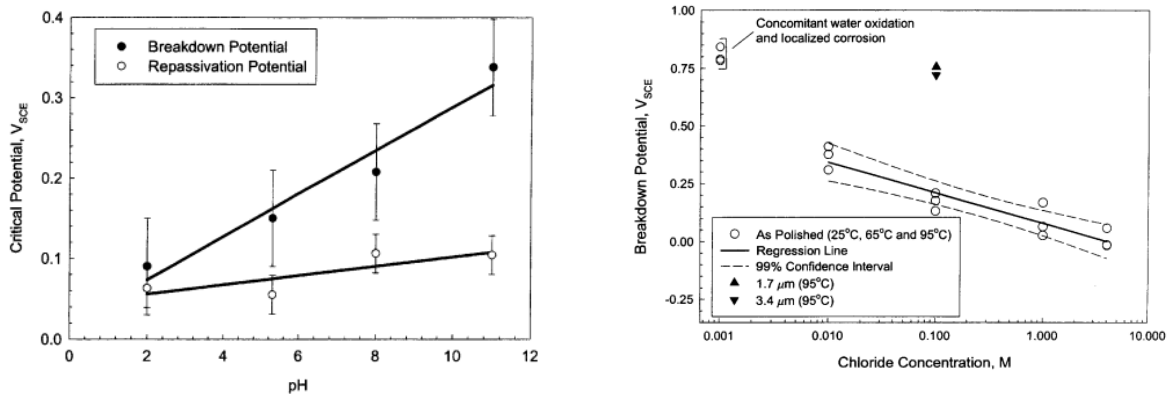

a) 0.1 M NaCl b) oxidized vs as-polished samples

Figure 35: Effect of pH (a) and chloride content (b) on the critical potentials measured on Zircaloy-4 in simulated J-13 well water at 95°C [BRO 2000, PAN 2001]

Despite highly oxidizing conditions and even sometimes degraded chemistry conditions, the pool waters of spent fuel wet storage do not induce pitting of Zircaloy cladding nuclear fuel [IAE 1998b]. Unpublished work performed by EDF to verify the corrosion resistance of spent fuel rods in long-term wet storage suggests that the risk of pitting is unlikely in waters containing ≤ 1 $g.L^{-1}$ Cl^- (28 mM). The susceptibility of Zr alloys (Zircaloy-4, M5^{TM}) to pitting was investigated by using the standard potentiodynamic technique in which the potential applied to the material is scanned to positive values until the pitting breakdown potential (E_p) is surpassed and then back again until the repassivation potential (E_{rp}) is reached, as illustrated above.. Various parameters were examined:

- Under no circumstances and whatever its surface condition (as-polished, oxidized, hydrided), Zircaloy-4 has been found sensitive to pitting corrosion in water at pH 5.5 and 80°C, in presence of chloride ions (1 $g.L^{-1}$), the free corrosion potential is in all cases considered significantly lower than the pitting potential ($E_p - E_{cor} > 200$ mV). Between 40 and 80°C, temperature has no significant effect on the pitting potential (Table 14). In the oxidized state, Zircaloy is insensitive to pitting corrosion (E_p above the water oxidation potential). Thus, with its oxide layer of ZrO_2, Zircaloy does not present any risk of pitting corrosion, the corrosion potential cannot be greater than the oxidation potential of water.
- The resistance to pitting corrosion of M5^{TM} was studied at 80°C as a function of pH, with a chloride content of 1 $g.L^{-1}$. On the alloy in the metallic state (i.e. as-polished), a potential sensitivity to pitting corrosion occurs at acidic pH ($E_{rp} < E_{corr} < E_p$), but not in neutral or alkaline waters ($E_{corr} < E_{rp} < E_p$) (Table 15). In contrast, the oxidized

samples show no susceptibility to pitting corrosion: the pitting and repassivation potentials are higher than the water oxidation potential (Table 16). The presence of highly oxidizing ions such as Fe^{3+} and Cu^{2+} makes the alloy potentially sensitive to pitting in the metallic state ($E_{rp} < E_{corr} < E_p$), but not in the oxidized state (Table 17).

Table 14: Corrosion potentials (E_{corr}) and pitting potentials (E_p) of low-tin Zircaloy-4 tubing in water (pH 5.5) at 80°C, containing 1 g.L^{-1} Cl^- and 15 mg.L^{-1} H_2O_2 (H_2O_2 was added to simulate the creation of oxidizing species by radiolysis of water; highly oxidizing conditions) [BEL 1999].

	Temperature (°C)	Metallic state	Oxidized state (1)	Hydrided state (2)	Cold worked condition (3)
E_p (mV_{SCE})	80	210 ± 10 *(480 ± 40)**	> 750	315 ± 5	265 ± 100
	60	225 ± 10	-	-	
	40	240 ± 10	-	-	-
E_{corr} (mV_{SCE})	80	- 150 ± 40	70 ± 15	75 ± 5	- 10 ± 10
	60	- 50 ± 10	-	-	-
	40	- 005 ± 50	-	-	-
$E_p - E_{corr}$ (mV)	80	110	> 430	- 10	25

(1) To represent the dense zirconia layer formed in reactor; oxide of thickness 2.5 µm formed in PWR primary water (3,700 h at 360°C).
(2) To simulate a possible exposure of the base metal with a dense hydrided layer in surface; sample hydrided by cathodic charging then annealed 26 h at 430°C (277 ppm of hydrogen)
(3) To study the influence of surface defects and simulate the expected effects of radiation damage.
* Pitting potential for a chloride content of 100 mg.L^{-1}.

Table 15: Pitting potentials (E_p), repassivation potentials (E_{rp}) and corrosion potentials (E_{corr}) of M5^{TM} alloy <u>in the metallic state</u> at 80°C as a function of pH, with 1 g.L^{-1} Cl^- and 15 mg.L^{-1} H_2O_2 [DAM 2000].

pH	1.5	2	3	4	5.8	10	12
E_p (mV_{SCE})	285	350	375	350	340	380	495
E_{rp} (mV_{SCE})	200	215	220	200	220	155	30
E_{corr} (mV_{SCE})	220	270	230	75	20	- 30	- 155

Table 16 Pitting potentials (E_p), repassivation potentials (E_{rp}) and corrosion potentials (E_{corr}) of M5™ alloy in the oxidized state at 80°C as a function of pH, with 1 g.L^{-1} Cl$^-$ and 15 mg.L^{-1} H_2O_2 [DAM 2000].

pH	1.5	4	12
E_p (mV_{SCE})	> potential of oxygen evolution reaction		
E_{rp} (mV_{SCE})	> potential of oxygen evolution reaction		
E_{corr} (mV_{SCE})	- 100	- 50	- 165

Table 17 Pitting potentials (E_p), repassivation potentials (E_{rp}) and corrosion potentials (E_{corr}) of M5™ alloy at 80°C, in presence of 1 g.L^{-1} Cl$^-$, 15 mg.L^{-1} H_2O_2 and 40 mg.L^{-1} Fe^{3+} or Cu^{2+} [DAM 2000].

	Metallic state		Oxidized state	
Environment	40 mg.L^{-1} Fe^{3+} pH 3.5	40 mg.L^{-1} Cu^{2+} pH 5.8	40 mg.L^{-1} Fe^{3+} pH 3.5	40 mg.L^{-1} Cu^{2+} pH 5.8
E_p (mV_{SCE})	340	370	> potential of oxygen evolution reaction	
E_{rp} (mV_{SCE})	215	205	> potential of oxygen evolution reaction	
E_{corr} (mV_{SCE})	305	245	- 5	- 15

The consequences of the Fukushima Daiichi accident in March 2011 resulted in the need to know the effect of inputs of high concentration of chloride (seawater) into the pools on the corrosion resistance of the Zircaloy cladding rods. Moreover, the falling of concrete blocks into the pools led to a significant increase in the pH of the pool. The corrosion behavior of the samples was evaluated using polarization curves in solutions containing 3 g.L^{-1} Cl$^-$ at pH values of 8 and 12, but without measuring the repassivation potential [LAV 2012]. The authors conclude to a slight decrease in the pitting susceptibility with an increase in the pH. Although the chloride ions widely decrease the passive range of the oxidized samples, the oxide layer substantially increases the pitting potential (Table 18).

Table 18: Pitting potentials (E_p) and corrosion potentials (E_{corr}) of Zircaloy-4 in solutions containing 3 g.L^{-1} Cl$^-$ at ambient temperature (average of 5 measurements; pH values obtained by additions of NaOH) [LAV 2012]

	Metallic state		Oxidized state
	E_p (mV_{SCE})	E_{corr} (mV_{SCE})	E_p (mV_{SCE})
pH 8	160	- 219 ± 42	600
pH 12	180	- 220 ± 6	600

Kurashige *et al.* conducted corrosion tests of Zircaloy-4 at 30 and 45°C in alkaline (pH 10.5 or 12.8) and high chloride (0.55 M) solutions, under anoxic conditions: pitting corrosion was

not observed after a test period of 400 or 500 days to the potential of free corrosion [KUR 1999].

The following trends can be drawn from all of the results reported:

- in neutral groundwaters with high chloride content (> 0.2 M), pitting corrosion of Zr alloys appears possible if a sufficient oxidant concentration is able to polarize E_{corr} beyond the threshold for pitting susceptibility;
- the susceptibility of Zr alloys to pitting corrosion by chloride ions decreases in alkaline waters;
- the oxide layer formed in reactor is protective and considerably improves the resistance of Zr alloys to pitting, even in the more oxidizing environments.

In summary, pitting corrosion can be considered as a mode of corrosion of Zr alloys unlikely in cementitious environments that will prevail in repository in the near field of the hulls waste packages.

5.2.2.2 Galvanic corrosion

In waste packages of compacted hulls and end-pieces (CSD-C), various metallic materials may be in contact with the Zr alloy hulls: austenitic stainless steel of end-pieces, nickel-based alloys of springs and lead-tin alloy used as coating material[3] of *galettes* (see Figure 17). This may result in a coupling and a risk of galvanic corrosion if the environment is sufficiently conducting and if the potential difference between the two metals in contact is sufficiently large. It is generally accepted that there is no coupling when the potential difference is less than 50 mV [NOR 2004].

When there is galvanic corrosion, the less noble material acts as an anode and sees its corrosion rate increase. *A contrario,* the noblest material acts as a cathode. For metals such as zirconium, some galvanic couplings may promote hydriding on the cathode, especially contacts with aluminum alloys [JOH 1977].

Galvanic corrosion is well known in aerated environments (in particular in seawater). The galvanic series allow to predict the behaviour of a couple of metallic materials under these conditions. However, these data can hardly be used for repository conditions, because they are representative of aerated conditions. To evaluate these coupling phenomena under repository

[3] The compaction cases in carbon steel are coated with a thin coating of Pb-Sn alloy which allows the self-lubrication of the case during the step of press compacting [AND 2013].

conditions, it would be necessary to know the corrosion potentials of the materials of the package in a typical water of the disposal cell, under anoxic conditions.

In the early phase of disposal, the presence of residual oxygen and the impact of water radiolysis could create oxidizing redox conditions. In a highly oxidizing water (dissolved O_2, 15 $mg.L^{-1}$ H_2O_2) at 80°C, as-polished Zircaloy-4 is passive and takes a free corrosion potential lower than that taken by the stainless steel AISI 304L and nickel-chromium alloys; the potential difference can reach 200 mV. But, when the metal is pre-oxidized, the potential difference is lower than 50 mV, and excludes any risk of coupling [BEL 1999]. The potentials of lead and tin are less noble than this one of zirconium in aerated environments [ZHA 2011]. Moreover, the high resistivity of zirconia layers (Figure 36) could only lead to coupling currents extremely low, less than a few $\mu A.m^{-2}$ [AND 2013]. The phenomenon of galvanic coupling may be neglected in the evaluation of the corrosion of zirconium alloys in disposal conditions.

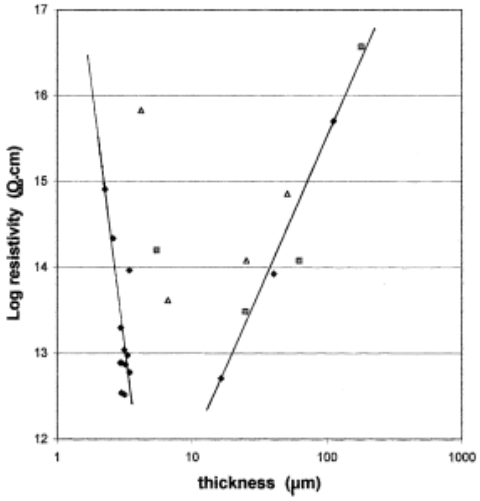

Figure 36: Dependence of resistivity on oxide layer thickness: ◆: alloy Zr1Nb, ■: Zirlo™, ▲: Zircaloy-4, [FRA 2002]

Andra and EDF have been testing galvanic coupling between Zircaloy-4 and the lead-tin alloy used in the CSD-C packages in deaerated cementitious environment: no negative influence of such coupling has been detected [AND 2013].

5.2.2.3 Microbiologically influenced corrosion

Microbiologically influenced corrosion (MIC) of Zr alloys might be a local corrosion mechanism of hulls where microbes produce a local acidic environment that could produce multiple penetrations through the hulls. There is no indication in the literature that MIC occurs on zirconium metal or alloys. This type of corrosion is considered extremely unlikely,

if not excluded, for the zirconium alloys in a geological repository environment [HIL 1998, SIE 2000].

In summary, most of the data appear to show that localized corrosion would not be significant for zirconium alloys under "normal" repository conditions. General (uniform) corrosion will be the main, if not the only, mode of corrosion expected in these conditions.

Before reviewing the state of knowledge on general corrosion of zirconium alloys, the possible influence of irradiation of the material in reactor on its subsequent behaviour after disposal is discussed in the next section.

5.2.3 Influence of neutron irradiation of cladding in reactor

Irradiation in reactor of zirconium alloys induces irradiation damage leading to a change of their microstructure (see § 2.1.2.2), of their mechanical properties and of their resistance to corrosion. These phenomena, which are observed under neutron flux, require very high dose rates and a neutron spectrum which do not occur in the waste packages. The question is therefore whether the (neutron) irradiation of claddings in reactor will affect the corrosion of hulls in repository conditions (out of neutron flux).

The general corrosion of claddings in reactor is accelerated by two phenomena: the irradiation and the precipitation of hydrides beyond a certain burn-up. The influence of these two parameters (hydriding and irradiation) was studied through corrosion tests in autoclave of claddings previously corroded in reactor [HÉL 2004]. These tests have shown that, in PWR water, at short term, the corrosion rate of cladding previously oxidized in reactor is higher than that of non-irradiated cladding, and that this effect is due to the presence of hydrides and radiation defects in the material. Then the corrosion rate progressively tends towards that of non-irradiated cladding as defects and hydrides are eliminated, mainly by slow annealing of the material due to the high temperature of autoclave tests.

Under repository conditions, the corrosion rates are extremely low, and the impact of irradiation damage is not considered likely to have any influence on the uniform corrosion of zirconium alloys [AND 2013]. Moreover, as noted above (see § 2.2.1), a partial recovery of irradiation defects is expected as consequence of transportation of fuel assemblies in dry cask at high temperature [EPR 2006].

The low temperature of disposal and the annealing of claddings during transportation should minimize the impact of irradiation in reactor on the corrosion rate in disposal conditions.

5.2.4 Uniform corrosion of Zr-based alloys in neutral waters

The Zr alloys exhibit an excellent resistance to uniform corrosion in the waters with a pH close to neutrality or slightly alkaline except in presence of fluoride. The presence of fluoride ion, even at low concentrations, is very detrimental, and promotes accelerated corrosion of zirconium for concentrations of a few $mg.L^{-1}$, even at low temperatures [PIN 1989, BAL 2000]. Such corrosion is likely due, as in an acid medium, to a complexation of Zr^{4+} ions preventing the metal from passivating:

$$Zr \rightarrow Zr^{4+} + n\,F^{-} \equiv [ZrF_n]^{4-n} \qquad \{3\}$$

Determining the uniform corrosion rate of Zr alloys in neutral waters is based on two complementary approaches:

- the extrapolation to the temperatures of interest for disposal of the considerable data set in water at high temperature (250 – 400°C);
- some observations and results of corrosion tests carried out at low temperatures.

5.2.4.1 At high temperature

As noted in paragraph 2.1.2.1.2, the zirconium alloys exhibit excellent corrosion resistance in water at temperatures up to 350°C, because it forms a protective oxide film of ZrO_2. The existence of various models developed to account for the kinetics of uniform corrosion of Zircaloy-2 and -4 in high temperature water between 250 and 400°C was also mentioned. Reviews of these various models have been made by several authors [GAR 1980, COX 1985, GRA 1988, IAE 1998, TAN 2013].

The most numerous are semi-empirical models with a cubic rate law for the pre-transition period and a linear post-transition kinetic regime (see Figure 3a). The corrosion equations are as follows:

- pre-transition period:

$$\Delta W^3 = k_{Co} \exp(-Q_C/RT)\, t \qquad \{4\}$$

- post-transition period :

$$\Delta W = k_{Lo} \exp(-Q_L/RT)\, t \qquad \{5\}$$

with : ΔW : weight gain ($mg.dm^{-2}$)

k_{Co}: rate constant for the pre-transition period ($mg^3.dm^{-6}.d^{-1}$)

k_{Lo}: rate constant for the post-transition period ($mg.dm^{-2}.d^{-1}$)

Q_C, Q_L: activation energy for the pre and post-transition respectively ($J.mol^{-1}$)

R: the universal gas constant ($8.314\ J.mol^{-1}.K^{-1}$)

t: exposure time (d)

It can be remarked that, for laboratory tests, measuring the weight gain of the test pieces after the test is a measure of general corrosion of Zr alloys in water, in so far as the release of oxidized species in the medium is considered negligible and the oxide layer does not flake. It is shown in Appendix 1 that:

- the relationship between oxide ZrO_2 thickness and weight gain is: 1 µm = 14.62 $mg.dm^{-2}$
- the relationship between loss of metal Zr and weight gain is: 1 µm = 22.83 $mg.dm^{-2}$.

Without sake of completeness, Table 19 gives the values of the different constants of this model, calculated by several authors from their own results or bibliographic compilations. With the exception of the Dalgaard's model below 360°C, all the earlier models are equivalent in the temperature range 280-400°C (Figure 37).

It should be also that, in addition to the models of Kass and Hillner [KAS 1969a, HIL 1977], Westinghouse has also developed an iterative model with a cyclic cubic kinetics [MAR 1978, CLA 1985].

Table 19: Values of the kinetic parameters of the corrosion models of Zircaloy-2 and Zircaloy-4 in high temperature water or steam (test in autoclaves between 250 and 400°C)

Author, year	Ref.	Pre-transition period		Post-transition period	
		k_{Co} ($mg^3.dm^{-6}.d^{-1}$)	Q_C ($kJ.mol^{-1}$)	k_{Lo} ($mg.dm^{-2}.d^{-1}$)	Q_L ($kJ.mol^{-1}$)
Dyce, 1964	[DYC 1964]	$5.07\ 10^{13}$	135.1	$6.53\ 10^{9}$	125.2
Van der Linde, 1965	[VAN 1965]	$1.99\ 10^{13}$	130.2	$2.30\ 10^{9}$	119.7
Kass, 1969	[KAS 1969a]	$6.36\ 10^{11}$	113.4	-	-
Stehle *et al.*, 1975	[STE 1975]	period neglected		$2.21\ 10^{9}$	118.0
Dalgaard, 1976	[DAL 1976]	period neglected		$1.84\ 10^{7}$	92.9
Westinghouse model Hillner, 1977	[HIL 1977]	$6.36\ 10^{11}$	113.4	$1.12\ 10^{8}$	104.2
MATPRO model Hagrman *et al.*, 1978	[HAG 1978]	$1.56\ 10^{13}$	130.2	$1.21\ 10^{9}$	117.1
Garzarolli *et al.*, 1980	[GAR 1980]	$5.07\ 10^{13}$	135.1	$2.21\ 10^{9}$	118.0
Billot *et al.*, 1991	[BIL 1991]	$3.56\ 10^{14}$	142.8	$5.85\ 10^{12}$	152.9
Forsberg *et al.*, 1995	[FOR 1995]	$1.55\ 10^{14}$	135.1	$2.34\ 10^{9}$	114.5
Hillner *et al.*, 1998 (see text)	[HIL 1998, HIL 2000]	$6.36\ 10^{11}$	113.4	1) $2.47\ 10^{8}$ 2) $3.47\ 10^{7}$	1) 107.1 2) 95.2

In 1998, Hillner *et al.* revisited all of their data covering then a maximum exposure time in autoclaves at 316°C of approximately 29 years and a maximum oxide thickness of ~ 114 µm

for an experiment at 338°C [HIL 1998, HIL 2000]. The objective of the study was to update the laws of uniform corrosion of Zircaloy in high temperature water, in order to make extrapolations to the lower temperatures anticipated in the repositories for the disposal of Zircaloy-clad fuel elements. Since spent fuel cladding will be in the post-transition region upon entry into a repository, the authors focus on post-transition kinetic region. The post-transition regime is described by two stages and two successive equations from stage 1 to stage 2 (Figure 38a), with the change occurring at about ~ 400 mg.dm^{-2} (i.e. an oxide thickness of ~ 27 µm, or else a loss of metal of ~ 17.5 µm). Both stage 1 and stage 2 linear rate constants appear to follow an Arrhenius-type temperature dependence (Figure 38b):

- Stage 1: K(1) ΔW (mg.dm^{-2}) = 2.47 10^8 exp (-12880/T) t (d) {6}
- Stage 2: K(2) ΔW (mg.dm^{-2}) = 3.47 10^7 exp (-11452/T) t (d) {7}

Considering the thickness of the oxide present on the Zircaloy cladding of spent fuel, the use of the equation {7} to estimate the amount of additional corrosion due to repository exposure, which is conservative, is recommended.

The authors put forward another argument for the use of a conservative law: the "memory" effect of prior irradiation of cladding (or hulls) [HIL 2000].

We will see in the next paragraph that the equation {7} was retained for the Yucca Mountain project by US DOE (OCRWM) at any temperature, provided that the pH is greater than 3.18 and the fluoride concentration is less than 5 ppm [BAL 2000].

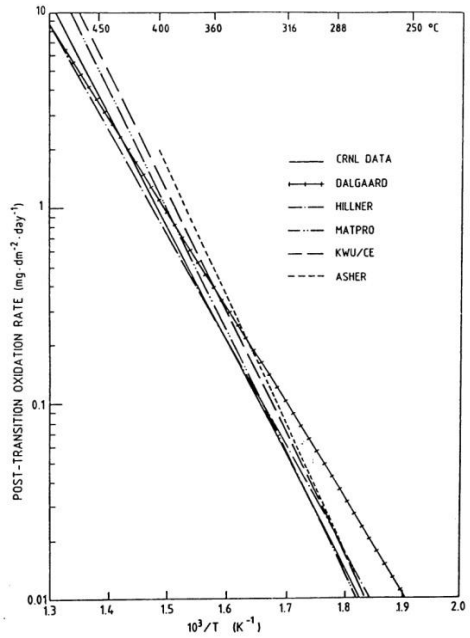

Figure 37: Comparison between post-transition corrosion rates for early models [COX 1985]

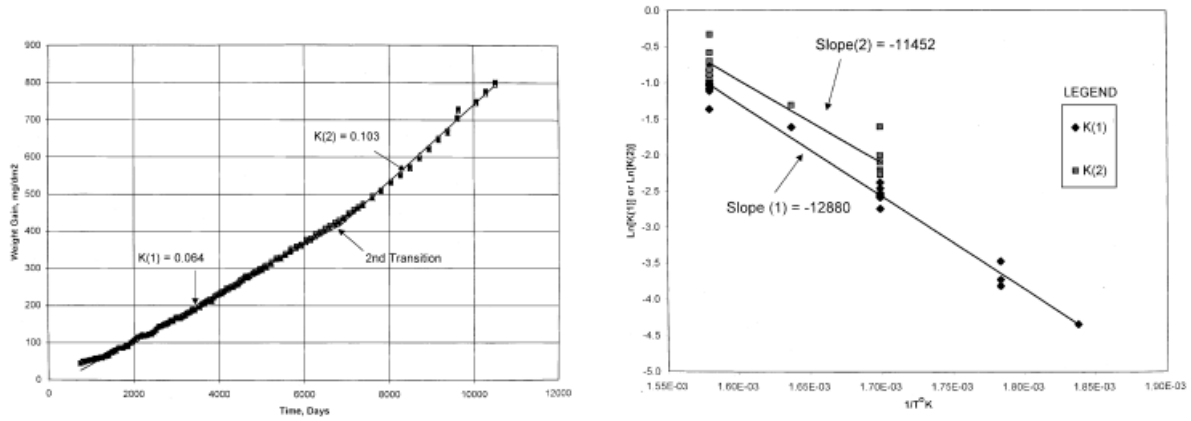

a) b)

Figure 38: (a) Variation of weight gain as a function of exposure time at 316°C and (b) Arrhenius-type plot of the stage 1 and stage 2 rate constants as function of the inverse absolute temperature [HIL 2000]

5.2.4.2 At low temperature (20 – 80°C)

a) Extrapolation of high temperature uniform corrosion rates

The excellent corrosion resistance of zirconium alloys in water makes it impractical to conduct meaningful corrosion tests at low temperature (20 – 80°C) in any reasonable time period. That explains why corrosion correlations based on data generated at high temperature were used to make extrapolations to the lower temperatures under repository conditions. The tacit assumption of this approach is that mechanisms do not change over the range of testing and extrapolation. Moreover, it is assumed that the corrosion rate is expected to be the same in pure water and in low salinity groundwaters [ROT 1984].

It is in this context that the Hillner's corrosion model was updated to meet the needs identified by the US DOE (OCRWM) for the Yucca Mountain project [HIL 1998, HIL 2000]. By retaining the relation {7}, the OCRWM was able to conclude that, under normal repository conditions, the very small level of general corrosion will not be expected to affect the integrity of nonfailed fuel elements with Zircaloy-4 cladding through the life of a repository [BAL 2000].

For the disposal of hull waste, the temperatures anticipated in the neighborhood of packages are generally in the range 20 – 50°C, depending on the age of packages and disposal concepts. To put some orders of magnitude, Table 20 gives the results of calculations of the corrosion rate of Zircaloy at 20 and 50°C in pure water, and the time to corrode a metal thickness of 0.5 mm (close to the end-of-life thickness of PWR cladding) on both sides.

Table 20: Comparison of metal loss rates predicted from the corrosion models of Zircaloy in high temperature water: general corrosion rates and times to corrode a hull thickness of 0.5 mm on both sides.

Author [Ref.]	at 20°C		at 50°C	
	r_{corr} ($nm.y^{-1}$)	$t_{0.5mm}$ (y)	r_{corr} ($nm.y^{-1}$)	$t_{0.5mm}$ (y)
Dyce [DYC 1964]	$5.0\ 10^{-9}$	$5.0\ 10^{13}$	$6.0\ 10^{-7}$	$4.2\ 10^{11}$
Van der Linde [VAN 1965]	$1.7\ 10^{-8}$	$1.5\ 10^{13}$	$1.6\ 10^{-6}$	$1.6\ 10^{11}$
Stehle *et al.* [STE 1975]	$3.2\ 10^{-8}$	$7.8\ 10^{12}$	$2.9\ 10^{-6}$	$8.6\ 10^{10}$
Dalgaard [DAL 1976]	$8.0\ 10^{-6}$	$3.1\ 10^{10}$	$2.8\ 10^{-4}$	$0.9\ 10^{9}$
Hillner [HIL 1977]	$4.8\ 10^{-7}$	$5.2\ 10^{11}$	$2.5\ 10^{-5}$	$1.0\ 10^{10}$
MATPRO [HAG 1978]	$2.6\ 10^{-8}$	$1.0\ 10^{13}$	$2.2\ 10^{-6}$	$1.1\ 10^{11}$
Garzarolli *et al.* [GAR 1980]	$3.2\ 10^{-8}$	$7.8\ 10^{12}$	$2.9\ 10^{-6}$	$8.6\ 10^{10}$
Billot *et al.* [BIL 1991]	$5.2\ 10^{-11}$	$4.8\ 10^{15}$	$1.8\ 10^{-8}$	$1.4\ 10^{13}$
Forsberg *et al.* [FOR 1995]	$1.5\ 10^{-7}$	$1.7\ 10^{12}$	$1.1\ 10^{-5}$	$2.3\ 10^{10}$
Hillner *et al.* [HIL 1998]	1) $3.2\ 10^{-7}$ 2) $5.9\ 10^{-6}$	1) $7.8\ 10^{11}$ 2) $4.2\ 10^{10}$	1) $1.9\ 10^{-5}$ 2) $2.2\ 10^{-4}$	1) $1.3\ 10^{10}$ 2) $1.1\ 10^{9}$

Thus, the extrapolation of all the models at low temperature leads to uniform corrosion rates extremely low, having no physical meaning or quantitative credibility, and consequently to lifetimes of hulls that give an idea of the eternity!

Studies conducted to measure the uniform corrosion rates of Zircaloy in neutral waters at low temperature are obviously unable to determine values so vertiginously low with techniques that are normally applied.

b) Examination of rod claddings stored in water pool

Over more than 40 years of experience with several million LWR rods, power reactor fuel with zirconium alloy cladding has had excellent durability in wet storage [IAE 2006]. US examinations after 20 years in wet storage indicated no detectable changes in Zircaloy PWR cladding characteristics compared with properties measured on rods from the same assembly soon after the fuel rods were first put into wet storage [BRA 1981]. Some wet storage materials studies have included Zircaloy specimens. Zircaloy coupons were thus exposed in two Hanford fuel storage pools for a period of three years; during this period, water chemistry excursions occurred that markedly accelerated corrosion of Al alloy and carbon steel specimens. After three years, the Zircaloy specimens retained their silver appearance, suggesting that oxide growth had not progressed into the first interference colour range (20 nm thickness). The rate is suggested to be less than 7 $nm.y^{-1}$. Weight measurements on the same coupons indicated rates lower than 10 $nm.y^{-1}$ [IAE 1998b, IAE 2006].

c) Corrosion tests at low temperatures

At low temperature, times to reach post-transition kinetics are considerably longer than experiments so far carried out. Because most experimental tests were carried out on metallic samples of Zircaloy and not on pre-oxidized samples, they have explored in fact the pre-transition region of the corrosion kinetics (Figure 39a). Unless the oxide layer is broken or spalled, these tests do not make so much account for the behaviour of hulls (claddings) which are in the post-transition region at the end of their life in reactor. To our knowledge, the corresponding tests are still missing, as far as they are necessary to complete. Furthermore, regardless of how the very low corrosion rate of the metallic samples can be evaluated, the corrosion measured in the pre-transition regime does not present a constant corrosion rate, but a decreasing rate (*a priori* according a cubic law, if the corrosion mechanism at low temperature is similar to that at high temperature). The "average" rate measured after the test durations t1, t2... is greater than the "instantaneous" corrosion rate, which can be better assessed by measuring the evolution of the metal loss between the times t1 and t2 (Figure 39b). We shall see below that only one laboratory [KAT 2013] has attempted to determine the rate constant of a cubic kinetics, but over relatively short periods.

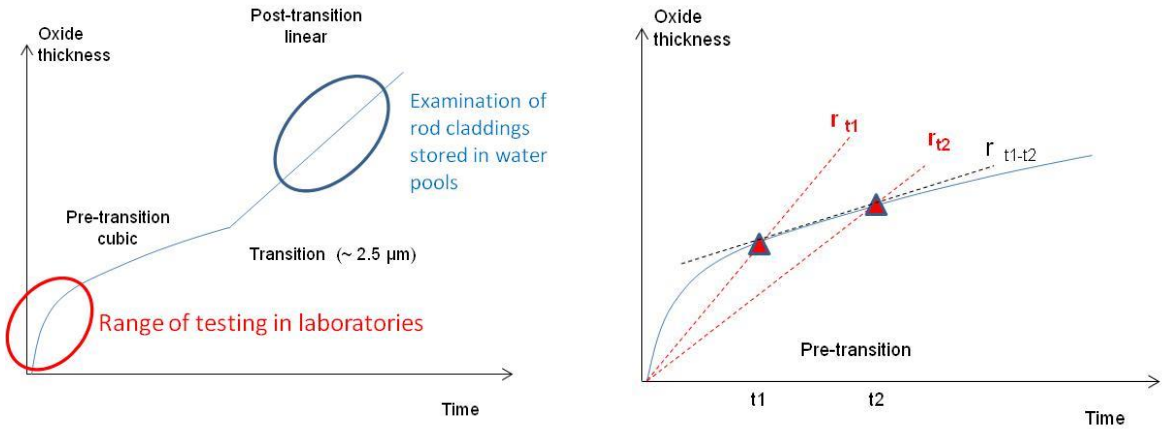

a) b)

Figure 39: Typical corrosion-time curve for Zircaloy corroding in water, showing the range explored with the corrosion tests (a) and how measured corrosion rate decreases with increasing measurement periods (b).

Table 21 presents a few results of some corrosion tests carried out in neutral waters.

Table 21: Conditions and results of corrosion tests of Zircaloy in neutral waters at low temperature

Author, Ref	Sample *	Solution	T (°C)	Test duration	Corrosion measurement	r_{corr} ($nm.y^{-1}$)
Johnson [JOH 1977]	Zy-2 no irradiated (M)	Columbia river water	~ 90	1.75 y 4.0 y	diffraction colors of the oxide film	3.3 (1) 2.0 (1)
	Zy-2 irradiated (M)			1.75 y 4.0 y		6.0 (1) 4.5 (1)
Fraker *et al.* [FRA 1990]	Zy-2, 4 (M)	J-13 water pH 8.3	95	-	electrochemistry	0.2 - 1
Kato *et al.* [KAT 2013] see text	Zy-4 (M)	pure water	30 50 80	180 d	hydrogen output + uptake	3 (2) 9 (2) 11 (2)

* Zy-2 (or 4) = Zircaloy-2 (or 4); (M): surface of sample in metallic condition (as-polished, pickled…)
(1) The thickening oxide rates have been converted into Zircaloy corrosion rates (see Appendix 1)
(2) Corrosion rates calculated over the period 90 – 180 days (see text)

Kato *et al.* [KAT 2013] carried out corrosion tests of 180 days in pure water at 30, 50 and 80°C, using a hydrogen measurement technique to determine equivalent corrosion rates (see equation {1}). A part of hydrogen generated by the anaerobic corrosion of Zircaloy in water is released as gas and the rest is absorbed in Zircaloy. Tests were performed on Zircaloy-4 in metallic state but not on pre-oxidized specimens. Their results are shown on Figure 40. As expected, the metal losses are very low and within the pre-transition period, where the kinetics of corrosion is *a priori* cubic. However the authors find that the data at pH 12.5 would be better represented initially by a parabolic law. One can calculate that the variations of the average losses of metal between 90 and 180 days would correspond, if the corrosion kinetics were supposed linear, to corrosion rates of 3 $nm.y^{-1}$ at 30°C and 11 $nm.y^{-1}$ at 80°C (Table 21).

It should be noted that the hydrogen pick-up ratio of Zircaloy-4 reaches values of about 90 % at 30 and 50°C. The pick-up ratio decreases with temperature and is about 35 % at 160°C [KAT 2013]. We have seen in paragraph 2.1.2.1.3 that the pick-up ratio ranges between 10 and 20 % in PWR primary water at high temperature.

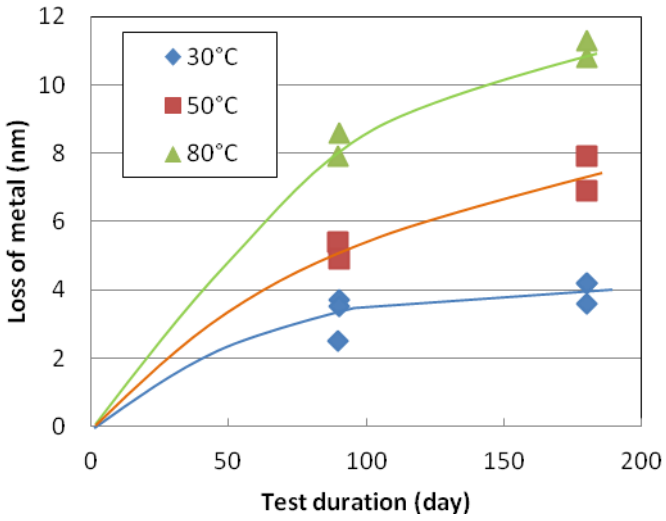

Figure 40: Evolution of metal loss (deduced from hydrogen measurement) of Zircaloy-4 in pure water between 30 and 80°C [KAT 2013]

Corrosion rates of Zircaloy in pure water were nevertheless calculated by fitting these data to a cubic rate law (see equation {4}) irrespective of actual time dependence [TAN 2013]. The rate constants thus calculated were compared with the data and pre-transition rate constant determined by Hillner. The results are shown on Figure 41. The pre-transition corrosion rate constant, k_{Co} in equation {4}, derived from low-temperature corrosion data gradually deviates from the estimate from the high-temperature corrosion equation and increases as temperature decreased. Tanabe *et al.* have identified possible reasons for corrosion rate constant deviation between high and low temperatures, in particular [TAN 2013]:

- method for calculating the constant rate by a cubic law while experience rather leads initially to a parabolic law;
- differences in properties of the oxides formed at low and high temperatures;
- low solubility of hydrogen in Zr alloys at low temperature (see Figure 7a) and effect of hydrides known to accelerate the kinetics of corrosion of Zircaloy in water at high temperature [BLA 1996, KID 1997, BLA 2000, KIM 2014].

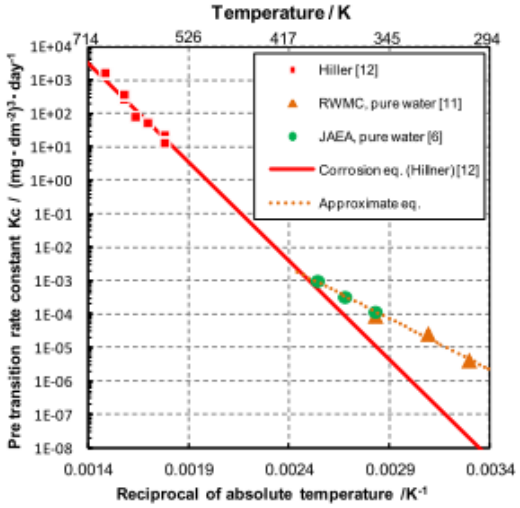

Figure 41: Corrosion of Zircaloy in pure water: pre-transition rate constant k_{Co} as function of the inverse absolute temperature [TAN 2013]

Table 22 mentions the corrosion rates recommended by nuclear waste management agencies or their partner laboratories, from their analysis of the literature, mostly in the context of direct disposal of spent fuel.

Table 22: Corrosion rates of Zircaloy recommended for deep repository conditions in neutral environments

Waste diposal agency or partner laboratory (see the glossary)	Waste *	Environment	r_{corr} ($nm.y^{-1}$)
LLNL [ROT 1984]	SNF	tuffaceous rock (Yucca Mountain)	2
SKB [SKB 1999, SKB 2006]	SNF	granitic groundwater	2 (5 **)
Nagra [JOH 2002]	Hulls	-	≤ 10
NWMO [SHO 2010]	SNF	granitic groundwater	< 1

* SNF: spent nuclear fuel
** conservative value corresponding to the growth of an oxide film of ~ 8 nm thickness during the first year and leading to the passivation of a freshly exposed surface.

At this point, we can state that corrosion rates of Zircaloy hulls coated with their zirconia layer are very likely lower than 1 $nm.y^{-1}$ in neutral free-fluoride waters at low temperature. Assuming that corrosion occurs on both sides of a hull, such a corrosion rate under deep geologic repository conditions would correspond to a lifetime of hulls (minimum thickness: 0.5 mm), assumed not fractured, of approximately 2.5 10^5 years, i.e. to a fraction corroded of

4 10^{-6} y^{-1}. In other words, the thickness of metal corroded on each side of hull for 10 half-lives (10 x 5,730 years) of ^{14}C would be only of ~ 60 µm.

5.2.5 Uniform corrosion of Zr-based alloys in alkaline environments

Determining the uniform corrosion rates of Zr alloys in alkaline (cementitious) waters at low temperatures by extrapolation from data set at high temperature does not appear as a rigorous and reliable approach, as in neutral waters, even if low corrosion rates were measured in dilute alkaline solutions at high temperatures. Indeed, the comparison of potential-pH diagrams of zirconium at 25 and 300°C (see Figure 30) does not permit such an approach. Nevertheless, through the results of some studies on the corrosion of Zircaloy in basic environments, the qualitative influence of some parameters can be perceived. However most of this section will be devoted to the analysis of test results at low temperatures (20 – 80°C).

5.2.5.1 At high temperature

Lithium hydroxide being used for pH control of PWR primary water, its influence on the corrosion rate of Zircaloy has been the subject of many works in the past. Other bases were also considered.

a) Lithium hydroxide solutions

For low concentrations of lithium hydroxide, the corrosion rate of Zircaloy is comparable to that measured in pure water. But when it exceeds a critical value, it increases suddenly (Figure 42). Zircaloy-2 and -4 behave identically. Above the critical concentration, corrosion is accompanied by a high hydriding of metal which becomes very brittle. The hydrogen uptake of Zircaloy-4 is much lower than that of Zircaloy-2 [HIL 1962, COR 1962], but higher than that of Zr-Nb alloys.

The threshold values of the critical concentration are given in Table 23. There is a marked influence of temperature.

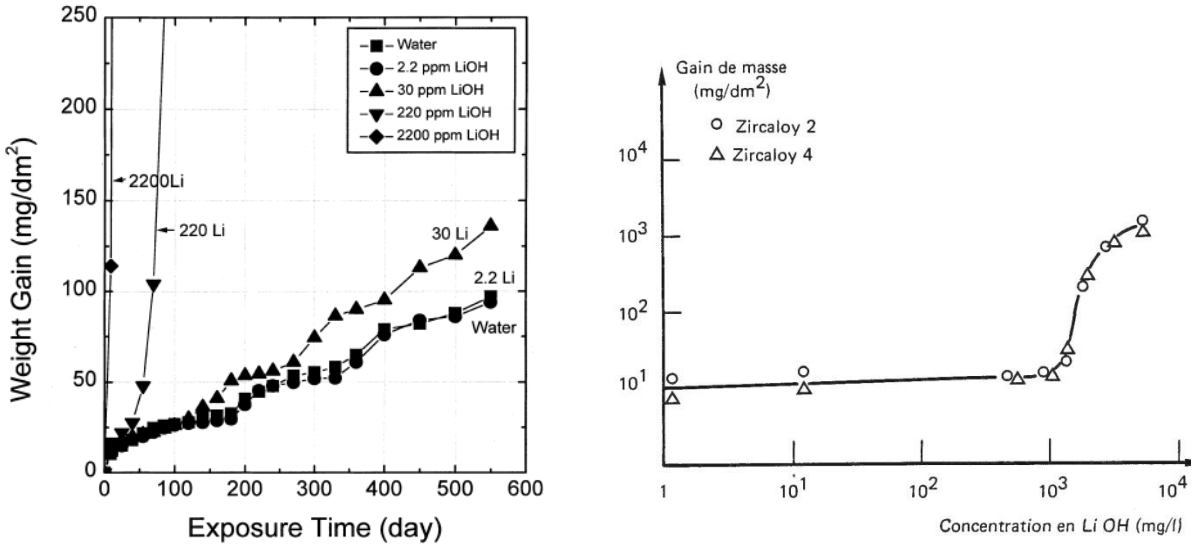

a) Zircaloy-4 in LiOH solutions at 350°C [JEO 1999]

b) Test of 3 days at 360°C [COR 1962]

Figure 42: Influence of LiOH concentration on general corrosion of Zircaloy in water.

Table 23: Threshold values of the critical LiOH concentration on corrosion of Zr alloys in high temperature water

Alloy	Test conditions		Critical concentration ($g.L^{-1}$ LiOH)	Ref.
	Temperature (°C)	Duration (d)		
Zircaloy-2 Zircaloy-4	360	-	0.04 ($pH_{25°C}$ 11.3)	[HIL 1962]
Zircaloy-2 Zircaloy-2 Zr-2.5Nb	360	3 3 3	1.0 1.0 0.1	[COR 1962] [URB 1984] [URB 1984]
Zircaloy-4	350	550	between 0.03 and 0.22 ($11.4 < pH_{25°C} < 12.2$)	[JEO 1999]
Zircaloy-4 Zr-2.5Nb Zr-1Nb	343	16	0.45 0.6 0.6	[MÜL 2013]
Zircaloy-2 Zr-2.5Nb	340	4	0.84	[MAN 1982]
Zircaloy-2 Zircaloy-4	300	- 3	5 > 4	[MUR 1967] [COR 1962]
Zircaloy-2	260	-	8	[CAU 1977]

The kinetics of corrosion of Zircaloy-4 in lithiated water at 360°C is shown in log-log coordinates in Figure 43 as a function of the LiOH concentration. At this temperature, for concentrations lower than 0.06 M (< 1.4 $g.L^{-1}$ LiOH), the corrosion kinetics is cubic then

linear, as in the pure water; for concentrations greater than or equal to 0.1 M (> 2 $g.L^{-1}$ LiOH), only a domain of linear kinetic corrosion is observed.

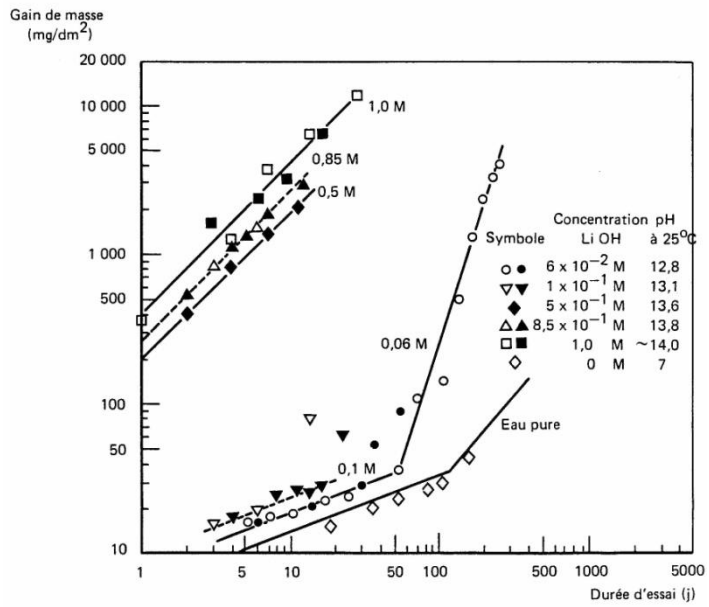

Figure 43: Kinetics of corrosion of Zircaloy-4 in water at 360°C as function of the lithium hydroxide concentration, after [HIL 1962, McD 1984].

The corrosion rate of Zircaloy in the post-transition region, expressed in weight gain, follows the relationship {8} established by Westinghouse, for LiOH concentrations between 10^{-2} and 10^{-1} M [McD 1984]:

$$\ln \frac{\Delta W}{\Delta t} \text{ (mg.dm}^{-2}\text{.d}^{-1}\text{)} = 25.39 + 185.6\,[\text{Li}] - 407.4\,[\text{Li}]^2 - \frac{(32{,}660 + 110{,}540\,[Li])}{RT} \qquad \{8\}$$

The hydrogen pick-up is much higher in presence of lithium hydroxide than in pure water. For solutions of concentration 0.1 M to 1 M LiOH, between 300 and 360°C, it is frequently exceeding 60 % [MUR 1967, KAS 1969b].

Several hypotheses have been proposed to explain the enhancement of corrosion rates of Zircaloy in lithiated waters at high temperature [PEC 1996, JEO 1999]:

- an increase of oxygen vacancies concentration in the oxide caused by the substitution of Li^+ for Zr^{4+} site in the zirconia lattice [HIL 1962];
- a modification of the growth mechanism and microstructure of zirconium oxide [GAR 1991, KIM 1999];
- the generation of pores caused by preferential dissolution of cubic ZrO_2 in zirconia layers exposed to more than 700 ppm Li;
- a detrimental effect of hydrogen [MAN 1982, MAY 1982].

b) Other bases

Corrosion of Zircaloy is much lower in other alkaline environments than in presence of LiOH solutions (Figure 44). The NaOH solutions are more aggressive than those of KOH (Table 24).

The corrosion rate of Zircaloy-2 and -4 in a 1 M KOH solution at 360°C is ~ 1.5 $mg.dm^{-2}.d^{-1}$ [HIL 1962], i.e. approximately 250 times less than in a 1 M LiOH solution with a pH at 360°C equivalent to that of a 0.1 M KOH solution.

The hydrogen pickup fraction decreases in the order: LiOH > NaOH > KOH [JEO 1999].

Table 24: Threshold values of the critical alkaline concentration with regard the corrosion of Zircaloy-2 in water at 360°C (tests of 3 days) [COR 1962]

Base	Critical concentration ($mol.L^{-1}$ OH^-)
LiOH	0.05 (see Figure 42b)
NaOH	0.3
KOH	> 0.5

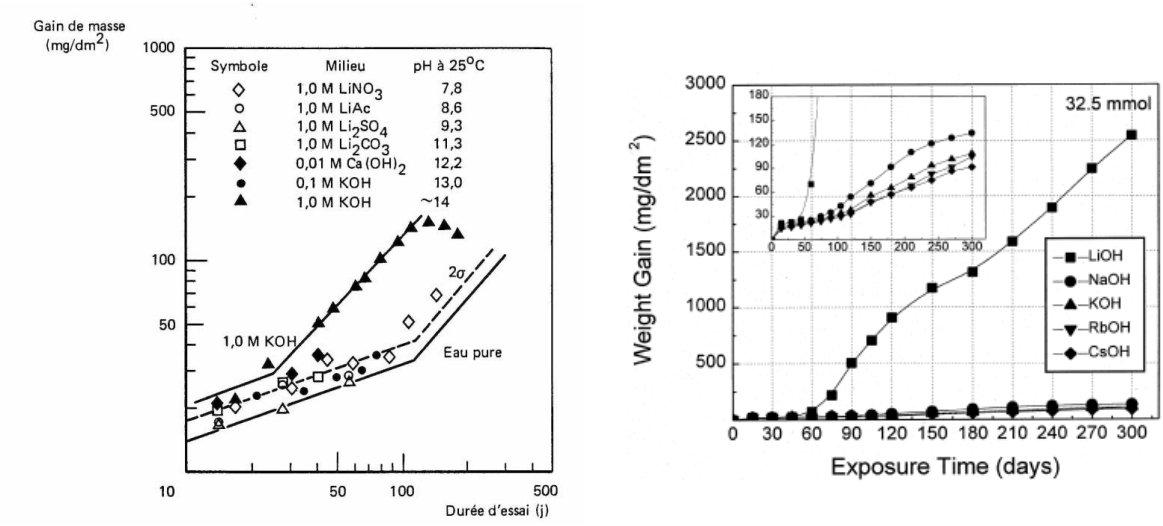

a) Zircaloy-2 at 360°C [HIL 1962] b) Zircaloy-4 at 350°C [JEO 1999]

Figure 44: Corrosion kinetics of Zircaloy in various alkali hydroxide solutions at high temperature.

In summary, alkaline environments at high temperature enhance general corrosion rates of Zircaloy, because of thermodynamic reasons. Moreover, there is a specific effect of the cation, lithium having the most adverse influence. However, the critical concentrations associated with a reversal in the kinetic behaviour of Zircaloy correspond to alkaline pH, significantly higher than those given by thermodynamics (see Figure 30b). Anyway, it is

inadvisable to use the corrosion data obtained at high temperature in alkali hydroxide solutions, even in low concentration, for extrapolation to low temperatures.

5.2.5.2 At low temperature (20 – 80°C)

The remarks made above about tests in neutral waters (see § 5.2.4.2.c) also apply to those in alkaline solutions:

- tests were generally carried out on metallic samples surfaces of zirconium alloy and not on pre-oxidized surfaces; so they explored the beginning of the pre-transition oxidation period;
- the metal losses are very low. Due to the passivation of the metal, the corrosion measured does not present a constant but a decreasing corrosion rate.

Table 25 lists the main data available on the corrosion resistance of zirconium alloys in alkaline environments relevant to the conditions in a low and intermediate level waste repository. The longest tests reach a duration of 5 years. Different methods for measuring the corrosion were used. Electrochemistry and weight measurements are insufficiently sensitive and accurate methods for measuring corrosion rates of the order of $nm.y^{-1}$. The measurement of hydrogen generation appears most suitable method for measuring very low corrosion rates, but requires taking into account not only the hydrogen recovered in the corrosion cell, but also the hydrogen absorbed in the corroded sample, which is very significant in low temperature [KAT 2013] (see below).

The works of Kurashige *et al.* [KUR 1999] and Wada *et al.* [WAD 1999] indicate that there is a higher corrosion rate initially, which gradually falls with time, evidence of the metal passivation. At pH 12.8 and 30°C, the hydrogen generation rate would be equivalent to a corrosion rate of 4 $nm.y^{-1}$ over the first 100 days, 1 $nm.y^{-1}$ averaged over 500 days and ~ 0 beyond 140 days. At 45°C, at pH 10.5 or 12.8, the corrosion rates deduced from the hydrogen-gas-generation is almost 0 beyond 40 days [KUR 1999]. However, these authors did not consider the hydrogen uptake by the metal during corrosion: their values therefore greatly underestimate the corrosion rates.

Kurashige *et al.* also tested samples which were pre-treated with steam at 400°C and 10.3 MPa for 3 days according to the standard ASTM-G2. It is well known that this test, routinely used as an acceptance test for Zircaloy tubing, provides on Zircaloy an oxide of average thickness ~ 1 µm (i.e. weight gain of ~ 15 $mg.dm^{-2}$), that is to say less than the oxide thickness associated with the phenomenon of break-away. The corrosion test was conducted

at pH 12.8 and 45°C: the hydrogen-gas-generation with pre-treated samples was of the same order of magnitude as for un-treated samples at each time [KUR 1999].

Andra and EDF [AND 2013] carried out long duration corrosion tests on Zircaloy-4, M5™, Zirlo™ in two types of alkaline media: a "nominal" cementitious medium (pH 12.5) at 20 and 50°C, a "carbonated" cementitious medium (pH 9) at 20°C. The weight measurements after 3 years do not allow to differentiate the behaviour of the three alloys, whatever the test medium, the mass variations are close to the measurement uncertainty (r_{corr} < 20 nm.y^{-1}). The oxide thicknesses measured by transmission electron microscopy (TEM) are very low, of the order of 15 nm after 3 years, which would correspond to an average corrosion rate of 3.2 nm.y^{-1} over this duration.

Table 25: Conditions and results of corrosion tests of zirconium alloys in alkaline or cementitious waters at low temperature.

Author, Ref	Sample *	Solution	T (°C)	Test duration	Corrosion measurement	r_{corr} (nm.y^{-1})
Hansson [HAN 1984, HAN 1985]	Zy-2 (M)	Cementious water anaerobic conditions pH 12.0 – 13.8	25	-	electrochemistry	< 10
Kurashige *et al.* [KUR 1999]	Zy-4 (M)	Groundwater (Japan) 0.55 M Cl^-, anaerobic pH 10.5 – 12.8	30 45	500 d 400 d	hydrogen output **	1 – 2 1 - 3
Wada *et al.* [WAD 1999]	Zy-4 (M)	"Sea water" + NaOH anaerobic conditions pH 10 – 12.5	30 50	300 d	hydrogen output **	0.2 0.3
Kogawa [KOG 2003]	Zircaloy	anaerobic alkaline	-	1 y	electrochemistry	~ 5
Hélie [HÉL 2004]	Zy-4 (M) M5™ (M)	Cementious water 35 mM Cl^- pH 10.5; 13.5	30 45	-	electrochemistry	6 – 8
EDF R&D [AND 2013]	Zy-4 (M),(H) M5™ (M) Zirlo™ (M)	Cementious water 35 mM Cl^- pH 9; 12.5	25 50	3 y	weighing TEM analysis	< 20 3.2
Kato *et al.* [KAT 2013]	Zy-2 (M) Zy-4 (M)	NaOH or $Ca(OH)_2$ or SGW *** pH 12.5	30 50 80	1825 d	hydrogen output TEM analysis	see Table 26

* Zy-2 (or 4) = Zircaloy-2 (or 4); (M): surface of sample in metallic condition (as-polished, pickled…); (H): pre-hydrided sample.
** The hydrogen uptake is not taken into account in evaluating the corrosion rates.
*** SGW: simulated groundwater: sea water derived groundwater equilibrated with cement. Its composition is the following (in mol.L^{-1}): 3 10^{-5} SiO_2, 1.4 10^{-5} HCO_3^-, 2.4 10^{-4} SO_4^{2-}, 0.6 Cl^-, 0.6 Na^+, 2.8 10^{-2} Ca^{2+}, 7.7 10^{-6} Al^{3+}.

The most precise work on the corrosion kinetics was performed by Kato *et al.* [KAT 2013] that we will now describe on the following figures. The authors conducted their experiments in various types of alkaline solutions (NaOH, $Ca(OH)_2$, simulated groundwater SGW) at pH 12.5 as they did in pure water (see § 5.2.4.2.c). The interest of this work is therefore also to allow a comparison between the two types of environments, all other things being equal (material studied, method of measuring corrosion, test methodology...).

Figure 45 shows the evolution of the metal loss, derived from the hydrogen generation rate, in NaOH solution at pH 12.5, as a function of time and temperature. Zircaloy-2 and 4 were tested; the difference between their corrosion behaviour is not significant. Figure 46 compares the uniform corrosion kinetics of Zircaloy-4 in NaOH solution and in pure water between 30 and 80°C. The average corrosion rates of Zircaloy-4 calculated over the first 2 years of exposure and over the only second year are given in Table 26, together with the corresponding average corrosion rates measured in pure water, but over shorter periods. The corrosion of Zircaloy-4 is equivalent in NaOH and $Ca(OH)_2$ alkaline waters at pH 12.5, but seems to be slightly higher in simulated groundwater SGW (Figure 47), indicating that an element of SGW other than pH causes an acceleration effect [KAT 2013], probably by a complexing effect.

Corrosion of Zircaloy appears slightly higher at pH 12.5 than in pure water (Figure 46), although it remains very low in alkaline medium at low temperatures. The corrosion rates calculated on the second year of exposure in NaOH pH 12.5 is between 1 $nm.y^{-1}$ at 30°C and 2.2 $nm.y^{-1}$ at 80°C. This effect of pH is consistent with the diagram potential – pH of the system zirconium – water (see Figures 29 and 30).

Table 26: Average corrosion rates (in $nm.y^{-1}$) of Zircaloy-4 in NaOH and in pure water over the indicated periods.

Temperature (°C)	NaOH pH 12.5			Pure water	
	Period 0 – 2 years	Period 1 – 2 years	Period 2 – 5 years	Period 0 – 180 days	Period 90 – 180 days
30	4	1.0	-	8	3
50	6	2.0	1.3	15	9
80	10	2.2	-	22	11

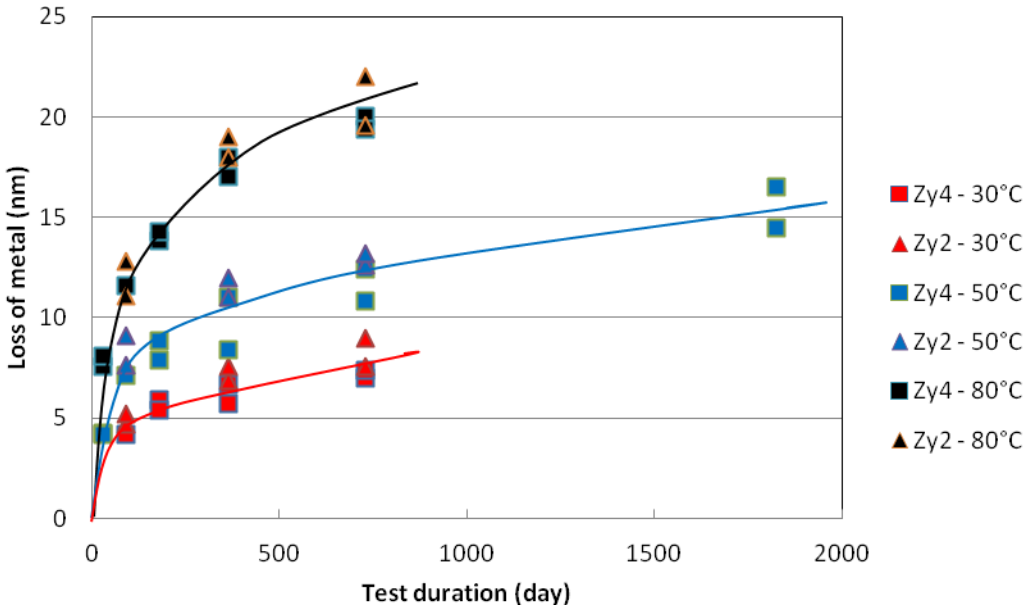

Figure 45: Evolution of the metal loss (deduced from hydrogen generation) of Zircaloy-2 (Zy2) and Zircaloy-4 (Zy4) in NaOH pH 12.5 between 30 and 80°C [KAT 2013]

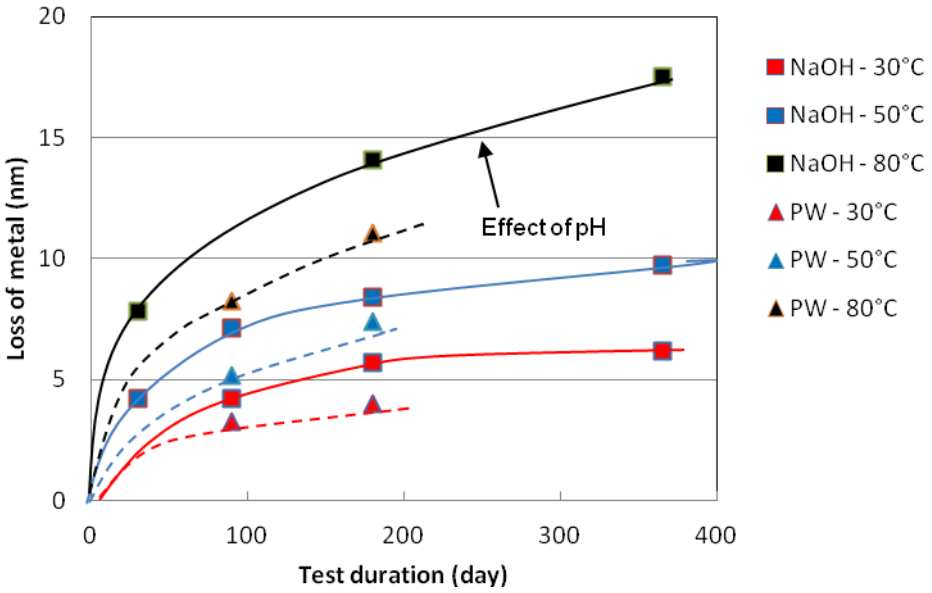

Figure 46: Evolution of the average metal loss (deduced from hydrogen generation) of Zircaloy-4 in NaOH pH 12.5 and in pure water (PW) between 30 and 80°C [KAT 2013]

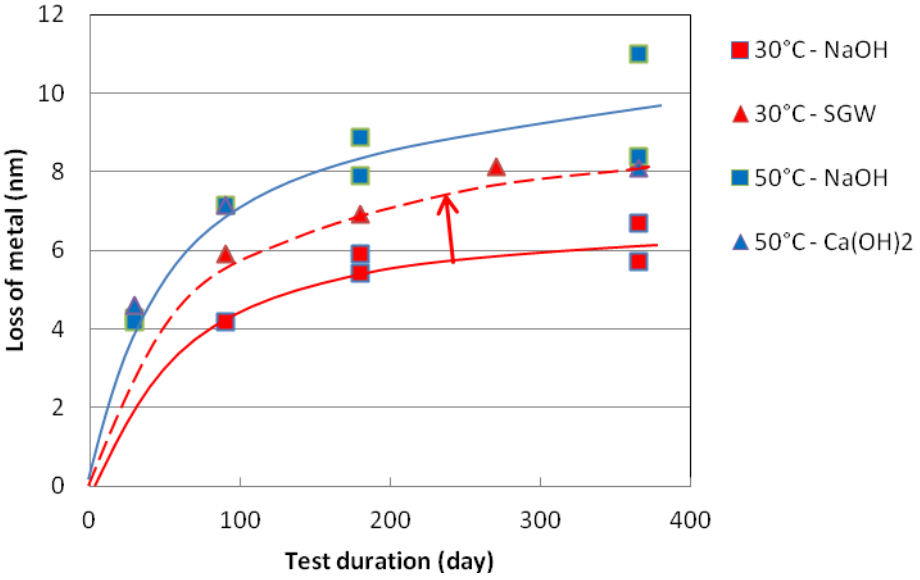

Figure 47: Comparison of the Zircaloy-4 corrosion (deduced from hydrogen generation) at pH 12.5 in NaOH and $Ca(OH)_2$ solutions at 50°C, and in NaOH and SGW solutions at 30°C [KAT 2013]

Failing to compare the variations of the rate constant (cubic law of corrosion) as a function of temperature, it can be noted that the difference of the long term corrosion rate between 30 and 80°C appears to become small (Figure 48).

The hydrogen pick-up ratio of Zircaloy-4 reaches values of about 90 % at 30 and 50°C in NaOH and $Ca(OH)_2$ at pH 12.5, of the same order of magnitude as in pure water at the same temperatures (Figure 49) [KAT 2013]. Thus, the hydrogen produced by the corrosion of hulls will be found predominantly in zirconium hydride insoluble in the zirconium alloy.

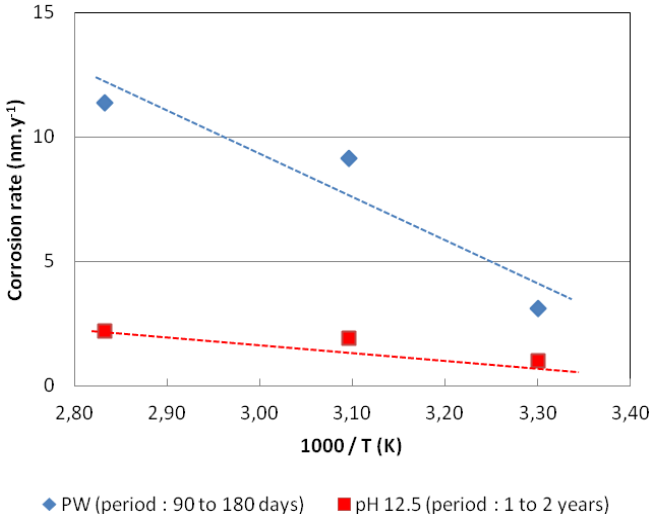

Figure 48: Corrosion rates of Zircaloy-4 calculated at short-term in pure water (PW) and at mean-term in NaOH pH 12.5 (values given in Table 26) as a function of temperature.

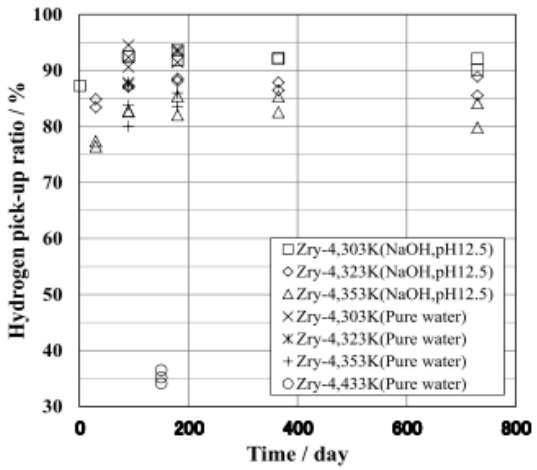

Figure 49: Hydrogen pick-up ratio of Zircaloy-4 during corrosion in pure water and in NaOH pH 12.5 [KAT 2013]

In summary, all these results, established on different Zr alloys and using different measurement techniques and different durations, are consistent, if one takes into account that the corrosion rate of a passive material gradually decreases with time and that a substantial fraction of the hydrogen of corrosion is uptaken in the metal. They lead to very low corrosion rates in alkaline solutions at low temperature, but slightly higher than in pure water, due to a lower stability of the zirconia layer in highly alkaline media. After a few years of exposure in alkaline environments at low temperature (20 to 50°C), the corrosion rate of Zr alloys is expected to be around 1 $nm.y^{-1}$. At short term (< 2 years), corrosion rates ≤ 10 $nm.y^{-1}$ can be measured. The envelope value of ≤ 20 $nm.y^{-1}$, which was sometimes adopted in assessment models, seems too conservative.

When fuel rods are unloaded from reactor, the thickness of unoxidized cladding is between 0.5 and 0.8 mm (see Table 1).

- For a corrosion rate of 1 $nm.y^{-1}$ representative of the hulls behaviour beyond a few years, the lifetime of hulls, assumed not fractured and corroded on both sides, would be of the order of 2.5 to 4 10^5 years, which corresponds to a corroded fraction of 2.5 to 4 10^{-6} y^{-1}. The thickness of metal corroded on each side of hull for 10 half-lives (10 x 5,730 years) of ^{14}C would be only of ~ 60 µm.
- At short term (< 2 years), that is to say especially during the early years of leaching tests, corroded fractions ten times higher (2.5 to 4 10^{-5} y^{-1}) could be measured.

However it should be noted that our knowledge on the corrosion resistance of zirconium alloys at low temperature regards the very beginning of the pre-transition corrosion regime, where the corrosion kinetics should follow a power law (*a priori* a cubic law). It is not

possible, at low temperature, to explore the corrosion regime which is beyond a possible phenomenon of break-away[4], where the corrosion kinetics could be pseudo-linear. Failing that, corrosion tests on samples pre-oxidized in autoclaves should complete the range of tests already performed on samples in metallic condition (as-polished, pickled…) or hydrided condition.

In addition, attention should be given to the fact that the non-corroded metal of hulls will be gradually transformed into zirconium hydride. This will generate on the external surface of hulls a high-density region of hydrides, acting as a brittle layer. In the current state of knowledge, it is difficult to further clarify the fate of this layer: is it capable of inhibiting the corrosion of hulls or should it be treated as waste?

5.3 Leaching experiments of hulls

5.3.1 Operating experience in reprocessing process

During the reprocessing of spent fuel, several situations are likely to lead to an instantaneous release of ^{14}C contained in the oxide layer, especially when the fuel assemblies stay in cooling pools and the hulls are washed in nitric acid then rinsed in hot water.

The experience feedback from industrial reprocessing about the ^{14}C release in aqueous media of the process could provide additional elements in this state of knowledge. It seems that there are no published data.

According to Smith, a washing in nitric acid, similar to that experienced by hulls during the dissolution treatment of spent fuel, does not appear to affect the amount or pattern of ^{14}C release [SMI 1993].

5.3.2 Japanese experiments

Some radionuclides distributed in the zirconium oxide, including ^{14}C, have been assumed to have an instantaneous release after disposal. For instance, it was shown that the release of iodine implanted into the zirconia in contact with an alkaline environment comprises two phases: a phase of rapid release and a phase of slow release [POU 2002]. The question arises in the same way for the release of ^{14}C from hulls. Is it only correlated to the dissolution rate of zirconia (respectively the corrosion rate of metal) or does it exist in the oxide as a labile

[4] The oxide thickness for which the break-away phenomenon is observed on Zircaloy in high temperature water is about 2.5 µm (corresponding to a weight gain of 30 to 40 $mg.dm^{-2}$).

fraction of ^{14}C easily mobilized in aqueous medium, through for example short circuits as grain boundaries?

As shown above (see § 4.2.2.2), the thermal diffusion of ^{14}C in the zirconia is also likely to play a role in the release process, even at room temperature. Strictly speaking, this mechanism should be taken into account in interpreting the results of leaching, especially if the release by other mechanisms (zirconia dissolution, grain boundary migration...) is very low.

Leaching tests were carried out by RWMC and its partners using irradiated Zircaloy claddings from PWR (burn-up: 47.9 $GWd.t^{-1}$, N content: 47 ppm) and BWR (burn-up: 39.7 $GWd.t^{-1}$, N content: 34 ppm) spent fuel to investigate the relationship between the hull corrosion and ^{14}C release behaviour [YAM 1999, TAN 2007, YAM 2013]. Tests were conducted on two types of specimen: hull specimen, hull specimen without oxide film (i.e. Zircaloy metal). The leaching solutions were a simulated groundwater at pH 12.5 (SGW; sea water derived groundwater equilibrated with cement whose the composition is given in Table 25) or a NaOH solution at pH 12.5, at room temperature, in anoxic conditions. The published leaching tests results are shown in Table 27 and Figure 50. These tests will be continued for 10 years [YAM 2013]. The characterization of chemical forms of ^{14}C released in these tests is presented in § 6.3.

Table 27: Results of leaching tests at room temperature performed by RWMC *et al.*

A. Tests on PWR hulls (32 kBq $^{14}C.g^{-1}$): fraction of ^{14}C inventory released after exposure in SGW at pH 12.5 [YAM 1999, TAN 2007]

Specimen	**Test duration (year)**			
	0.25	**0.46**	**0.75**	**0.96**
Hull specimen compressed	$4.26\ 10^{-4}$	$3.65\ 10^{-4}$	-	-
Hull specimen	-	$2\ 10^{-4}$	$3.1\ 10^{-4}$	$3.3\ 10^{-4}$
Hull metal (without oxide)	-	$2\ 10^{-5}$	$3\ 10^{-5}$	$3\ 10^{-5}$

B. Tests on BWR hulls (17.4 kBq $^{14}C.g^{-1}$): total fraction of ^{14}C inventory released after exposure in NaOH at pH 12.5. Several analyses were performed on the same test leachate [YAM 2013]

Specimen	**Test duration (year)**			
	0.5	**0.75**	**1.0**	**2.0**
Hull metal (without oxide)	$3.50\ 10^{-6}$ $2.85\ 10^{-6}$	$3.54\ 10^{-6}$ $3.24\ 10^{-6}$	$1.34\ 10^{-6}$ $1.24\ 10^{-6}$	$2.33\ 10^{-5}$ $3.38\ 10^{-5}$ $7.06\ 10^{-6}$ $6.59\ 10^{-6}$

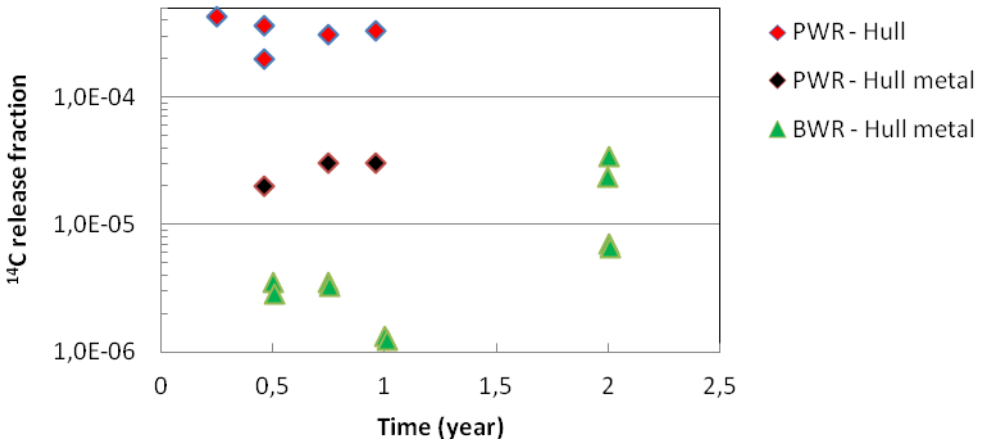

Figure 50: Fraction of ^{14}C inventory released during leaching tests of PWR and BWR hulls in SGW or NaOH solutions at pH 12.5 at room temperature [TAN 2007, YAM 2013]

These results show that the ^{14}C radioactivity leached from a hull specimen without oxide layer is one order less compared to ^{14}C leached from the same hull specimen with its oxide layer, and that the BWR samples present a lower ^{14}C release fraction than the PWR samples during the first year of testing. To explain this last result as well as the results obtained on BWR hulls after two-year immersion, the authors confess that further investigations based on longer-term test results will be needed to better understand the origin of the measured releases, considering low concentrations, uncertainties and scattering associated with this type of test [YAM 2013].

One source of uncertainty is related to the fate of ^{14}C released during the corrosion of Zircaloy: there is a possibility of a mechanism in which ^{14}C is not released immediately by corrosion but is incorporated into the oxide film and then released by diffusion or during the zirconia dissolution [YAM 1999].

Note: one can try to treat the inverse problem by assuming that the ^{14}C release is congruent with the oxide dissolution or Zircaloy corrosion. What would be the released fraction corresponding to a given alteration of the oxide layer or Zircaloy, knowing the initial thickness of oxide or metal? Figure 51 shows the variations of the release fraction as a function of the thickness of oxide dissolved (on its external face) or metal corroded (on both sides of the hull). This figure verifies or confirms:

- the higher apparent release of oxide layer, thinner than the metal (one order of magnitude for an oxide thickness of 20 µm);
- the low level of alteration of hulls (oxide and metal) in alkaline solutions at pH 12.5.

In summary, the present results do not show the existence of an instantaneous ^{14}C release of hulls in the conditions studied (alkaline solutions at pH 12.5 at room temperature). The ^{14}C release seems to be congruent with the oxide layer dissolution and metal corrosion.

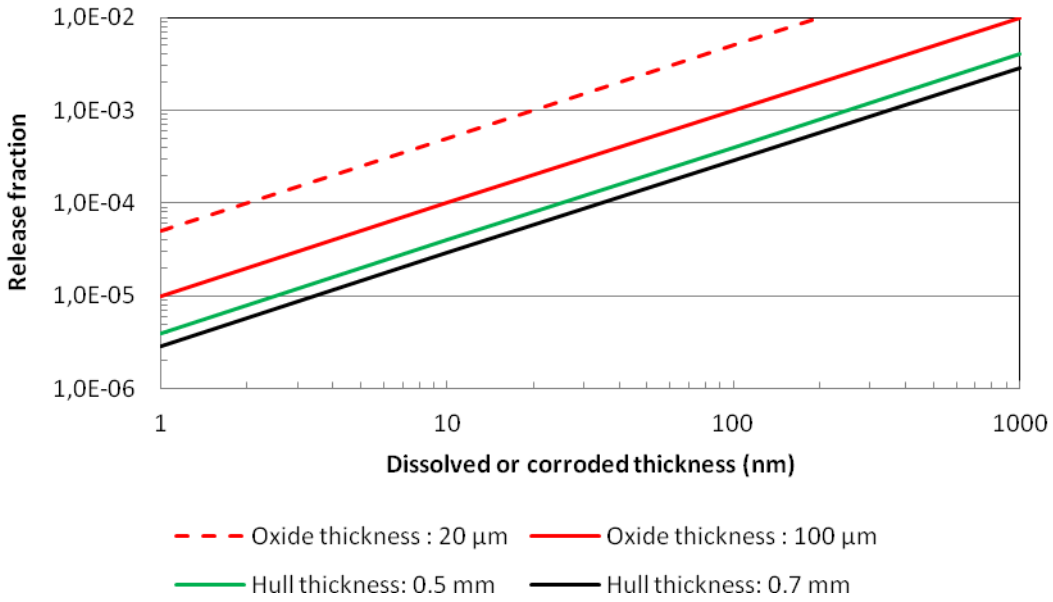

Figure 51: Variations of the release fraction assumed to be congruent with the dissolution of oxide layer or to the hull corrosion as a function of the altered thickness and the initial thickness of oxide or metal cladding. The oxide dissolution is assumed to occur only on its external face, the metal corrosion on both sides of hull.

6 Speciation of released ^{14}C

In addition to the rate of release, the chemical form of ^{14}C controls its fate in the cementitious or argillaceous near field of ILW cells. Indeed the assessment of the long-term behaviour of ^{14}C in the near field requires to know the speciation of ^{14}C released from the hulls during the course of anoxic corrosion of Zr alloys. Is ^{14}C released from hulls in inorganic species (CO_2, carbonate) or labelled organic compounds? Is it mobilized in gaseous species (CO, CO_2, CH_4) or dissolved in aqueous solutions? Other questions arise, related to the interaction (sorption, precipitation…) with cement or clay, but these do not fall within the scope of the present report.

It is generally considered that there is evidence for a high percentage of organic ^{14}C release from activated metals [JOH 2003] and that the organic form of ^{14}C has a potential for volatilization under repository conditions. However, the origin and the reaction mechanism of organic molecules are not fully understood. The versatile chemistry of carbon

(organic/inorganic) has in recent years raised its importance concerning nuclear waste disposal.

This chapter presents the results published in the literature on the chemical forms of carbon released in atmosphere at relatively high temperature (§ 6.2) or during the course of zirconia dissolution and Zircaloy corrosion (§ 6.3). At first, we will try to see what are the expected species based on thermodynamic predictions (§ 6.1).

6.1 Thermodynamics of the C – H – O system

Carbon has one of the richest chemistry among the elements. As for all elements, the chemical form of ^{14}C is controlled by the redox potential (or pe), the pH and the temperature of the system. Carbon can exist in various oxidation states, from the +IV state (in CO_2 and carbonic species) to the -IV state (as methane). Several intermediate states exist, in inorganic and organic forms. Potential – pH diagrams display the domains of stability of possible solids or gases, and the domains of dominance of soluble species. By way of examples, Figure 52 shows Pourbaix diagrams of the C-H-O system, as determined by considering the predominance of gaseous carbon derivatives CH_4 and CO_2, or formate and carbonates. So Figure 52a reflects the ^{14}C chemical species produced in the effluents of LWRs, where 80 to 95 % of the ^{14}C is released in gaseous form. The molecular form of the ^{14}C in PWR gaseous effluents is 75 to 90 % hydrocarbons (primarily methane), whereas a BWR releases about 95 % as CO_2 and 5 % as hydrocarbons [EPR 1995].

In the specific framework of the release of ^{14}C from activated wastes, PSI has examined all the work performed on the thermodynamic modelling of the C-H-O system. This work shows the spectacularly rich organic chemistry of carbon, especially if one takes into account that complete stable redox equilibrium is seldom achieved in the C-H-O system, at least at moderate temperatures [WIE 2010].

Hence, Wieland and Hummel have explored the chemical thermodynamics of the C-H-O system for small organic molecules (containing one up to five carbon atoms); organic compounds in the solid or gaseous state have not been considered in their study [WIE 2010]. The predominant dissolved species in the case of complete thermodynamic equilibrium are $CO_2(aq)$, HCO_3^-, CO_3^{2-} and methane $CH_4(aq)$ (Figure 53). All other organic species are found at trace levels or are thermodynamically unstable. The maximum equilibrium concentrations of these organic species do not exceed 10^{-8} M, i.e. five orders of magnitude below the total dissolved organic carbon.

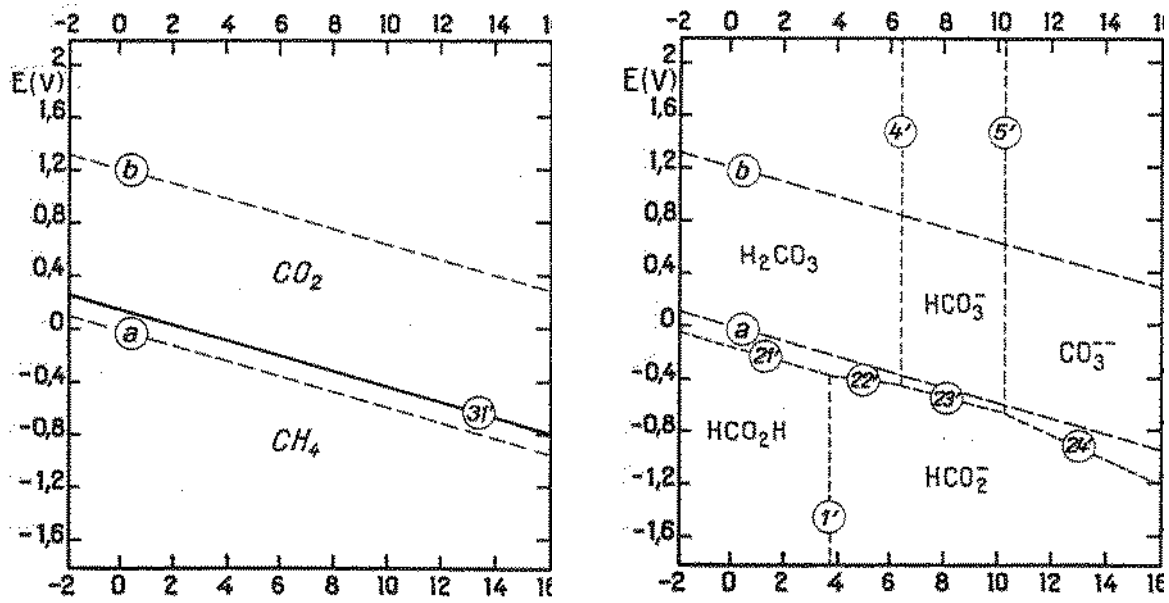

a) b)

Figure 52: Domains of relative predominance of the gaseous carbon derivatives CH_4 and CO_2 (stable equilibrium) (a) and domains of relative predominance of carbon in the form of formate and carbonates at 25°C (b) [POU 1963].

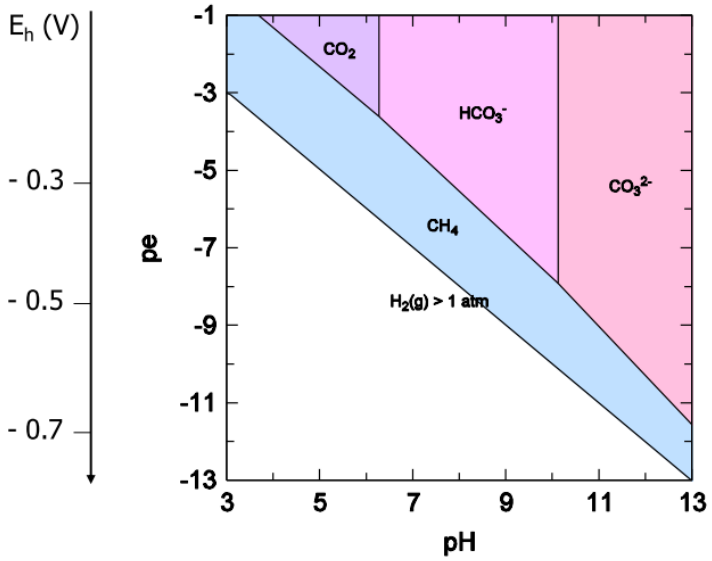

Figure 53: Predominance diagram of aqueous species for complete thermodynamic equilibrium in the C-H-O system at 25°C. Total dissolved carbon = 10^{-3} $mol.kg_{H2O}^{-1}$ [WIE 2010].

At pH 7.5, the trace organic species calculated in the ppm to ppb range are formate $HCOO^-$ > acetate CH_3COO^- > ethane C_2H_6(aq). Formic acid HCOOH(aq) and acetic acid CH_3COOH(aq) are in the ppb to ppt range. In the ultra-trace range below the ppt level, at the

verge of insignificance, we find methanol $CH_3OH(aq)$, propane $C_3H_8(aq)$, propanoate $C_2H_5COO^-$ and oxalate $C_2O_4^{2-}$ (Figure 54a).

At pH 12, the calculated speciation becomes much simpler; the trace organic species found below a concentration of 10^{-9} M, i.e. below the ppm level of total dissolved organic carbon, are only formate $HCOO^-$ > acetate CH_3COO^- ≈ ethane C_2H_6 (aq) (Figure 54b).

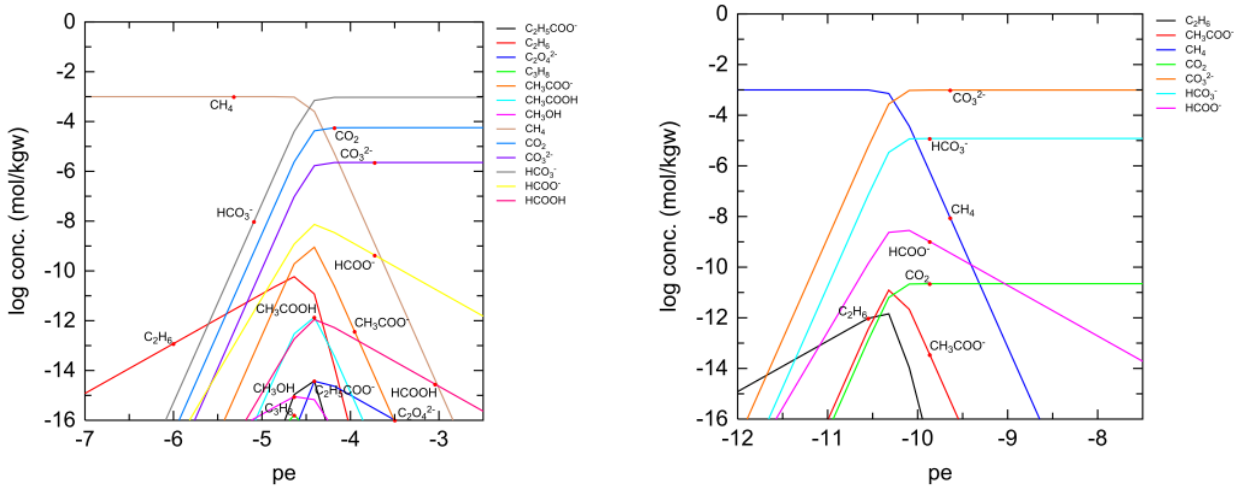

a) at pH 7.5 b) at pH 12

Figure 54: Aqueous species distribution for complete thermodynamic equilibrium in the C-H-O system at 25°C. Total dissolved carbon = 10^{-3} mol.kg$_{H2O}^{-1}$ [WIE 2010].

To take into account the fact that complete stable redox equilibrium is seldom achieved in the C-H-O system at moderate temperatures, Wieland and Hummel have also calculated partial thermodynamic equilibria, assuming, as a first step, that dissolved methane, the most reduced form of carbon, is not formed, then, in a second step, that dissolved alkanes, i.e. methane, ethane, propane, butane and pentane are not formed. With these assumptions, the authors established the diagram of Figure 55 and calculated the distributions shown in Figure 56.

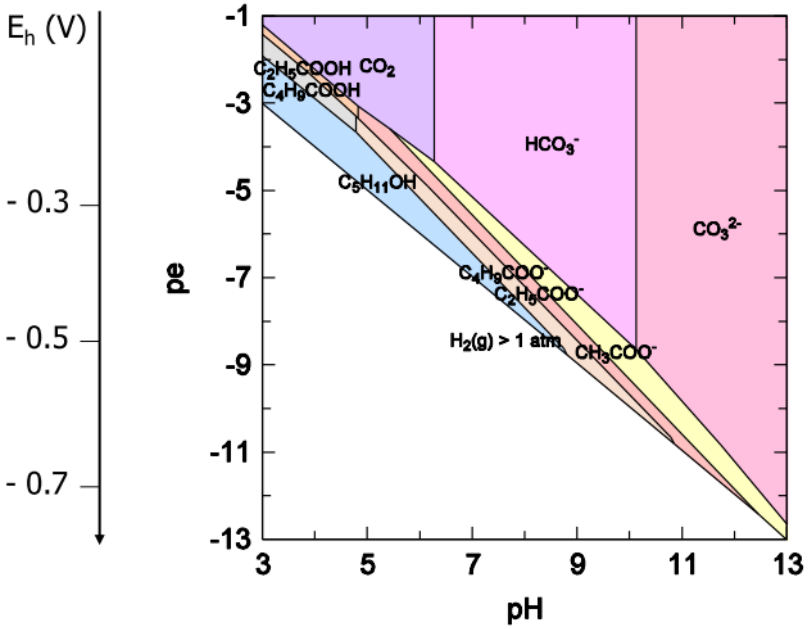

Figure 55: Predominance diagram of aqueous species for partial thermodynamic equilibrium in the C-H-O system at 25°C. It is assumed that no alkanes are formed. Total dissolved carbon = 10^{-3} mol.kg$_{H2O}^{-1}$ [WIE 2010].

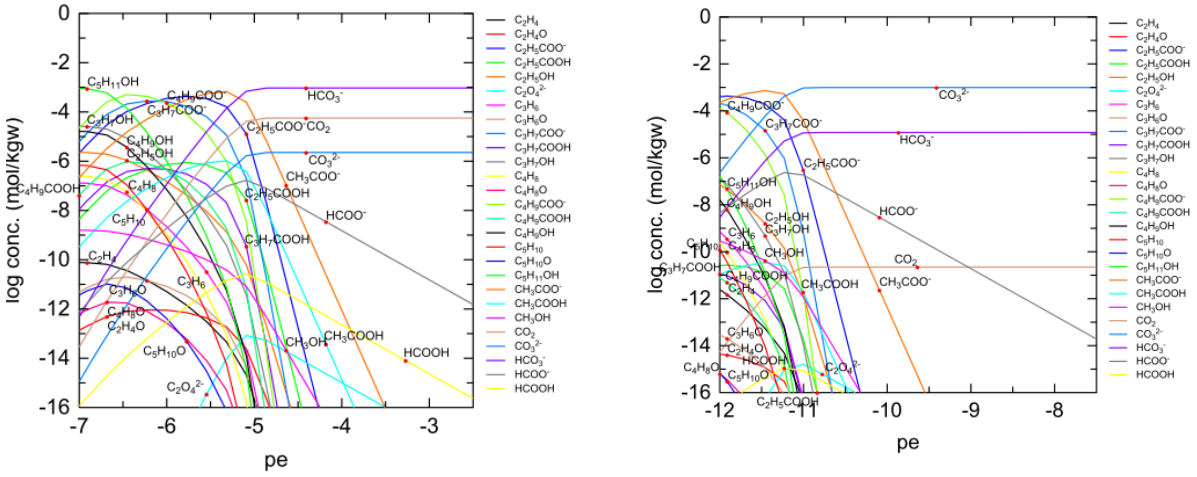

a) at pH 7.5 b) at pH 12

Figure 56: Aqueous species distribution for partial thermodynamic equilibrium in the C-H-O system at 25°C. It is assumed that no alkanes are formed. Total dissolved carbon = 10^{-3} mol.kg$_{H2O}^{-1}$ [WIE 2010].

In the case of partial thermodynamic equilibrium where no alkanes are formed, the predominant dissolved species are the carboxylic acids and, at low pH and very reducing conditions, a higher alcohol (Figure 55). The stability field of these organic species with respect to carbonate is much smaller than the stability field of methane in the case of complete equilibrium (Figure 53). Especially at high pH, metastable carboxylic acids are in partial

thermodynamic equilibrium with carbonate only under very reducing conditions at the verge of the stability of water (Figure 55).

At pH 7.5 and -7 < pe < -5, the predominant species are the carboxylic acids acetate CH_3COO^-, propanoate $C_2H_5COO^-$, butanoate $C_3H_7COO^-$, pentanoate $C_4H_9COO^-$ (Figure 56a). Formate $HCOO^-$ remains a minor species with a maximum concentration of 100 ppm. Under the most reducing conditions at the border of the water stability, equilibria between different alcohols are calculated, with l-pentanol $C_5H_{11}OH(aq)$ as the dominating species, l-butanol $C_4H_9OH(aq)$ and l-propanol $C_3H_7OH(aq)$ in the per cent range, ethanol $C_2H_5OH(aq)$ at the per mille (!) level and methanol $CH_3OH(aq)$ at the ppm level. The aldehydes acetaldehyde $C_2H_4O(aq)$, propanal $C_3H_6O(aq)$, butanal $C_4H_8O(aq)$ and pentanal $C_5H_{10}O(aq)$ remain trace species well below the ppm level. In summary, when dissolved alkanes are assumed to be not formed, bicarbonate is found to be in metastable equilibrium with carboxylic acids at pH 7.5, and, under the most reducing conditions, also with alcohols and alkenes. The latter are minor species.

At pH 12, the stability range of organic species is restricted to a very narrow range between pe = -10 and the stability of water at pe = -12 (Figure 56b). The predominant (metastable) species are acetate CH_3COO^- and propanoate $C_2H_5COO^-$, with butanoate $C_3H_7COO^-$ and pentanoate $C_4H_9COO^-$ in the per mille to per cent range. Formate $HCOO^-$ remains a minor species with a maximum concentration of 100 ppm, as at pH 7.5. The alcohols ethanol, l-propanol, l-butanol and l-pentanol are the only other organic species in metastable equilibrium above the ppm level.

Wieland and Hummel conclude that the aqueous C-H-O system in complete thermodynamic redox equilibrium would be dominated by carbonate and methane, with insignificant trace amounts of formate, acetate and ethane present at the predominance boundary carbonate – methane. However, complete stable redox equilibrium is seldom achieved in the C-H-O system at moderate temperatures, and this situation is the main cause of uncertainty concerning organic carbon speciation in aqueous systems [WIE 2010]. In other words, the major uncertainties in modelling the C-H-O system are not the uncertainties associated with the thermodynamic data but the model uncertainties, i.e. the question of metastability.

6.2 Chemical forms of ^{14}C released in atmosphere at high temperature

The release of ^{14}C in atmosphere from spent fuel cladding occurs very predominantly in the form of $^{14}CO_2$ [VAN 1991, EIN 1991]. However, we noted above (see § 4.2.2) that, during

dry storage of spent fuel, the analysis of the cask cover gas had revealed not only $^{14}CO_2$ but also ^{14}CO releases [EPR 1989, STE 1996, EPR 2000].

For the disposal project envisaged in Yucca Mountain under oxidizing conditions, it was considered that ^{14}C would be released in the form of $^{14}CO_2$ [COD 1992].

More precisely, the work performed by Smith and Baldwin shows that the initial release observed under both air and argon atmospheres occurs as a desorption of $^{14}CO_2$ from the surface. The reduction in release rate after a short time under argon suggests either that oxidation in air is important for release, or that natural CO_2 in the air facilitates release by exchanging with adsorbed $^{14}CO_2$ on the cladding [SMI 1993].

6.3 Chemical forms of ^{14}C generated during corrosion of zirconium alloys

Most of this research was performed in the framework of the Japanese disposal program for radioactive waste. Essentially, the results have been presented in workshop proceedings: ICEM'99 at Nagoya, Japan; Nagra/RWMC Workshop 2003 at Wettingen, Switzerland [JOH 2003]; Mobile Fission and Activation Products in Nuclear Waste Disposal Workshop 2007 at La Baule, France; and the MRS Symposium 2013 at Barcelona, Spain.

Table 28 summarizes the conditions of tests performed by the Japanese teams (RWMC, Toshiba, Mitsubishi, KEPCO). Essentially, tests were carried out either on irradiated oxidized hulls or on hulls specimen without oxide layer (oxide layer removed mechanically) (see § 5.3.2). Specific tests were also undertaken to clarify the nature of the organic species released in the liquid phase and to explore the effect of the chemical state of carbon in the matrix material: zirconium powder (carbon content: 0.02 wt. %), zirconium carbide ZrC and a mixture of carbon powder and zirconium powder were used for these tests [KAN 2002].

A study on the chemical speciation of ^{14}C leached was carried out by a German team under quite different conditions, in a very corrosive environment for the alloys of zirconium (saturated NaCl solution containing 100 ppm fluoride), at 200°C [KIE 2012].

In the Japanese experiments [YAM 1999, TAN 2007, TAK 2013], samples of the gaseous and liquid phase are withdrawn and analysed after test. Chemical analysis of the liquid phase is based on acid treatment and oxidation followed by CO_2 measurements (Figure 57). Separation and recovery of the gaseous compounds in NaOH is followed by oxidation to generate CO_2 and subsequent CO_2 measurements. The analytical procedure allows the organic from the inorganic ^{14}C chemical form to be distinguished in the liquid phase. In the gaseous phase the

selected analytical procedure allows three types of carbon species to be distinguished: CO_2, CO, and reduced hydrocarbons (e.g., CH_4). ^{14}C is measured with a liquid scintillation counter.

Table 28: Conditions of the tests performed by the Japanese teams (all tests were conducted at room temperature in anoxic conditions).

Material			Leaching solution	Test duration (y)	Ref.
Metal	**Irradiated**	**Oxide (ZrO_2)**			
Zircaloy-4	47.9 GWd.t^{-1}	with	SGW* pH 12.5	≤ 0.92	[YAM 1999, TAN 2007, TAK 2013]
	yes	without	-	≤ 0.92	[YAM 1999]
Zircaloy-2	39.7 GWd.t^{-1}	without	NaOH pH 12.5	≤ 2	[YAM 2013]
Zr (0.02 wt% C) ZrC Zr + C (powder)	no	no	NaOH pH 8 NaOH pH 12.5	≤ 1.33	[KAN 2002, SAS 2003a]

* SGW: sea water derived groundwater equilibrated with cement whose the composition is given in Table 25.

Specific analytical tools such as gas chromatography – mass spectrometry (GC/MS) and high performance liquid chromatography (HPLC) were used to identify the organic carbon compounds in the liquid phase [KAN 2002].

Figure 58 shows the distribution of the ^{14}C chemical form analysis results of the Japanese tests carried out on irradiated hulls.

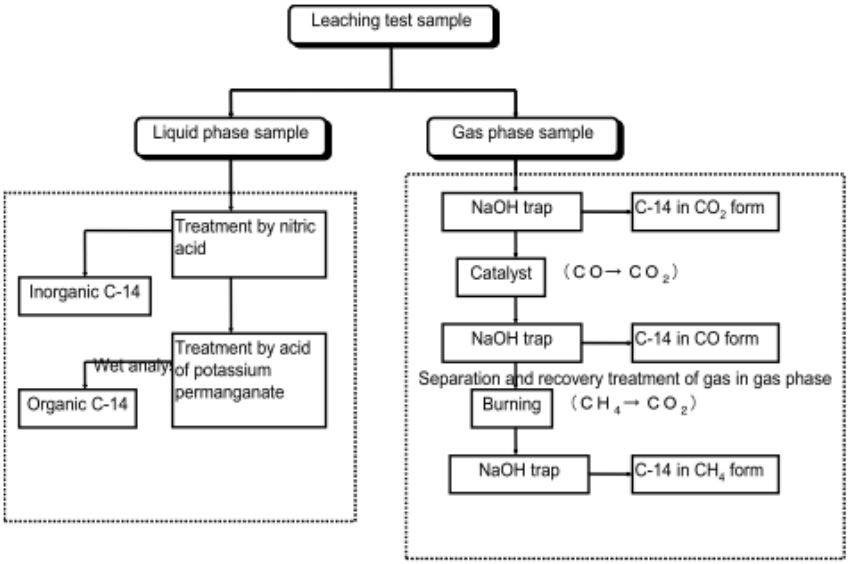

Figure 57: Flowchart of analysis procedure for leaching test used in the Japanese studies [YAM 1999, TAN 2007, YAM 2013].

Material		Time (y)	Ratio of ^{14}C chemical form			Ref.
Zircaloy-4	with oxide	0.25	100 %			[YAM 1999]
		0.46	21.1 %	78.9 %		
		0.92	100 %			
	without oxide	0.46	21 %	79 %		
		0.92	100 %			
Zircaloy-2	without oxide	0.5	20 %	30 %	~ 50 %	[YAM 2013]
		0.75	18 %	32 %	~ 50 %	
		1.0	72 %		28 %	
		2.0	20 %	80 %		

Figure 58: ^{14}C chemical forms leached from hulls in Zircaloy, with or without oxide layer, in alkaline solutions at room temperature:

liquid phase: inorganic carbon

liquid phase: organic carbon

gaseous phase

Yamaguchi *et al.* find that ^{14}C released from PWR samples is detected mainly in the liquid phase and most of the ^{14}C is the organic form, but the ^{14}C labelled hydrocarbons could not be identified separately (compound-specific analysis) for these tests because their concentration was too low [YAM 1999, TAN 2007]. ^{14}C is not present in the gaseous phase neither as CO_2, CO nor CH_4. The chemical form of inorganic carbon in solution, when it is detected after 5.5 months exposure time, is expected to be CO_3^{2-} at pH 12.5. The comparison of the results of Yamaguchi *et al.* and those reported by Takahashi *et al.* [TAK 2013] in an article which focuses on analytical techniques would suggest that the chemical forms of ^{14}C are independent of the presence or not of the oxide layer.

The results obtained by Yamashita *et al.* [YAM 2013] on BWR samples seem to present more variability. Until 9 months and at 2.5 years, ^{14}C exists in the gaseous phase. In the liquid phase, both organic and inorganic ^{14}C co-exist, but the amount of organic ^{14}C is higher than that of inorganic ^{14}C, except in the samples immersed for 1 year.

Another study was carried out by Japanese researchers with the aim of identifying the dissolved carbon species, using no irradiated materials: powder of zirconium, carbide ZrC and mixture of powders of zirconium and carbon [KAN 2002, SAS 2003a, SAS 2003b]. The metallic powders were immersed in solutions of pH adjusted to 8 or 12.5 with NaOH solution. The liquid-to-solid ratio of experimental samples was 1 $mL.g^{-1}$. The authors observe that the portion of carbon in the gaseous phase is small (~ 0.01 %), in the form of alkanes and alkenes

of low molecular weight. Both organic and inorganic carbon species are found to exist in the liquid phase:

- 55 to 85 % of organic carbon species for experiment with the Zr (0.02 wt % C) metallic powder, ~ 90 % for ZrC;
- 15 to 45 % of inorganic carbon species for experiment with the Zr powder, ~ 10 % for ZrC.

While inorganic carbon is expected to be present as HCO_3^- or CO_3^{2-}, depending on pH, organic carbon species are identified as low-molecular weight alcohols, carboxylic acids and aldehydes (Figure 59). The identified carboxylic acids are formic acid (HCOOH) and acetic acid (CH_3COOH) from HPLC, and the aldehyde is formaldehyde (HCHO). Methanol (CH_3OH) and ethanol (C_2H_5OH) are also highlighted. The experimental techniques and analytical protocols used in this study being particularly delicate to implement, Wieland and Hummel consider these results to have much uncertainty [WIE 2010].

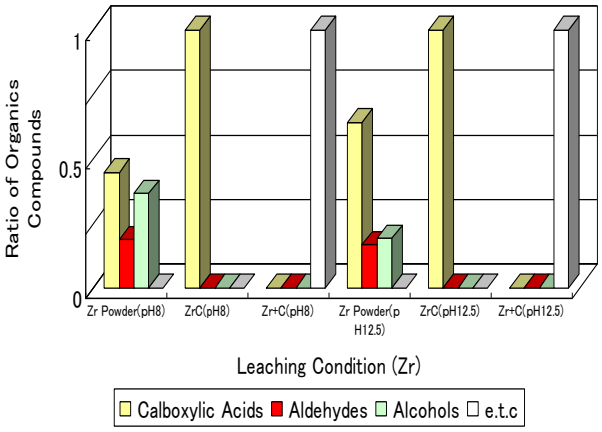

Figure 59: Ratio of organic compounds in leaching solutions for experiments with zirconium, ZrC and a mixture of zirconium and carbon, at pH 8 or 12.5 [KAN 2002]

The stability of the oxygenated hydrocarbons formic and acetic acid, formaldehyde, acetaldehyde, ethanol and methanol was further investigated in batch-type experiments at pH 8 and 12.5 over a duration of 14 months [SAS 2003b]. Decomposition is found to be slightly faster at pH 12.5 than at pH 8, and the extent of decomposition is the same for all compounds.

The results reported by Kienzler *et al.* [KIE 2012] contrast with those of Japanese teams, but they were obtained under very different experimental conditions in terms of pH and corrosion, and above all temperature. Corrosion tests (rather than leaching) were carried out in fluoride solution at 200°C. The ^{14}C results obtained under these conditions indicated that cladding

corrosion mobilizes about 50 % of the ^{14}C in PWR hulls and about 90 % of the ^{14}C in BWR hulls. The mobilized ^{14}C was found ~95 % in the $^{14}CO/^{14}CH_4$ fraction, whereas $^{14}CO_2$ at ~ 5 % represented a minor part (Table 29).

Table 29: Measured speciation of ^{14}C leached from Zircaloy in saturated NaCl + 100 ppm F^-, at 200°C [KIE 2012]

	PWR (Bq.g^{-1})		BWR (Bq.g^{-1})	
	$^{14}CO_2$	^{14}CO / $^{14}CH_4$	$^{14}CO_2$	^{14}CO / $^{14}CH_4$
Gaseous phase	28	10^4	78	$2.4\ 10^4$
Solution	350	16	250	< 19
Solid	98	< 14	< 100	< 50
Sum	480	10^4	420	$2.4\ 10^4$

It is likely we have here an illustration of the influence of temperature on achieving a stable equilibrium in the C-H-O system. A complete stable equilibrium is seldom achieved at moderate temperatures [WIE 2010], whereas it can be more easily reached 200°C.

7 Conclusions

The aim of the present work was to review the current status of knowledge on various aspects related to the release of ^{14}C from zirconium alloys waste (hulls), which is of importance for long-term safety analyses of final repositories for long-lived Intermediate level waste.

7.1 Inventory and distribution of ^{14}C in Zircaloy cladding

In zirconium alloy claddings, the neutron activation of ^{14}N, impurity element of these alloys, is the main source of ^{14}C. ^{17}O coming from the UO_2 (or $(U\text{-}Pu)O_2$) oxide fuel and from water coolant is also a significant precursor of ^{14}C in the zirconia oxide layers formed in reactor on the internal and external sides of cladding respectively. The actual nitrogen content of zirconium alloys is of the order of 30 to 40 ppm, that is to say, about half the maximum level of 80 ppm set as specified or contractual values.

Inventories of ^{14}C in hulls were determined either by calculation or more rarely by direct measurement. For a fuel irradiated at ~ 45 GWd.t_U^{-1}, the production of ^{14}C in cladding is 30 ± 10 kBq.g^{-1}. The analysis of the collected data shows that the power-related ^{14}C production amounts to 1.9 ± 0.4 GBq/GWyr.ppm N. The Japanese experience suggests that the

calculation overestimates the inventory, even when the calculation is carried out with the actual value of the nitrogen content in alloy.

Distribution of ^{14}C between the metal cladding and the zirconia oxide layer depends on the thickness of the oxide. On PWR fuels irradiated at burn-up ≥ 45 GWd.t_U^{-1}, the external oxide layer contains ≤ 20 % of the ^{14}C inventory. On BWR fuels, the thinner external oxide layer contains a lower inventory.

There is a lack of reliable data on the chemical state of ^{14}C in the metal and in the zirconium oxide layer. A modelling approach at the atomic scale would be needed to identify the ^{14}C insertion sites in the metal and in the oxide.

7.2 Release rates of ^{14}C from Zircaloy hulls

The mechanisms and the rate of ^{14}C release from hulls are expected to be controlled in large part by the uniform corrosion rate of Zircaloy, the diffusion rate of ^{14}C from zirconia oxide layers and/or the dissolution rate of zirconia oxide layers, at the time of the contact between hulls and the infiltrated water under the repository conditions. However various questions arise regarding the physical condition of these hulls, i.e., their state of division and fragmentation, at this time. Indeed, the bulk Zircaloy of hulls is hydrided in reactor, which makes the metal brittle and probably more or less fragmented, linked to the extent of burn-up, after press compaction.

7.2.1 Corrosion rates of zirconium alloys

Zirconium alloys are highly resistant to uniform corrosion at low or moderate temperatures, and their susceptibility to localized corrosion (pitting or crevice corrosion) and stress corrosion cracking appears unlikely in anaerobic groundwaters. However, as mentioned above, considerable uncertainties remain regarding the possibility of hydrogen-induced cracking of the press compacted hulls under repository conditions. Nevertheless, regardless of the degree of division of hulls, it can be considered that ^{14}C in the bulk metal of hulls is released congruently with corrosion loss of zirconium alloy. During the corrosion of Zircaloy, there is a possibility of a mechanism in which ^{14}C is not released immediately by corrosion but is incorporated into the oxide film and then released by diffusion or during the zirconia dissolution. It is supported by the fact that measured ^{14}C specific concentration in zirconia oxide layers is about twice of that of Zircaloy metal after irradiation in a reactor.

Various studies show that the uniform corrosion rates of zirconium alloys are very low in anaerobic neutral or alkaline waters at low temperature. The envelope value of 20 nm.y^{-1},

which was sometimes adopted in assessment models, seems excessively conservative. The most recent results lead to corrosion rates of 1 to 2 nm.y^{-1} after a few years of corrosion test. For a corrosion rate of 1 nm.y^{-1}, the lifetime of hulls, assumed not fractured and corroded on both sides, would be of the order of 2.5 to 4 10^5 years, which corresponds to a corroded fraction of 2.5 to 4 10^{-6} y^{-1}. The thickness of metal corroded on each side of hull for 10 half-lives of ^{14}C would be only of ~ 60 µm. In other words, such low corrosion rates will lead to decay of much of the inventory of ^{14}C before release can occur.

However it should be noted that our knowledge on the corrosion resistance of zirconium alloys at low temperature regards the very beginning of the corrosion regime (Figure 60). Now the study of the corrosion behaviour of Zircaloy in high temperature water has shown that, when the zirconia oxide layer reaches a critical thickness of ~ 2.5 µm (corresponding to a weight gain of 30 to 40 mg.dm^{-2}), there is a change of the corrosion regime: the corrosion kinetics firstly follows a power law (*a priori* a cubic law) and after the break-away point a pseudo-linear kinetics. It is not possible, at low temperature, to explore the corrosion regime which is beyond a possible phenomenon of break-away, where the corrosion kinetics could be pseudo-linear. Corrosion tests on pre-oxidized samples (oxide thickness > 10 µm) or hulls should complete the range of tests already performed.

The hydrogen pick-up ratio for Zircaloy reaches values of about 90 % in alkaline and in pure water between 30 and 50°C. So attention should be given to the fact that the non-corroded metal of hulls will be gradually transformed into brittle zirconium hydride, as it will corrode. This will generate on the external surface of hulls a high-density region of hydrides, acting as a brittle layer, and presumably having a corrosion behaviour different from that of zirconium metal.

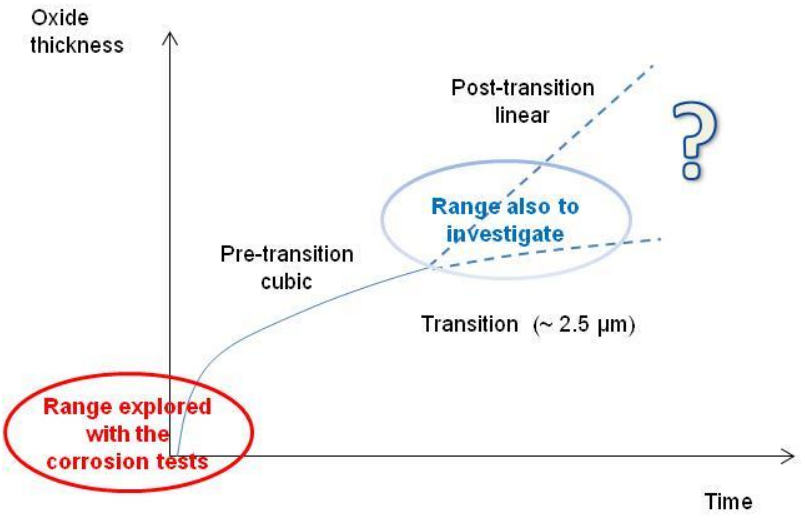

Figure 60: Typical corrosion-time curve of Zircaloy in neutral and alkaline waters

7.2.2 Dissolution rates of zirconia oxide layer

The zirconia oxide layer formed on spent fuel rod cladding is chemically very stable in pure water (a solubility of 10^{-9} M can be considered as a conservative and realistic estimate) The solubility increases with increasing alkaline concentrations, and reaches values of the order of 10^{-6} M at pH 12.5 at ambient temperature. The zirconia solubility remains very low for carbonate concentrations lower than 10^{-2} M. At low to moderate concentrations, chloride ions do not seem to have any significant effect on the zirconia solubility, except in $CaCl_2$ solutions of concentration higher than 0.05 M at pH > 10, due to the formation of a highly soluble complex with calcium.

The dissolution rates of zirconia are less well known and were less studied than the corrosion rates of Zircaloy. In addition, not knowing if the release of radionuclides can be considered as congruent with the dissolution of zirconia, this has led to the conservative assumption in performance assessment studies that oxide layer provides no delay to the release of radionuclides. However, in light of some recent results, a realistic value, but possibly not conservative, of the dissolution rate of zirconia in neutral groundwaters or in cementitious environments, weakly carbonated (< 0.01 M) and fluoride-free, could be very low (order of magnitude: 1 $nm.y^{-1}$).

The recent Japanese experiments of leaching in alkaline solutions at pH 12.5 at room temperature suggest that ^{14}C release would be congruent with the oxide layer dissolution and metal corrosion.

7.3 Chemical forms of ^{14}C released

The aqueous C-H-O system in complete thermodynamic redox equilibrium would be dominated by carbonate and methane. However, complete stable redox equilibrium is seldom achieved in the C-H-O system at moderate temperatures. So the major uncertainties in modelling the C-H-O system are not the uncertainties associated with the thermodynamic data but the model uncertainties, i.e. the question of metastability at moderate temperatures (Figure 61). The chemical stability of organic compounds under the repository conditions is poorly known.

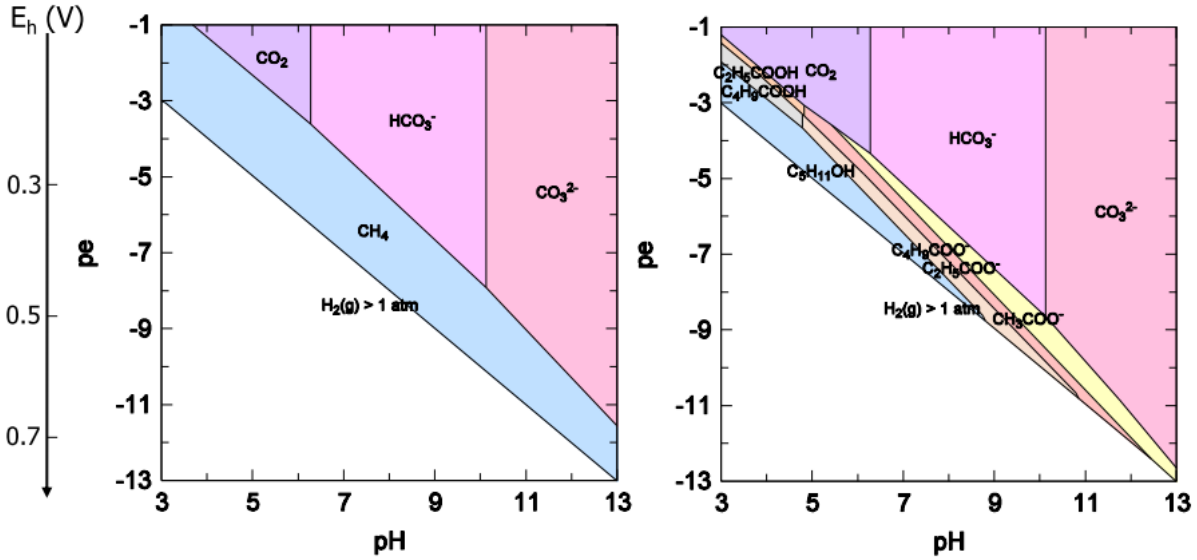

Figure 61: Comparison of complete (left) and partial (right) thermodynamic equilibrium [WIE 2010]

Both organic and inorganic carbons have been identified in leaching experiments with irradiated hulls or no-activated Zr-based materials (powder of Zr, ZrC), although clearly a higher proportion was released as small organic molecules. The origin of these compounds and their reaction mechanisms are not fully understood. The finding that small organic molecules such as short-chain carboxylic acids, alcohols and aldehydes are dominant species raises many questions regarding the ultimate fate of such molecules. Some significant uncertainties remain with respect to speciation of ^{14}C (inorganic vs. organic), as well as the nature of the organic ^{14}C.

References

[ADA 2007] Adamson R., Garzarolli F., Cox B., Strasser A., Rudling P., *Corrosion mechanisms in zirconium alloys*, Advanced Nuclear Technology International Europe AB (ANT International®), October 2007.

[AGA 1975] Agarwala R.P., Paul A.R., *Diffusion of carbon in zirconium and some of its alloys*, J. of Nuclear Materials 58 (1975) 25-30.

[ALL 2012] Allen T.R., Konings R.J.M., Motta A.T., *Corrosion of zirconium alloys*, in Comprehensive Nuclear Materials, Konings R.J.M. ed., vol. 5 (2012) 49-68.

[AMB 2010] Ambard A., Baron D., Blat-Yrieix M., Bouffioux P., Leclerc S., Legras L., *Livre blanc Matériaux du combustible*, EDF R&D Report HT-29-2009-03788-FR, May 2010, 547 pages (in French).

[AND 2005] Andra, *Référentiel de comportement des colis de déchets à haute activité et à vie longue*, Andra Technical Report *Dossier 2005*, Réf. C.RP.ASCM.04.0017.A, 2005, p. 105 (in French).

[AND 2005b] Andra, *Référentiel du comportement des radionucléides et des toxiques chimiques d'un stockage dans le Callovo-Oxfordien jusqu'à l'homme. Tome 2*. Andra Technical Report *Dossier 2005*, Réf. C.RP.ASCM.04.0032.A, 2005, chapter 5, p. 41 (in French).

[AND 2012] *Référentiel du comportement des colis de déchets HA-MAVL. Tome 1. Combustibles usés*, Andra Technical Report, Réf. CG.RP.ASCM.12.0026, octobre 2012 (in French).

[AND 2013] *Référentiel du comportement des colis de déchets HA-MAVL. Tome 3. Déchets MAVL*, Andra Technical Report, Réf. CG.RP.ASCM.12.0026, avril 2013 (in French).

[AOM 2007] Aomi M., Baba T., Miyashita T., Kamimura K., Yasuda T., Shinohara Y., Takeda T., *Evaluation of hydride reorientation behavior and mechanical property for high burnup fuel cladding tube in interim dry storage*. Proceedings of the 15th International Symposium on Zirconium in the Nuclear Industry, June 24-28, 2007, Sunriver, Oregon.

[ASM 1992] ASM Handbook. Volume 3: Alloy phase diagrams, H. Baker editor, ASM International, 1992.

[AST 2002] ASTM B353-02, Standard specification for wrought zirconium and zirconium alloy seamless and welded tubes for nuclear service.

[BAL 2000] Bale M., *Clad degradation – local corrosion of zirconium and its alloys under repository conditions*, US DOE – OCRWM, Report ANL-EBS-MD-000012 REV00, 24 March 2000.

[BAE 1976] Baes C.F., Mesmer R.E., The Hydrolysis of Cations, John Wiley and Sons, New York, 1976.

[BIL 1991] Billot Ph., Giordano A., *Comparison of Zircaloy corrosion models from the evaluation of in-reactor and out-of-pile loop performance*. Zirconium in the Nuclear Industry: 9th Int. Symposium, ASTM-STP 1132, 1991, pp. 539-565.

[BIL 2013] Billone M.C, Burtseva T.A., Einziger R.E., *Ductile-to-brittle transition temperature for high-burnup cladding alloys exposed to simulated drying-storage conditions*, J. of Nuclear Materials 433 (2013) 431-448.

[BLA 1996] Blat M., Noel D., *Detrimental role of hydrogen on the corrosion rate of zirconium alloys*, ASTM STP 1295, 1996, pp. 319-337.

[BLA 1997] Blat M., Bourgoin J., *Corrosion behavior of Zircaloy-4 cladding material: evaluation of the hydriding effect*. International Topical Meeting on Light Water reactor Fuel Performance, Portland, March 1997, ANS, pp. 250-257.

[BLA 2000] Blat M., Legras L., Noel D., Amanrich H., *Contribution to a better understanding of the detrimental role of hydrogen on the corrosion rate of Zircaloy-4 cladding materials*, ASTM STP 1354, 2000, pp. 563-590.

[BLE 1987] Bleier A., Kroebel R., Neeb K.H., Wiese H.W., *Carbon-14 inventories and behaviour in LWR spent fuel rods during reprocessing*, Proc. Int. Conf. on Nuclear Fuel Reprocessing and Waste Management Recod 87, Paris 1987, Vol. 3, pp. 1089-1094.

[BON 1974] Bonka H., Brüssermann K., Schwarz G., *Umweltbelastung durch Radiokohlenstoff aus Kertechnischen Analagen*, Reaktortagung, Berlin, april 1974. Referenced in [FOW 1976].

[BON 1992] Bonnet C., Giraud C., *Dry storage developments in France build on Cascad experience*, Turbomachinery International, October 1992, p. 31.

[BOR 2008] Bordier M., EDF, Division Combustible Nucléaire, private communication, 2008.

[BOS 2004] Bossis Ph., Pêcheur D., Hanifi K., Thomazet J., Blat M., *Comparison of the high burn-up corrosion on M5^{TM} and low tin Zircaloy-4 alloy*, 14th Int. Symposium Zirconium in the Nuclear Industry, Stockholm, 13-17 June 2004, ASTM STP 1467 (2006) pp. 494-525.

[BOS 2007] Bossis Ph, Verhaeghe B., Doriot S., Gilbon D., Chabretou V., Dalmais A., Mardon J.P., Blat M., Miquet A., *In PWR comprehensive study of high burn-up corrosion and growth of M5^{R} and recrystallized low-tin Zircaloy 4*, 15th Int. Symposium Zirconium in the Nuclear Industry, Sunriver, 25-27 June 2007, Journal of ASTM International 6 (2009) 430-457.

[BOU 2000] Bourgeois M., *Retraitement du combustible. Principales opérations*, Techniques de l'ingénieur, Traité Génie nucléaire, article BN 3650, juillet 2000 (in French).

[BOU 2003] Boulanger D., Gens R., Dierckx A., Van Humbeeck H., De Cannière P., *C-14 source term characterization and migration behaviour of C-14 labelled bicarbonate in Boom clay*, Proceedings of a Nagra/RWMC Workshop on the release and transport of C-14 in repository environments, Wettingen, Switzerland, 27-28 october 2003, Nagra Technical Report NAB 08-22, May 2008, p. 94.

[BRA 1981] Bradley E.R., Bailey W.J., Johnson A.B., Lowry L.M., *Examination of Zircaloy-clad spent fuel after extended pool storage*, PNL, Report PNL-3921, 1981.

[BRE 2007] Brendebach B., Altmaier M., Rothe J., Neck V., Denecke M. A., *EXAFS study of aqueous Zr^{IV} and Th^{IV} complexes in alkaline $CaCl_2$ solutions: $Ca_3[Zr(OH)_6]^{4+}$ and $Ca_4[Th(OH)_8]^{4+}$*, Inorg. Chem. 46 (2007) 6804-6810.

[BRO 2000] Brossia C.S., Greene C.A., Dunn D.S., Cragnolino G.A., *Effects of environmental and electrochemical factors on the localized corrosion of Zircaloy-4*, Congress Corrosion Nace, Paper 2210, March 2000.

[BRU 1997] Bruno J., Cera E., de Pablo J., Duro L., Jordana S., Savage D., *Determination of radionuclide solubility to be used in SR97. Uncertainties associated to calculated solubilities*, SKB Technical Report TR-97-33, December 1997, p. 89.

[BUR 2010] Burtseva T.A., Yan Y., Billone M.C., *Radial hydride induced embrittlement of high burnup Zirlo cladding exposed to simulated drying conditions*. NRC Report ML1016-20301 (2010).

[CAU 1977] Causey A., Urbanic V., Coleman C., *In-reactor oxidation of crevices and cracks in cold-worked Zr-2.5Nb*, J. of Nuclear Materials 71 (1977) 25-35.

[CHE 1983] Chen C.M., Aral K., Theus G.J., *Computer-calculated potential pH diagrams to 300°C. Volume 2: Handbook of diagrams*, EPRI Technical Report NP-3137, vol. 2, June 1983.

[CLA 1985] Clayton J.C., Fisher R.L., *Corrosion and hydriding of Zircaloy fuel rod cladding in 633K water and reactor environments*, ANS Topical Meeting on Light Water Reactor Fuel Performance, Orlando, Vol. 1, pp. 3-1 to 3-16, 21-24 April 1985.

[COD 1992] Codell R.B., Murphy W.M., *Geochemical model for ^{14}C transport in unsaturated rock*, High Level Radioactive Waste Management Proceedings of the 3rd International Conference, Las Vegas, Nevada, 12-16 April 1992, pp. 1959-1965.

[COH 1980] Cohen P., Water coolant technology of power reactors, American Nuclear Society, 1980.

[COL 1985] Coleman C.E., Cheadle B.A., Ambler J.F.R, Lichtenberger P.C., Eadie R.L., *Minimizing hydride cracking in zirconium alloys*, Canadian Metallurgical Quaterly Vol. 24 (3), 1985, pp. 245-250.

[COR 1962] Coriou H., Grall L., Meunier J., Pelras M., Willermoz H., *Corrosion du Zircaloy dans divers milieux alcalins à haute température*, J. of Nuclear Materials 7 (1962) 320-327 (in French).

[COX 1973] Cox B., *Zirconium alloys in high temperature water*, in High temperature high pressure electrochemistry in aqueous solutions, Nace-4, D.G. Jones and R.W. Staehle eds., 1973, pp. 67-105.

[COX 1976] Cox B., *Oxidation of zirconium and its alloys*, in Advances in corrosion science and technology, Vol. 5, M.G. Fontana and R.W. Staehle eds, Plenum Press, 1976, pp. 173-391.

[COX 1985] Cox B., *Assessment of PWR waterside corrosion models and data*, EPRI Technical Report NP-4287, October 1985.

[COX 1990] Cox B., E*nvironmentally-induced cracking of Zirconium alloys – A review*, J. of Nuclear Materials 170 (1990) 1-23.

[COX 2005] Cox B., *Some thoughts on the mechanisms of in-reactor corrosion of zirconium alloys*, J. of Nuclear Materials 336 (2005) 331-368.

[CUR 1999] Curti E., Hummel W., *Modeling the solubility of zirconia in a repository for high-level radioactive waste*, J. of Nuclear Materials 274 (1999) 189-196.

[CUR 2002] Curti E., Degueldre C., *Solubility and hydrolysis of Zr oxides: A review and supplemental data*, Radiochimica Acta 90 (2002) 801-804.

[DAL 1976] Dalgaard S.B., *Long-term corrosion and hydriding of Zircaloy-4 fuel clad in commercial PWR with forced convective heat transfer*. 149th Meeting of the Electrochemical Society, Washington, May 1976 (extended abstract).

[DAV 1977] Davis W., *Carbon-14 production in nuclear reactors*, ORNL/NUREG/TM-12, February 1977.

[DEG 2007] Degueldre C., *Zirconia inert matric for plutonium utilisation and minor actinides disposition in reactors*, J. of Alloys and Compounds 444-445 (2007) 36-41.

[DEH 2000] Dehaudt P., Dubois S., Maguin J.C., Huet F., Pelletier M., Lacroix B., Pasquet B., Guérin Y., Hourdequin N., Salot R., Desgranges L., Delette G., Struzik C, *Le combustible nucléaire et son état physico-chimique à la sortie des réacteurs*. Rapport CEA-R-5923 (2000) (in French).

[DOE 1992] US Department of Energy, Office of Civilian Radioactive Waste Management, *Characteristics of potential repository wastes*, DOE/RW-0184-R1, Volume 1, 1992.

[DOU 1971] Douglass D.L., The metallurgy of zirconium, IAEA Rev. (Suppl. 1971).

[DUR 2006] Duro L., Grivé M., Cera E., Gaona X., Domènech C., Bruno J., *Determination and assessment of the concentration limits to be used in SR-Can*, SKB Technical Report TR-06-32, December 2006.

[DYC 1964] Dyce I.H., *Corrosion of Zircaloy fuel cladding – The influence of high heat fluxes*. Nuclear Engineering 9 (1964) 253.

[EIN 1991] Einziger R.E., *Effects of an oxidizing atmosphere in a spent fuel packaging facility*, Focus 1991 Nuclear Waste Packaging, Las Vegas, NV, 29 Sept. – 2 Oct. 1991.

[EIN 2005] Einziger R.E., Brown C.L., Hornseth G.P., Interrante C.G., *Data needs for storage and transportation of high-burnup fuel*, Radwaste Solutions March/april 2005, pp. 44-56.

[ELL 1968] Ells C.E., *Hydride precipitates in zirconium alloys*, J. of Nuclear Materials 28 (1968) 129-151.

[EPR 1989] McKinnon M.A., Michener T.E., Jensen M.F., Rodman G.R., *Testing and analysis of the TN-24P PWR spent-fuel dry storage cask loaded with consolidated fuel*, EPRI Technical Report NP-6191, February 1989.

[EPR 1995] Vance J.N., Cline J.E., *Characterization of carbon-14 generated by the nuclear power industry*, EPRI Technical Report TR-105715, November 1995.

[EPR 2000] Kessler J.H., *Dry cask storage characterization project*, EPRI Technical Report 1000157, June 2000.

[EPR 2006] Adamson R., *Recovery of irradiation damage by post-irradiation thermal annealing. Relevance to hydrogen solubility and dry storage issues*, EPRI Technical Report 1013446, June 2006.

[EPR 2010] *Estimation of carbon-14 in nuclear power plant gaseous effluents*, EPRI Technical Report 1021106, December 2010.

[FOR 1995] Forsberg K., Limback M., Massih A.R., *A model for uniform Zircaloy clad corrosion in pressurized water reactors*, Nuclear Engineering and Design 154 (1995) 157-168.

[FOW 1976] Fowler T.W., Clark R.L., Gruhlke J.M., Russel J.L., *Public health considerations of carbon-14 discharges from the light-water cooled nuclear power industry*, Technical Note ORP/TAD-76-3, Technology assessment division, US Environmental Protection Agency, July 1976.

[FRA 1990] Fraker A.C., Harris J.S., *Corrosion behavior of zirconium alloy nuclear fuel cladding*, Mat. Res. Soc. Symp. Proc. 176 (1990) 549-556.

[FRA 2002] Frank H., *Transport properties of zirconium alloy oxide films*, J. of Nuclear Materials 306 (2002) 85-98.

[GAR 1979] Garzarolli F., von Jan R., Stehle H., *The main causes of fuel element failure in water-cooled power reactors*, IAEA-Atomic Energy Review (1979), Vol. 17, n°1, 31-128.

[GAR 1980] Garzarolli F., Jorde D., Manzel R., Parry G.W., Smerd P.G., *Review of PWR fuel rod waterside corrosion behavior*, EPRI Technical Report NP-1472, August 1980.

[GAR 1991] Garzarolli F., Seidel H., Tricot R., Gros J.P., *Oxide growth mechanisms on zirconium alloys*, Zirconium in the Nuclear Industry, ASTM STP 1132 (1991) 395-415.

[GAR 2011] Garzarolli F., Rudling P., *Performance evaluation of new advanced Zr alloys for PWRs/VVERs*, Advanced Nuclear Technology International Europe AB (ANT International®), October 2011.

[GRA 1988] Gras J.M., *Étude bibliographique de la corrosion généralisée des alliages Zircaloy dans les conditions intéressant le fonctionnement des réacteurs à eau légère*, EDF R&D Technical Report HT-45 PVD654, March 1988, 150 pages (in French).

[GUE 1994] Guenther R.J., Blahnik D.E., Wildung N.J., *Radiochemical analysis of several spent fuel approved testing materials*, Pacific Northwest Laboratory, Technical Report PNL-10113, September 1994.

[GUE 1996] Bailly H., Ménessier D., Prunier C., Le combustible nucléaire des réacteurs à eau sous pression et des réacteurs à neutrons rapides, Eyrolles, 1996 (in French).

[GUI 2009] Guipponi C., *Effets de la radiolyse de l'air humide et de l'eau sur la corrosion de la couche d'oxyde du Zircaloy-4 oxydé*, Thesis, Lyon, December 2009 (in French).

[HAG 1978] Hagrman D.L., Reymann G.A., *Cladding oxidation (Corros and Cobild)*, in A handbook of materials properties for use in the analysis of the LWR fuel rod behavior, MATPRO code 14, US report TREE-NUREG-1280, p. 439.

[HAN 1984] Hansson C.M., *The corrosion of zircaloy 2 in anaerobic synthetic cement pore solution*, SKB Technical Report 84-13, December 1984.

[HAN 1985] Hansson C.M., *The corrosion of steel and zirconium in anaerobic concrete*, Mat. Res. Soc. Symp. Proc. 50 (1985) 475-482.

[HAY 1977] Hayes D.W., MacMurdo K.W., *Carbon-14 production by the nuclear industry*, Health Physics 32 (1977) 215-219.

[HÉL 2004] Hélie M., *Dossiers de synthèse sur le comportement à long terme des colis : dossier de référence phénoménologique CSD-C 2004*, CEA Technical Report, Réf. DPC/SCCME 04-685-A, December 2004 (in French).

[HIL 1962] Hillner E., Chirigos J.N., *The effect of lithium hydroxide and related solutions on the corrosion rate of Zircaloy in 680°F water*, Westinghouse, Report WAPD-TM-307, August 1962.

[HIL 1977] Hillner E., *Corrosion in zirconium-base alloys – An overview*, Zirconium in the nuclear industry, ASTM STP 633 (1977), p. 211.

[HIL 1998] Hillner E., Franklin D.G., Smee J.D., *The corrosion of Zircaloy-clad fuel assemblies in a geological repository environment*, Westinghouse, Bettis Atomic Power Laboratory, Report WAPD-T-3173, 1998, 45 p.

[HIL 2000] Hillner E., Franklin D.G., Smee J.D., *Long-term corrosion of Zircaloy before and after irradiation*, J. of Nuclear Materials 278 (2000) 334-345.

[HSU 2011] Hsu H.H., Tsay L.W., *Effect of hydride orientation on fracture toughness of Zircaloy-4 cladding*, J. of Nuclear Materials 408 (2011) 67-72.

[HUM 2002] Hummel W., Berner U., Curti E., Pearson F.J., Thoenen T., *Nagra/PSI Chemical Thermodynamic Data Base 01/01*, Nagra Technical Report 02-16, July 2002.

[IAE 1998] IAEA, Waterside corrosion of zirconium alloys in nuclear power plants, IAEA-TECDOC-996, 1998.

[IAE 1998b] IAEA, Durability of spent nuclear fuels and facility components in wet storage, IAEA-TECDOC-1012, April 1998.

[IAE 2004] IAEA, Management of waste containing tritium and carbon-14, IAEA Technical Reports Series n°421, 2004, p. 26.

[IAE 2006] IAEA, Understanding and managing ageing of material in spent fuel storage facilities, IAEA Technical Reports Series n°443, 2006, p. 26.

[IRS 2001] IRSN, *Fiche radionucléide Carbone-14*, août 2001 (in French).

[JEO 1999] Jeong Y.H, Baek J.H., Kim S.J., Kim H.G., Ruhmann H., *Corrosion characteristics and oxide microstructures of Zircaloy-4 in aqueous alkali hydroxide solutions*, J. of Nuclear Materials 270 (1999) 322–333.

[JOH 1977] Johnson A.B., *Behavior of spent nuclear fuel in water pool storage*, PNL, Technical Report BNWL-2256 UC70, September 1977.

[JOH 2002] Johnson L.H., McGinnes D.F., *Partitioning of radionuclides in Swiss power reactor fuels*, Nagra Technical Report 02-07, August 2002, p. 21.

[JOH 2003] Johnson L.H., Schwyn B. (eds), *Proceedings of a Nagra/RWMC Workshop on the release and transport of C-14 in repository environments*, Wettingen,

Switzerland, 27-28 October 2003, Nagra Technical Report NAB 08-22, May 2008.

[KAN 2002] Kaneko S., Tanabe H., Sasoh M., Takahashi R., Shibano T., Tateyama S., *A study on the chemical forms and migration behavior of carbon-14 leached from the simulated hull waste in the underground condition*. Scientific Basis of Nuclear Waste Management, MRS Fall Meeting, Boston, 2-6 December 2002.

[KAS 1969a] Kass S., *Aqueous corrosion of the Zircaloys at low temperatures*, J. of Nuclear Materials 29 (1969) 315-321.

[KAS 1969b] Kass S., *Corrosion and hydrogen pickup of Zircaloy in concentrated lithium hydroxide solutions*, Corrosion Nace 25 (1969) 30-46.

[KAT 2013] Kato O., Tanabe H., Sakuragi T., Nishimura T., Tateishi T., *Corrosion tests of Zircaloy hull waste to confirm applicability of corrosion model and to evaluate influence factors on corrosion rate under geological disposal conditions*, Scientific Basis for Nuclear Waste Management XXXVII, Barcelona, Spain, 29 September – 3 October 2013, Mat. Res. Soc. Symp. Proc. 1518.

[KAW 1974] Kawanishi H., Ishino S., Mishima Y., *Directionality of the grain boundary hydride in Zircaloy-2*, in Zirconium in Nuclear Applications, ASTM STP 551 (1974) pp. 201-211.

[KEL 1975] Kelly G.N., Jones J.A., Bryant P.M., Morley F., *The prediction radiation exposure of the population on the European Community resulting from discharges of krypton-85, tritium, carbon-14 and iodine-129 from the nuclear power industry to the year 2000*, Commission of the European Communities, Luxembourg, Doc. V/2676/75, September 1975.

[KID 1997] Kido T., Kanasugi K., Sugano M., Komatsu K., *PWR Zircaloy cladding corrosion behavior: quantitative analyses*, J. of Nuclear Materials 248 (1997) 281-287.

[KIE 2012] Kienzler B., Altmaier M., Bube C., Metz V., *Radionuclide source term for HLW glass, spent nuclear fuel, and compacted hulls and end pieces (CSD-C waste)*, Karlsruhe Institute of Technology, Report-Nr. KIT-SR 7624, 2012.

[KIM 1999] Kim Y.S., Kwon S.C., *Crystallization and degradation of zirconium oxide in various pH solutions*, J. of Nuclear Materials 270 (1999) 165–173.

[KIM 2014] Kim Y.S., Jeong Y.H., Son S.B., *A study on the effects of dissolved hydrogen on zirconium alloys corrosion*, J. of Nuclear Materials 444 (2014) 349-355.

[KNI 1984] Knittel D.R., Bronson A., *Pitting corrosion on zirconium – A review*, Corrosion Nace 40 (1984) 9-14.

[KOB 2007] Kobayashi T., Sasaki T., Takagi I., Moriyama H., *Solubility of zirconium (IV) hydrous oxides*, J. Nucl. Sci. Technol. 44 (2007) 90-94.

[KOG 2003] Kogawa N., *Migration of C-14 in activated metal under anaerobic alkaline condition*, Workshop on C-14 release and transport in repository environments, Wettingen, Switzerland, 27-28 October 2003, Nagra Technical Report NAB 08-22, May 2008.

[KOP 1990] Kopp D., Munzel H., *Release of volatile carbon-14 containing products from Zircaloy*, J. of Nuclear Materials 173 (1990) 1-6.

[KUR 1999] Kurashige T., Fujisawa R., Inagaki Y., Senoo M., *Gas generation behavior of zircaloy-4 under waste disposal conditions*, Radioactive waste management and environmental remediation, ICEM Conference Proceedings, ASME, Nagoya, Japan, 26-30 Sept.1999.

[KUW 1983] Kuwae R., Sato K., Higashinakagawa E., Kawashima J., Nakamura S., *Mechanism of Zircaloy nodular corrosion*, J. of Nuclear Materials 119 (1983) 229-239.

[LAU 2003] Laugier F., *Inventaire radiologique et thermique des assemblages REP usés : combustible UOX 4.95 %*, EDF R&D Technical Report HI-28/2003/022-A, June 2003 (in French).

[LAV 2012] Lavigne O., Shoji T., Sakaguchi K., *On the corrosion behavior of zircaloy-4 in spent fuel pools under accidental conditions*, J. of Nuclear Materials 426 (2012) 120-125.

[LEM 2010] Lemaignan C., *Nuclear materials and irradiation effects*, in Handbook of nuclear engineering, D.G. Cacuci ed., Springer Science, Business Media, Chapter 13, 2010.

[LUM 1999] Lumpkin G.R., *Physical and chemical characteristics of baddeleyite (monoclinic zirconia) in natural environments: an overview and case study*, J. of Nuclear Materials 274 (1999) 206-217.

[MAG 2007] Magnusson Å, *^{14}C produced by nuclear power reactors. Generation and characterization of gaseous, liquid and solid waste*, Doctoral thesis, Lund, Sweden, August 2007.

[MAN 1982] Manolescu A.V., Mayer P., Simpson C.J., *Effect of LiOH on corrosion rate of Zr-2.5Nb in 340°C water*, Corrosion Nace 38 (1982) 23-31.

[MAR 1978] Marino G.P., Fisher R.L., *Corrosion of Zircaloy-4 tubing in 680°F water (LWBR development program)*, WAPD-TM-1322, December 1978.

[MAR 2003] Marimbeau P., Esbelin E., *N and C-14 content of spent fuel*, Proceedings of a Nagra/RWMC Workshop on the release and transport of C-14 in repository environments, Wettingen, Switzerland, 27-28 October 2003, Nagra Technical Report NAB 08-22, May 2008.

[MAR 2004] Marimbeau P., *Recommandations pour les inventaires initiaux d'impuretés dans les assemblages combustibles des PWR, pastilles UOx et MOx et structures*. CEA Report SPRC/LECy 2003-331/DR, 24 février 2004 (in French).

[MAR 2008] Mardon J.P., *Matériaux des tubes de gainage pour réacteurs à eau pressurisée*, Techniques de l'ingénieur, Traité Génie nucléaire, article BN 3700, juillet 2008 (in French).

[MAY 1982] Mayer P., Manolescu A.V., Rasile E.M., *Hydrogen absorption during corrosion of zirconium alloys in concentrated alkaline solutions at 340°C*, 3ème Congress Hydrogen and Materials, Chatenay-Malabry, France, 7-11 June 1982.

[McD 1984] McDonald S.G., Sabol G.P., Sheppard K.D., *Effect of lithium hydroxide on the corrosion behavior of Zircaloy-4*, ASTM STP 824, 1984, pp. 519-530.

[MIN 2013] Min S.J., Kim M.S., Kim K.T., *Cooling rate- and hydrogen content-dependent hydride reorientation and mechanical property degradation of Zr–Nb alloy claddings*, J. of Nuclear Materials 441 (2013) 306-314.

[MIN 2014] Min S.J., Won J.J., Kim K.T., *Terminal cool-down temperature-dependent hydride reorientations in Zr–Nb alloy claddings under dry storage conditions*, J. of Nuclear Materials 448 (2014) 172-183.

[MÜL 2013] Müller S., Lanzani L., *Corrosion of zirconium alloys in concentrated lithium hydroxide solutions*, J. of Nuclear Materials 439 (2013) 251-257.

[MUR 1967] Murgatroyd R.A., Winton J., *Hydriding of Zircaloy-2 in lithium hydroxide solutions*, J. of Nuclear Materials 23 (1967) 249-256.

[NAK 1993] Nakatsuka M., *Potential application of Zircaloy chemical embrittlement to volume reduction of spent-fuel cladding*, Nuclear Technology 103 (1993) 426-433.

[NEE 1997] Neeb K.H., The radiochemistry of nuclear power plants with light water reactors, de Gruyter, 1997.

[NIS 1997] Nishino Y., Endo M., Ibe E., Yasuda T., *Formation and dissolution of oxide film on zirconium alloys in 288°C pure water under γ-ray irradiation*, J. of Nuclear Materials 248 (1997) 292-298.

[NIS 2009] NISA, *Long-term integrity of the dry metallic casks and their contents in the spent fuel interim storage facilities – Attachment 3*, Nuclear and Industrial Safety Subcommittee of the Advisory Committee for Natural Resources and Energy – Nuclear Fuel Cycle Safety Subcommittee. Interim Storage Working Group and Transportation Working Group, 25 juin 2009.

[NOR 2004] Normand B., Pébère N., Richard C., Wery M., Prévention et lutte contre la corrosion : une approche scientifique et technique, Presses Polytechniques et Universitaires Romandes, 2004, 775 p. (in French).

[PAN 2001] Pan Y.M., Brossia C.S., Cragnolino G.A., Jain V., Pensado O., Sridhar N., *Effect of in-package chemistry on the degradation of vitrified high-level radioactive waste and spent nuclear fuel cladding*, Center for Nuclear Waste Regulatory Analyses, Report CNWRA 2002-01, October 2001, pp. 37-52.

[PEC 1996] Pêcheur D., Godlewski J., Billot Ph., Thomazet J., *Microstructure of oxide films formed during the waterside corrosion of Zircaloy-4 cladding in lithiated environment*, ASTM STP 1295, 1996, pp. 94-113.

[PIC 1972] Pickman D.O., *Properties of Zircaloy cladding*, Nuclear Engineering and Design 21 (1972) 212-236.

[PIN 1989] Pinard-Legry G., Pelras M., Turluer G., *Corrosion resistance of metallic materials for use in nuclear fuel reprocessing*. A Working Party Report on Corrosion in the Nuclear Industry, EFC Publications, The Institute of Metals, n°1, 1989, pp. 47-51.

[POU 1963] Pourbaix M., Atlas d'équilibres électrochimiques à 25°C. Gauthier-Villars, Paris, 1963.

[POU 1970] Pourbaix M., *Significance of protective potential in pitting and intergranular corrosion*, Corrosion Nace 26 (1970) 431-438.

[POU 2001a] Poulard K., *Étude de l'influence de la corrosion en milieu basique sur le relâchement d'activité par la zircone : application au stockage des coques*, Thesis, University Claude Bernard-Lyon 1, n°151-2001, 27 September 2001 (in French).

[POU 2001b] Poulard K., Chevarier A., Moncoffre N., Trocellier P., Crusset D., *Study of zircaloy-4 fuel cladding using ion beams. Application to long-term disposal of nuclear wastes*, Nuclear Instruments and Methods in Physics Research B 181 (2001) 640-643.

[POU 2002] Poulard K., Chevarier A., Moncoffre N., Crusset D., *Iodine release from oxidised Zircaloy cladding in contact with an alkaline solution*, J. of Nuclear Materials 306 (2002) 99-104.

[QIU 2009] Qiu L., Guzonas D.A., Webb D.G., *Zirconium dioxide solubility in high temperature aqueous solutions*, J. of Solution Chemistry 38 (2009) 857-867.

[RAS 2002] Rashid J., Machiels A., *A perspective on spent fuel integrity under dry storage and transportation conditions*, Nuclear Safety Research Conference, Washington, 28-30 October 2002.

[ROB 1989] Robertson J., *Modelling of corrosion and corrosion release in PWR primary circuits*, Proceedings of the congress Water Chemistry of Nuclear Reactor Systems 5, London, BNES, 1989, pp. 81-87.

[ROT 1984] Rothman A.J., *Potential corrosion and degradation mechanisms of Zircaloy cladding on spent nuclear fuel in a tuff repository*, LLNL, Technical Report UCID 20172, 1984.

[SAK 2013] Sakuragi T., Tanabe H., Hirose E., Sakashita A., Nishimura T., *Estimation of carbon 14 inventory in hull and end piece wastes from Japanese commercial reprocessing operation*, Proceedings of the ASME 2013 15th International Conference on Environmental Remediation and Radioactive Waste Management, ICEM2013, 8-13 September 2013, Brussels, Belgium, Paper n°96110.

[SAS 2003a] Sasoh M., *The study for the chemical forms of C-14 released from activated metals*, Proceedings of a Nagra/RWMC Workshop on the release and transport of C-14 in repository environments, Wettingen, Switzerland, 27-28 October 2003, Nagra Technical Report NAB 08-22, May 2008.

[SAS 2003b] Sasoh M., *Study on chemical behavior of organic C-14 under alkaline condition*, Proceedings of a Nagra/RWMC Workshop on the release and transport of C-14 in repository environments, Wettingen, Switzerland, 27-28 October 2003, Nagra Technical Report NAB 08-22, May 2008.

[SIE 2000] Siegmann E., *Clad degradation – FEPs screening arguments*, US DOE – OCRWM, Report ANL-WIS-MD-000008 REV00, 28 April 2000.

[SIN 2004] Singh R.N., Kishore R., Singh S.S., Sinha T.K., Kashyap B.P., *Stress-orientation of hydrides and hydride embrittlement of Zr-2.5 wt% Nb pressure tube alloy*, J. of Nuclear Materials 325 (2004) 26-33.

[SHO 2010] Shoesmith D.W., Zagidulin D., *The corrosion of zirconium under deep geologic repository conditions*, NWMO, Technical Report TR-2010-19, October 2010; 2nd source: J. of Nuclear Materials 418 (2011) 292-306.

[SKB 1999] SKB, *SR97 Processes in the repository evolution*, Technical Report TR-99-07, November 1999, pp. 34-35.

[SKB 2006] SKB, *Fuel and canister process report for the safety assessment SR-Can*, Technical Report TR-06-22, October 2006, pp. 50-52.

[SMI 1993] Smith H.D., Baldwin D.L., *An investigation of thermal release of carbon-14 from PWR Zircaloy spent fuel cladding*, J. of Nuclear Materials 200 (1993) 128-137.

[STE 1975] Stehle H., Kaden W., Manzel R., *External corrosion of cladding in PWRs*, Nuclear Engineering and Design 33 (1975) 155-169.

[STE 1996] Stewart L., McKinnon M.A., *Spent fuel behavior in long-term dry storage*, IMechE Conference Transaction 1996-7, pp. 183-194, 1996.

[TAK 2013] Takahashi R., Sasoh M., Yamashita Y., Tanabe H., Sakuragi T., *Improvement of inventory and leaching rate measurements of C-14 in hull waste, and separation of organic compounds for chemical species identification*, Mater. Res. Soc. Symp. Proc. 1518, Scientific basis for nuclear waste management XXXVII, Barcelona, Spain, 29 september – 3 october 2013.

[TAN 2007] Tanabe H., Nishimura T., Kaneko M., Sakuragi T., Nasu Y., Asano H., *Characterization of hull waste in underground condition*, Proceedings of the International Workshop on Mobile Fission and Activation Products in Nuclear Waste Disposal, L'Hermitage, La Baule, France, January 16-19, 2007.

[TAN 2013] Tanabe H., Sakuragi T., Miyakawa H., Takahashi R., *Long-term corrosion of Zircaloy hull waste under geological disposal conditions: Corrosion correlations, factors Influencing corrosion, corrosion test data, and preliminary evaluation*. Mater. Res. Soc. Symp. Proc. 1518, Scientific basis for nuclear waste management XXXVII, Barcelona, Spain, 29 september – 3 october 2013.

[TER 2014] Terrani K.A., Zinkle S.J., Snead L.L., Advanced oxidation-resistant iron-based alloys for LWR fuel cladding, J. of Nuclear Materials 448 (2014) 420-435.

[URB 1984] Urbanic V.F., *Observations of accelerated hydriding in zirconium alloys*, ASTM STP 824, 1984, pp. 554-571.

[VAN 1965] Van der Linde A., *Calculation of the safe lifetime expectancy of zirconium alloy canning in the fuel elements of the NERO reactor*. Petten, Netherlands, RCN-41, July 1965.

[VAN 1985] Van Konynenburg R.A., Smith C.F., Culham H.W., Otto C.H., *Behavior of carbon-14 in waste packages for spent fuel in a repository in tuff*, Scientific Basis of Nuclear Waste Management, MRS 44 (1985) 405-412.

[VAN 1991] Van Konynenburg R.A., *Gaseous release of carbon-14: why the high level waste regulations should be changed*, 1991 International High-Level Radioactive Waste Management Conference Las Vegas, NV, 28 April – 3 May 1991.

[VID 1975] Videm K., *Uniform corrosion and hydrogen pickup of zirconium-base cladding materials in boiling water reactors*, Nuclear Engineering and Design 33 (1975) 170.

[VRI 1994] Vrignaud E., Dugué P., *Apport des contrôles sur sites du combustible à l'analyse du comportement en service de l'assemblage combustible*. Actes du colloque international Fontevraud III (1994), Contribution des expertises sur matériaux à la résolution des problèmes rencontrés dans les réacteurs à eau pressurisée, Vol. 2, p. 650 (in French).

[WAD 1999] Wada R., Nishimura T., Fujiwara K., Tanabe M., Mihara M., *Experimental study on hydrogen gas generation rate from corrosion of zircaloy and stainless steel under anaerobic alkaline conditions*, 7th Int. Conf. on Radioactive waste management and environmental remediation, ICEM Conference Proceedings, ASME, Nagoya, Japan, 26-30 Sept.1999.

[WIE 2010] Wieland E., Hummel W., *The speciation of ^{14}C in the cementitious near field of a repository for radioactive waste*, PSI, Technical Report TM-44-10-01, December 2010.

[YAM 1999] Yamaguchi T., Tanuma S., Yasutomi I., Nakayama T., Tanabe H., Katsurai K., Kawamura W., Maeda K., Kitao H., Saigusa M., *A study on chemical forms and migration behavior of radionuclides in hull wastes*, ICEM 1999, September, Nagoya, 1999.

[YAM 2013] Yamashita Y., Tanabe H., Sakuragi T., Takahashi R., Sasoh M., *C-14 release behavior and chemical species from irradiated hull waste under geological disposal conditions*. Mater. Res. Soc. Symp. Proc. 1518, Scientific basis for nuclear waste management XXXVII, Barcelona, Spain, 29 September – 3 October 2013.

[ZHA 2011] Zhang X.G., *Galvanic corrosion*, in Uhlig's Corrosion Handbook, 3rd edition, Chapter 10, John Wiley & Sons, 2011.

Appendix 1 Correspondence between the units used for the uniform corrosion measurement of zirconium alloy

In laboratory tests, measurement of weight gain of the specimens by weighing before and after the test is used for determining the general (or uniform) corrosion of zirconium alloys in water. It is recognized in fact that the release of the oxidized species in the environment is negligible and the oxide layer is perfectly adherent.

Below are given the corresponding relationships between the different parameters used for the evaluation of general corrosion of zirconium alloys in these conditions.

The weight gain ΔW ($mg.dm^{-2}$) is considered as entirely due to the oxygen atoms[5] constituting the oxide ZrO_2. The corresponding weight of the oxide is equal to:

$$\Delta W_{Ox} = \frac{[Zr]+[O]}{2[O]} \Delta W \qquad \{A1\}$$

with: [Zr]: molar mass of zirconium (91.2)

[O]: molar mass of oxygen (16.0)

The corresponding weight of oxidized metal is:

$$\Delta W_{Zr} = \frac{[Zr]}{2[O]} \Delta W \qquad \{A2\}$$

The corresponding thickness *t* of the oxide layer can be inferred from the following two ways:

- knowing the density of the oxide (ρ_{Ox} = 5.6 $g.cm^{-3}$):

$$t_{Ox}\ (\mu m) = \frac{[Zr]+[O]}{2[O]} \Delta W\ (mg.dm^{-2})/10\ \rho_{Ox} \qquad \{A3\}$$

- from the value of the Pilling-Bedworth ratio (ratio of volume of oxide to volume of metal), namely 1.56, and the density of zirconium (ρ_{Zr} = 6.5 $g.cm^{-3}$):

$$t_{Ox}\ (\mu m) = 1.56\ \frac{[Zr]}{2[O]} \Delta W\ (mg.dm^{-2})/10\ \rho_{Zr} \qquad \{A4\}$$

The relationships {A3} and {A4} lead to expression:

$$t_{Ox}\ (\mu m) = 0.0684\ \Delta W\ (mg.dm^{-2}) \qquad \{A5\}$$

or else:

$$\boxed{1\ \mu m \text{ of oxide} = 14.62\ mg.dm^{-2}} \qquad \{A6\}$$

[5] In all strictness, the absorption of hydrogen in the metal also contributes to the change in weight of specimens. Thus, it could be shown that, for a hydrogen pick-up of 20 %, the contribution of this

We can also calculate the corresponding loss of metal t_{Zr}:

$$t_{Zr}\ (\mu m) = \frac{[Zr]}{2\,[O]}\ \Delta W\ (mg.dm^{-2})/10\ \rho_{Zr} \qquad \{A7\}$$

and finally:

$$t_{Zr}\ (\mu m) = 0.0438\ \Delta W\ (mg.dm^{-2}) = 0.641\ t_{Ox}\ (\mu m) \qquad \{A8\}$$

or else:

$$\boxed{1\ \mu m \text{ of metal loss (Zr)} = 22.83\ mg.dm^{-2}} \qquad \{A9\}$$

The above relationship enables to easily establish the other corresponding relationships between the kinetics of weight gain and the kinetics corrosion of the base metal:

$$1\ \mu m.y^{-1}\ (\text{loss of metal}) = 1.56\ \mu m.y^{-1}\ (\text{thickening of the oxide layer}) = 6.26\ 10^{-2}\ mg.dm^{-2}.d^{-1}\ (\text{weight gain of specimen}) \qquad \{A10\}$$

hydrogen in the measured weight gain is of 2.5 %.

Glossary: Abbreviations and acronyms

Andra	Agence nationale pour la gestion des déchets radioactifs (France)
BWR	Boiling Water Reactor
CEA	Commissariat à l'énergie atomique et aux énergies alternatives (France)
CNWRA	Center for Nuclear Waste Regulatory Analyses, Southwest Research Institute (USA)
CSD-C	Standard Canister for compacted hulls, end-pieces and spacers (Colis Standard de Déchets Compactés)
DOE	US Department of Energy (USA)
EDF	Électricité de France
EPRI	Electric Power Research Institute (USA)
HMi	Heavy Metal initial
ILW	Long-lived Intermediate Level nuclear Waste
J-13	Well water used for corrosion tests in connection with the Yucca Mountain project (USA)
KEPCO	Kansai Electric Power Corporation (Japan)
KWU	Kraftwerk Union (Germany)
LLNL	Lawrence Livermore National Laboratory (USA)
LWR	Light Water Reactor
MOX	Nuclear fuel of mixed uranium and plutonium oxide $U(Pu)O_2$
Nagra	National cooperative for the disposal of radioactive waste (Switzerland)
NDA	Nuclear Decommissioning Authority (UK)
NPP	Nuclear Power Plant
NWMO	Nuclear Waste Management Organization (Canada)
OCRWM	Office of Civilian Radioactive Waste Management (USA)
PNL	Pacific Northwest Laboratory (USA)
PSI	Paul Scherrer Institute (Switzerland)
PWR	Pressurized Water Reactor
RWMC	Radioactive Waste Management Funding and Research Center (Japan)
SCC	Stress Corrosion Cracking
SCE	Saturated Calomel Electrode (+ 0.24 V versus the standard hydrogen electrode at 25°C)
SGW	Simulated Groundwater
SKB	Svensk Kärnbränslehantering AB (Sweden)
SNF	Spent Nuclear Fuel
UOX	Nuclear fuel of uranium oxide UO_2